

THE ROLE OF MICROSCOPIC MIXING IN THE DESCRIPTION
OF TURBULENT DIFFUSION IN FLUID CONTINUUM

by

Ya Guo

Department of Renewable Resources

McGill University, Montreal

December, 1991

A thesis submitted to
the Faculty of Graduate Studies and Research
in partial fulfillment of the requirements for
the degree of Doctor of Philosophy

© Ya Guo, 1991

Suggested short title:

THE ROLE OF MICROSCOPIC MIXING IN THE DESCRIPTION
OF TURBULENT DIFFUSION

Abstract

Ph.D.

Ya Guo

Renewable Resources

The role of molecular mixing (as opposed to molecular-collision transport) in the description of turbulent diffusion in continuum framework is examined. This is done by comparing a new virtual fluid parcel treatment with the classical fluid particle treatment of the BMDFE (Basic Macroscopically Describable Fluid Element). It is found that the classical fluid particle treatment conceptually excludes molecular mixing between different BMDFEs, due to its postulated constraint that individual BMDFEs maintain their integrities in motion. The new virtual fluid parcel treatment, on the other hand, conceptually incorporates molecular mixing between different BMDFEs, by relaxing this constraint to permit disintegration of individual BMDFEs. The main improvement made by the new virtual fluid parcel treatment lies in the introduction of a feedback mechanism in the form of physically coupled disintegration and integration of the BMDFEs. This improvement suggests that molecular mixing is a controlling agent of the mixing mechanism in every time-step of turbulent diffusion, whose significance would increase cumulatively. By applying the two treatments to the evolution of the diffusion cloud on the level of single time-step diffusion redistribution, it is shown that molecular mixing persistently and cumulatively influences the evolution of the diffusion cloud by reducing the diffusion distribution variance. This indicates that the exclusion of molecular mixing in the classical fluid particle treatment would lead to a potential mathematical-physical inconsistency in the description of turbulent diffusion by exaggerating the diffusion distribution variance. The results of this analysis are qualitatively supported by experiments of passive scalar diffusion in water flow with moderate turbulence intensity. As a preliminary test, a

simplified numerical modeling of scalar diffusion based on the virtual fluid parcel treatment is executed in two wind tunnel models. In this case, measurements are used to directly estimate the fractional redistribution density of the scalar so as to bypass technical difficulties in solving the disintegration equation. The numerical predictions show general agreement with experimental observations.

Résumé

Ph.D.

Ya Guo

Ressources Renouvelables

Le rôle de l'échange moléculaire (échange de molécules par contraste avec la 'diffusion moléculaire' par collision) est examiné dans la description de la diffusion turbulente en cadre continu. Une nouvelle méthode, basée sur des 'éléments virtuels' du fluide, est comparée à la méthode classique de la description du BMDFE (élément de base pour la description macroscopique du fluide). Cette description classique est exclue, par la contrainte que le BMDFE maintienne son intégrité le long des trajectoires, tout échange de molécules parmi les BMDFE. Par contre, l'échange moléculaire est incorporé dans la nouvelle description 'virtuelle', permettant la désintégration des BMDFE. Ceci est exécuté, du point de vue technique, par un feed-back d'intégrations et de désintégrations des BMDFE. Cette modification suggère que l'échange moléculaire influence même la diffusion turbulente à chaque intervalle de temps, avec une importance cumulative croissante. En appliquant les deux méthodes à la diffusion d'un scalaire passif au niveau de redistribution continue de la concentration dans chaque intervalle de temps, on constate que l'échange moléculaire, de façon persistente et cumulative, influence le processus de diffusion, en réduisant la variance de la distribution de la concentration. Ceci suggère que l'exclusion de l'échange moléculaire par le traitement classique devrait mener à une inconsistance dans la description mathématique, par rapport aux réalités physiques, en exagérant cette variance. Les conclusions de cette analyse sont supportées par des expériences de diffusion d'un scalaire passif dans un courant d'eau avec intensité de turbulence modérée. Comme essai supplémentaire et préliminaire, une simulation numérique simplifiée de la diffusion turbulente est également comparée à la simulation expérimentale exécutée

avec deux modèles de soufflerie. Dans ce cas, des observations expérimentales de vitesse servent à l'estimation approximative de la densité de redistribution du scalaire, évitant des difficultés techniques dans la solution de l'équation de désintégration. En général, les simulations numériques se conforment aux simulations expérimentales.

Acknowledgements

The author wishes to extend his sincere gratitude to Dr P H. Schuepp, the research supervisor, for his continued support, advice, encouragement and assistance, and to Dr. N.N. Barthakur, for his encouragement and assistance during the course of this study

The author wishes to express his sincere appreciation to Dr. P.J Sullivan (Applied Mathematics, University of Western Ontario) for helping to clarify the concept of molecular mixing, and to Dr. A.S. Mujumdar (Chemical Engineering, McGill University) and Dr. V.M. Canuto (NASA Goddard Space Flight Center, New York) for their encouragement. Constructive or critical comments by Dr. S B Pope (Mechanical and Aerospace Engineering, Cornell University), Dr. Y Chen (NASA Goddard Space Flight Center, New York), Dr. P. Durbin (NASA Ames Research Center, California), Dr. G.W. Thurtell (Land Resource Science, University of Guelph), Dr. J.W Deardorff (Atmospheric Sciences, Oregon State University), Dr. P. Taylor (Pure and Applied Science, York University), Dr. J Hunt (Applied Mathematics and Theoretical Physics, University of Cambridge) and Dr. J.M. Chen (Geography, University of British Columbia) were also appreciated.

The author gratefully acknowledges the financial support from the Natural Sciences and Engineering Research Council of Canada, from McGill University in the form of tuition waiver, from the McGill University Computing Center for non-funded computing time and from the Department of Meteorology of McGill University for the hospitable charge-free access to their computer.

The author is indebted to Dr. G.R. Mehuys, Dr. R.D. Titman and Mr. P Kirby of Renewable Resources, Dr. W.D. Marshall of Agricultural Chemistry and

Food Science and Dr. M.Y. Leclerc (University of Quebec) for their help during this study.

Special thanks are extended to Ms. G. Pelletier and Mr. S. Kaharabata who helped with quality jobs of data collection and processing in the water tunnel experiments, and to my other fellow graduate students, Mr M. Duncan, P. Caramori and Z Lin, for their good humour, interest and encouragement, as well as to the community of the Department of Renewable Resources for its friendly atmosphere.

My deepest gratitude is extended to my dear wife Ying for her love, patience, understanding and bearing the family burden during the course of this study, and to my mother-in-law Mian Sun for her love and help during the most difficult time of this study.

Contribution to Knowledge

This thesis examines the effect of molecular mixing on turbulent diffusion in continuum framework, through comparison of the fundamental conceptualization (or mathematical treatment) of the BMDFE (Basic Macroscopically Describable Fluid Element), with and without consideration of molecular mixing. To the author's knowledge, the following aspects of the thesis constitute original contributions to knowledge.

1. Molecular collision-transport and molecular mixing are conceptually distinguished. Molecular collision-transport is a process involving transport of physical properties (such as momentum, heat, etc) through surface contact between different BMDFEs, while molecular mixing is a process involving exchange of individual molecules, carrying physical properties across the boundaries of different BMDFEs.

2. The randomization of the classical fluid particle treatment of BMDFE is shown not to alter the fact that molecular mixing is excluded by this treatment, because it does not change the nature of the postulated fluid particle moving as an entity.

3. Based on the classical random fluid particle treatment, the Lagrangian and Eulerian variables in the ensemble of realizations of a turbulent flow are shown to be related by statistical multi-to-one Lagrangian-Eulerian transformations, instead of one-to-one transformations. The multi-to-one Lagrangian-Eulerian transformations deny the statistical equivalence between the Lagrangian variables of a single fluid particle and the Eulerian variables at one space-time point.

4. According to the statistical multi-to-one Lagrangian-Eulerian transformations, turbulent diffusion under the classical random fluid particle

treatment can only be described as random fluid particle dispersions, in the form of statistical superimpositions of contributions from individual fluid particles. The limitations of this description, with its lack of a feedback mechanism in the statistical superimpositions, is demonstrated

5. A new virtual fluid parcel treatment of BMDFE is proposed to extend the classical fluid particle treatment. The new treatment conceptually incorporates molecular mixing by permitting disintegration of individual BMDFEs.

6. The main improvement made by the new treatment in the description of turbulent diffusion is the introduction of a feedback mechanism in the form of physically coupled disintegration and integration of the BMDFEs. This improvement suggests that molecular mixing could be a controlling agent of the mixing mechanism in every time-step of turbulent diffusion, whose significance would be cumulatively increased.

7. A comparison of the new and classical treatments in application to the diffusion cloud evolution, with experimental support, suggests that molecular mixing persistently and cumulatively influences diffusion by reducing the diffusion distribution variance. This means that due to the exclusion of molecular mixing, the classical fluid particle treatment must be expected to exaggerate the diffusion distribution variance.

8. A first test of the new treatment is presented by comparing simplified numerical modeling of scalar turbulent diffusion against experimental observations of diffusion in two wind tunnel models. The numerical predictions show a general agreement with the experimental observations.

Thesis Statement

This thesis is presented as a series of four parts in paper manuscript format with the relevant literature review contained in each part. Each part is relatively independent, but serves as an integral part of the thesis under the same main topic. Connection between the different parts is naturally provided by the introduction and conclusion to each part. Mathematical symbols and terminology used in this thesis are carefully chosen to match common conventions, unless specified otherwise. Bold face symbols represent vectors.

The thesis conforms to the conditions, concerning authorship, as outlined in the Guidelines Concerning Thesis Preparation which are excerpted as follows:

"The inclusion of manuscripts co-authored by the candidate and others is acceptable but the candidate is required to make an explicit statement on who contributed to such work and to what extent, and supervisors must attest to the accuracy of the claims, e.g. before the oral committee. Since the task of the examiners is made more difficult in these cases, it is in the candidate's interest to make the responsibilities of authors perfectly clear. Candidates following this option must inform the Department before it submits the thesis for review."

Part 3 and part 4 are co-authored by this author and P.H. Schuepp. Dr. Schuepp was the student's supervisor who undertook the administrative operation of the project, helped to set up the experiments for electrochemical simulations, and contributed as well in the general guidance and editorial work on the manuscripts.

Table of Contents

	Page
Abstract	ii
Résumé	iv
Acknowledgements	vi
Contribution to Knowledge	viii
Thesis Statement	x
Table of Contents	xi
List of Tables	xv
List of Figures	xvi
General Introduction	1
REFERENCES	4
Part 1. The Limitation of the Fluid Particle Treatment	5
Abstract	5
1. Introduction	6
2. Review of the fluid particle treatment	6
2.1. The fluid particle treatment	6
2.2. The conservation principles	8
2.3. The potential limitation	12
3. The randomization supplement and the Lagrangian-Eulerian transformations	14
3.1. The randomization supplement	14
3.2. The Lagrangian-Eulerian transformations	15
4. The description of turbulent diffusion	25
	xi

4.1. Formulations of $\bar{\rho}_L$, $\bar{\theta}_L$ and $\bar{\Psi}_L$	25
4.2. The turbulent diffusion mechanism	30
5. Conclusion	33
REFERENCES	35
Part 2. The Virtual Fluid Parcel Treatment	39
Abstract	39
1. Introduction	40
2. The virtual fluid parcel treatment	41
2.1. Concept	41
2.2. The description of the fluid dynamic variables	42
3. The mixing processes	47
3.1. Disintegration	47
3.2. Integration	53
4. The description of turbulent diffusion	54
4.1. Approximations of F_M , F_V and F_C , or $\tilde{\rho}$, $\tilde{\theta}$ and $\tilde{\Psi}$	54
4.2. The turbulent diffusion mechanism	58
5. Conclusion	62
REFERENCES	64
Part 3. Application to the Diffusion Cloud	66
Abstract	66
1. Introduction	67
2. Diffusion redistributions and the effect of molecular mixing	72
2.1. Formal description of redistributions	72

2.2. The means and variances of the redistributions	80
2.3. The effect of molecular mixing	85
3. Experimental test	87
3.1. Design	87
3.2. Setup	89
3.3. Results	91
4. Conclusion	95
REFERENCES	97

Part 4. A Preliminary Simulation of Scalar Turbulent Diffusion

under the Virtual Fluid Parcel Treatment	98
Abstract	98
1. Introduction	99
2. Alternative approximate disintegration	101
3. Experimental details	103
3.1. Laboratory set-up	103
3.2. Measurements	106
4. Numerical details	110
4.1. Interpolations	110
4.2. Gridding	115
5. Results	116
5.1. Comparison of numerical simulations with experimental observations	116
5.2. Development of the numerical plumes	120
6. Error analyses	126
7. Conclusion	129

REFERENCES	131
General Summary	132
Suggestions for Future Study	134

List of Tables

	Page
Part 4.	
Table 1. List of simulation parameters.	117

List of Figures

	Page
Part 3.	
Figure 1. Design of experiments.	88
Figure 2. Schematic diagram of the experimental arrangement. ...	90
Figure 3. The arrangement of principal measurement sensors B to N and supplementary measurement sensors A_1 to A_{12}	92
Figure 4. The integrated two-dimensional contour (a) and surface (b) plots of the natural joint diffusion distribution P_n of the joint puff measured in the second sub-design (a1 and b1), and the diffusion distribution P_r calculated in principle of the statistical superimposition of the separate puffs individually measured in the first sub-design (a2 and b2), averaged from 10 repetitions. * gives data position.	93
Part 4.	
Figure 1. Schematic diagram of wind tunnel (a), artificial plant canopy diagram (b) and photograph (c).	104
Figure 2. The arrangements of concentration measurement positions: A_1 , A_2 , A_3 , B_1 , B_2 and B_3 are measurement profiles, each with five sensors at levels of 2.4, 7.2, 9.6, 14.4 and 19.2 cm respectively. Sensors are located at centers of cell patterns in the canopy model.	107
Figure 3. The design of hot-film sensors for the measurement of the values of the three components of the Eulerian wind velocity (a), the direction of v (b) and the direction of w (c). A_1 , A_2 , A_3 , B_1 , B_2 , C_1 and C_2 are sensors.	109
Figure 4. The profiles of mean velocities \bar{U} and turbulence intensities TI at source height in along-wind direction (a1, b1), cross-wind direction (a2, b2) and vertical direction (a3, b3), in the middle of the simulation sections. Measurements are taken at centers of cell patterns in the canopy model.	111

Figure 5.	Spectra for u measured at $x = 90\text{cm}$, $y = 0\text{cm}$ in open-surface model (a) and at $x = 62.4\text{ cm}$, $y = 0\text{ cm}$ in canopy model (v).	112
Figure 6.	Linear (a) and proportional (b) interpolation procedures: V is the interpolated value, $V_1, V_2, V_3, V_4, V_5, V_6, V_7$ and V_8 are measured values. Circles represent trees.	114
Figure 7.	NH_3 concentration profiles of the steady numerical plume (S) and steady experimental plume (M) from continuous point source in the open-surface model at three downwind distances (x) from the source, on each of two xz planes at $y = 0$ (a) and $y = 8$ (b).	118
Figure 8.	NH_3 concentration profiles of the steady numerical plume (S) and steady experimental plume (M) from continuous point source in the canopy model at three down-wind distances (x) from the source, on each of two xz planes at $y = 0$ (a) and $y = 8$ (b).	119
Figure 9.	The developments of NH_3 concentration contours on the central xz plane ($y = 0$) of the numerical plumes from continuous point sources in the open-surface model (a) and the canopy model (b) at simulation times 0.1s (a1, b1), 0.5s (a2, b2), 2.0s (a3, b3), 10.0s (a4) and 16.0s (b4).	121
Figure 10.	The developments of NH_3 concentration contours on the xy plane ($z = 8$, source height) of the numerical plumes from continuous point sources in the open-surface model (a) and the canopy model (b) at simulation times 0.1s (a1, b1), 0.5s (a2, b2), 2.0s (a3, b3), 10.0s (a4) and 16.0s (b4).	123
Figure 11.	NH_3 concentration contours of the steady numerical plumes from continuous point sources in the open-surface model (a) and the canopy model (b) on different xz planes at $y = 0$ (a1, b1), $y = 4$ (a2, b2), $y = 8$ (a3, b3) and $y = 18$ (a4, b4).	124
Figure 12.	NH_3 concentration profiles of the steady numerical plumes from continuous point sources in the open-surface model (C) and the canopy model (C) at three down-wind distances (x) from the source, on each of three xz planes at $y = 0$ (a1), $y = 8$ (a2) and $y = 18$ (a3).	125

Figure 13. NH_3 concentration profiles of the steady numerical plumes from continuous point sources in the open-surface model (O) and the canopy model (C) at three crosswind distances (y), on each of three yz planes at $x = 21$ (O) or 20 (C) in (a1), $x = 67$ (O) or 52 (C) in (a2) and $x = 150$ (O) or 100 (C) in (a3).

.....

General Introduction

Understanding the role of microscopic molecular mixing in turbulent fluids is important to the description of the real diffusion, mixing, dilution, combustion and chemical reactions in turbulent flows. It has been given increased attention in recent years (Pope 1979; Chatwin & Sullivan 1979; Durbin 1980; Hunt 1985; Sawford & Hunt 1986; Stapountzis et al. 1986; Kaplan & Dinar 1988; Chatwin & Sullivan 1991). This renewed discussion should not be regarded as a simple review of the old issue about the comparison between molecular collision-transport and turbulent transport.

In the continuum perception of real fluids, molecular diffusion in general may involve two different processes: One is collision-transport, described by molecular kinematic and scalar viscosities ν and κ (collision-transport coefficients for momentum and scalar), through which the collision-transportable physical properties (such as momentum, heat, etc.) are transmitted, by contact, between fluid elements. The other is mixing through which individual molecules carrying physical properties are exchanged from one fluid element to another. The distinction between these two processes will become clear later in the study and the terminology (possibly inappropriate) may be subject of further debate. Although the first process may have been intensively studied and well understood, there is still something to be learned about the second process.

Consideration of molecular mixing in the description of turbulent diffusion in continuum framework would introduce additional difficulties into the conceptualization (or mathematical treatment) of the BMDFE (Basic Macroscopically Describable Fluid Element). Because of the cascaded transport of turbulent energy from large scales down to fine scales, the BMDFE, as the starting

point of the description in continuum mechanics, may face disintegration of its integrity in turbulent fluids (Durbin 1980) Ultimately, the real mixing in turbulent fluids takes place through molecular mixing, or through molecular diffusion in general, at fine scales, irrespective of the macroscopic flow character (Chatwin & Sullivan 1991).

Although the contribution of molecular mixing to the large-scale transport of physical properties may be relatively small, its effect in smoothing fine-scale structure enhanced by turbulent motion should not generally be neglected, as realized by the previous studies (Chatwin & Sullivan 1979; Durbin 1980, Hunt 1985; Sawford & Hunt 1986; Stapountzis et al. 1986; Kaplan & Dinar 1988; Chatwin & Sullivan 1991). Molecular mixing may continuously cause disintegration of "old" BMDFEs, and hence integration of "new" BMDFEs in turbulent fluids, and may essentially become a persistent controlling agent of the mixing mechanism.

In this thesis, an attempt is made to explain the role of molecular mixing as such a controlling agent in the description of turbulent diffusion in continuum framework. Emphasis is on comparison of different conceptual treatments of the BMDFE, excluding and including molecular mixing. Turbulent diffusion, in this context, is applied broadly to the transport phenomena of both vector and scalar physical properties. The bulk of the work is covered in three studies given in the first three chapters: (Part 1) A critical investigation of the classical fluid particle treatment of the BMDFE and its potential limitation in the description of turbulent diffusion due to exclusion of molecular mixing; (Part 2) An exploratory proposal of a new "virtual fluid parcel" treatment of the BMDFE with incorporation of molecular mixing, and examination of its formal improvement in the description of turbulent diffusion; (Part 3) An attempt to clarify, analytically

and experimentally, the effect of molecular mixing on turbulent diffusion, by comparing the application of the classical and new treatments to the evolution of the diffusion cloud.

As a preliminary trial, a simplified numerical modeling of scalar diffusion based on the virtual fluid parcel treatment, and associated experimental tests, are presented in the last chapter (Part 4).

REFERENCES

- Chatwin, P.C. & Sullivan, P.J. 1979 The relative diffusion of a cloud of passive contaminant in incompressible turbulent flow. *J Fluid Mech.* **91**, 337-355
- Chatwin, P.C. & Sullivan, P.J. 1991 The use of exact but idealized results in turbulent diffusion problems Submitted to *Combustion Conference on Fluid Mechanics*, Trinidad.
- Durbin, P.A. 1980 A stochastic model of two-particle dispersion and concentration fluctuations in homogeneous turbulence. *J. Fluid Mech.* **100**, 279-302
- Hunt, J.C.R. 1985 Turbulent diffusion from sources in complex flows. *Ann. Rev. Fluid Mech.* **17**, 447-485.
- Kaplan, H. & Dinar, N. 1988 A stochastic model for dispersion and concentration distribution in homogeneous turbulence. *J Fluid Mech* **190**, 121-140.
- Pope, S.B. 1979 The statistical theory of turbulent flames. *Phil Trans. R Soc Lond.* **A291**, 529-568.
- Sawford, B.L. & Hunt, J.C.R. 1986 Effects of turbulence structure, molecular diffusion and source size on scalar fluctuations in homogeneous turbulence. *J Fluid Mech.* **165**, 373-400.
- Stapountzis, H., Sawford, B.L., Hunt, J.C.R. and Britter, R.E. 1986 Structure of the temperature field downwind of a line source in grid turbulence *J. Fluid Mech.* **165**, 401-424.

Part 1. The Limitation of the Fluid Particle Treatment

Abstract

The classical fluid particle treatment of the BMDFE (Basic Macroscopically Describable Fluid Element) in continuum framework, and its description of turbulent diffusion, are critically examined. It is found that the fluid particle treatment excludes molecular mixing between different BMDFEs. The randomization of the fluid particle is shown not to alleviate this fact because it does not change the nature of the postulated fluid particle moving as an entity. Instead, it leads to the statistical multi-to-one Lagrangian-Eulerian transformations which deny the statistical equivalence of the random Lagrangian and Eulerian variables in turbulent flows.

According to the statistical multi-to-one Lagrangian-Eulerian transformations, turbulent diffusion under the random fluid particle treatment can only be described as random fluid particle dispersions, processed in the statistical superimposition of the "shadow-like" ensemble mean contributions from individual fluid particles. The non-feedback mechanism in this description may lead to a potential mathematical-physical inconsistency in the understanding of turbulent diffusion in real turbulent fluids, because the mixing between real BMDFEs, caused by molecular mixing, does not lend itself to such superimposition.

1. Introduction

The conceptualization (or mathematical treatment) of the Basic Macroscopically Describable Fluid Element (BMDFE) is a primary problem in the description of turbulent diffusion in continuum framework. The BMDFE has been classically defined as the fluid particle which maintains its integrity in motion. However, due to molecular mixing, molecules may cross the boundaries of different BMDFEs. When this process has had a significant cumulative effect, it becomes meaningless to refer to the classical concept of fluid particles and to consider mass contained within the same individual fluid particles (Chatwin & Sullivan 1979). It is then reasonable to conjecture that the non-consideration of this aspect by the classical description, based on the fluid particle treatment, may lead to difficulties in the interpretation of turbulent diffusion mechanisms in real fluids.

In this study, we attempt to explore the above conjecture through a critical examination of the classical fluid particle treatment, and its potential limitation in the description of turbulent diffusion due to exclusion of molecular mixing. Discussion will be restricted to incompressible fluids for reason of simplicity, without jeopardizing the validity of the basic argument.

2. Review of the fluid particle treatment

2.1. The fluid particle treatment

Real fluids are composed of individual molecules and thus discrete when considered microscopically at the molecular level. These molecules usually exist separately, with separation distances that are large compared to their sizes. In fluid mechanics, generally in continuum mechanics, attention is primarily paid to the macroscopic phenomena of fluid motion, where detailed properties of individual molecules need not be taken into account. Instead, the average effects of many molecules are of

interest. Therefore, except for special situations such as gases at low pressure, where intermolecular distances approach the characteristic dimensions of the problem, a continuum hypothesis is applied, that treats a fluid as a macroscopically continuous medium composed indiscretely of the BMDFEs (Lamb 1932; Townsend 1956; Longwell 6-7pp 1966; Pao 6-7pp 1966; Batchelor 1967; Owczarek 3pp 1968; Mironer, 10pp 1979; Lu 11pp 1979; Massey 3pp 1983; John & Haberman 9pp 1988). Under this hypothesis, the macroscopic physical properties of a fluid, such as mass density ρ , velocity \mathbf{V} , and mass-specific concentration C of any other scalar, are assumed to vary continuously in space \mathbf{X} and time t , described by the Eulerian variables $\rho_E(\mathbf{X},t)$, $\mathbf{V}_E(\mathbf{X},t)$ and $C_E(\mathbf{X},t)$, respectively.

The classical definition of the BMDFE in continuum framework is based on the fluid particle treatment, subject to the following assumed constraints: On the one hand, it has dimensions that are large compared to the separation distances between molecules, so that the macroscopic physical properties of a fluid can be reasonably defined and measured by averaging molecular properties within that element. On the other hand, its dimensions are sufficiently small compared to the distance over which the macroscopic physical properties of the fluid may change significantly. It can then be regarded as a point-like "particle" of uniform state in space, relative to the macroscopic flow scale, moving as a whole in motion (Pao 7pp 1966; Owczarek 3pp 1968; Monin & Yaglom 528pp 1971; Lu 11pp 1979; Mironer 10pp 1979; Richardson 3-4pp 1989).

The description of the physical behaviour of an individual fluid particle necessarily involves, implicitly or explicitly, the Lagrangian variables of a fixed entity. They include the Lagrangian trajectory $\mathbf{X}_L(\mathbf{X}_0,t)$, mass density $\rho_L(\mathbf{X}_L,t; \mathbf{X}_0,t_0)$, velocity $\mathbf{V}_L(\mathbf{X}_L,t; \mathbf{X}_0,t_0)$, and mass-specific concentration $C_L(\mathbf{X}_L,t; \mathbf{X}_0,t_0)$ of any other scalar of an individual fluid particle identified by its

initial position \mathbf{X}_0 at initial time t_0 .

Here $\rho_L(\mathbf{X}_L, t; \mathbf{X}_0, t_0)$, $\mathbf{V}_L(\mathbf{X}_L, t; \mathbf{X}_0, t_0)$ and $C_L(\mathbf{X}_L, t; \mathbf{X}_0, t_0)$ are purposely written in the explicit forms of \mathbf{X}_L in order to emphasize that the Lagrangian variables of physical properties are defined by following the trajectory of the same fluid particle. They explicitly denote the Lagrangian mass density, velocity and mass-specific concentration of any other scalar of the fluid particle \mathbf{X}_0 when it appears at position \mathbf{X}_L at time t . The argument \mathbf{X}_L in these variables is a function of time t , given as $\mathbf{X}_L(\mathbf{X}_0, t)$. These notations, which should not be considered to be different from the conventional implicit-in- \mathbf{X}_L notations such as $\rho_L(\mathbf{X}_0, t)$, $\mathbf{V}_L(\mathbf{X}_0, t)$ and $C_L(\mathbf{X}_0, t)$, can bring convenience to the following analyses.

2.2. The conservation principles

A major advantage of the fluid particle treatment may lie in the convenience it offers for the mathematical formulation of changes of physical properties of fluids. Under this treatment, a fluid is visualized as a group of fluid particles which, in sum, produce a macroscopically continuous medium. Since each fluid particle in this medium is assumed as a point-like system moving as a whole, the conservation principles of classical particle mechanics are readily applied to it (Lamb 1932; Pao 1966; Batchelor 1967; Massey 1983; Richardson 1989).

The conservation of mass expresses the constancy of material of a fluid particle during its motion. In vector (printed in bold face) form, it is written as

$$\frac{d}{dt}(\rho_L(\mathbf{X}_L, t; \mathbf{X}_0, t_0) \cdot \delta \mathbf{X}_L) = 0 \quad (2.1)$$

where $\delta \mathbf{X}_L$ is the volume of the fluid particle \mathbf{X}_0 at position \mathbf{X}_L at time t .

Suppose the fluid particle \mathbf{X}_0 has its position $\mathbf{X}_L(\mathbf{X}_0, t)$ at time t . At time

$t + dt$, it moves to another position $\mathbf{X}_L + d\mathbf{X}_L$ along its trajectory. In this process, the change of its mass density due to advection would be

$$(d\mathbf{X}_L \cdot \nabla_{\mathbf{x}_L}) \cdot \rho_L(\mathbf{X}_L, t; \mathbf{X}_0, t_0)$$

and the change due to time would be

$$\frac{\partial}{\partial t} \rho_L(\mathbf{X}_L, t; \mathbf{X}_0, t_0) \cdot dt$$

so, the total change rate would be (Pao 15pp 1966)

$$\frac{d}{dt} \rho_L(\mathbf{X}_L, t; \mathbf{X}_0, t_0) = \frac{\partial}{\partial t} \rho_L(\mathbf{X}_L, t; \mathbf{X}_0, t_0) + \left(\frac{d}{dt} \mathbf{X}_L \cdot \nabla_{\mathbf{x}_L} \right) \cdot \rho_L(\mathbf{X}_L, t; \mathbf{X}_0, t_0) \quad (2.2)$$

where $\nabla_{\mathbf{x}_L}$ is del operator with respect to \mathbf{X}_L .

Considering also that

$$\frac{d}{dt} \mathbf{X}_L(\mathbf{X}_0, t) = \mathbf{V}_L(\mathbf{X}_L, t; \mathbf{X}_0, t_0) \quad (2.3)$$

(2.1) can be written in the conventional form

$$\begin{aligned} \frac{d}{dt} \rho_L(\mathbf{X}_L, t; \mathbf{X}_0, t_0) &= \frac{\partial}{\partial t} \rho_L(\mathbf{X}_L, t; \mathbf{X}_0, t_0) + (\mathbf{V}_L(\mathbf{X}_L, t; \mathbf{X}_0, t_0) \cdot \nabla_{\mathbf{x}_L}) \cdot \rho_L(\mathbf{X}_L, t; \mathbf{X}_0, t_0) \\ &= - \frac{\rho_L}{\delta \mathbf{X}_L} \cdot \frac{d}{dt} (\delta \mathbf{X}_L) \end{aligned} \quad (2.4)$$

In an incompressible fluid, δX_L should be kept constant, i.e.

$$\frac{d}{dt}(\delta X_L) = 0$$

or

$$\delta X_L = \delta X_0$$

δX_0 is the volume of the fluid particle X_0 at initial time t_0 .

Then, (2.4) becomes

$$\begin{aligned} \frac{d}{dt}\rho_L(\mathbf{X}_L, t; \mathbf{X}_0, t_0) &= \frac{\partial}{\partial t}\rho_L(\mathbf{X}_L, t; \mathbf{X}_0, t_0) + (\mathbf{V}_L(\mathbf{X}_L, t; \mathbf{X}_0, t_0) \cdot \nabla_{\mathbf{x}_L}) \cdot \rho_L(\mathbf{X}_L, t; \mathbf{X}_0, t_0) \\ &= 0 \end{aligned} \quad (2.5)$$

which indicates that mass density of an individual fluid particle is kept constant during motion in an incompressible fluid. For convenience of identification in the subsequent analysis, however, we retain the original notation as $\rho_L(\mathbf{X}_L, t; \mathbf{X}_0, t_0)$.

Similarly, the conservation of momentum of a fluid particle is expressed by Newton's Second Law

$$\begin{aligned} \frac{d}{dt}\mathbf{V}_L(\mathbf{X}_L, t; \mathbf{X}_0, t_0) &= \frac{\partial}{\partial t}\mathbf{V}_L(\mathbf{X}_L, t; \mathbf{X}_0, t_0) + (\mathbf{V}_L(\mathbf{X}_L, t; \mathbf{X}_0, t_0) \cdot \nabla_{\mathbf{x}_L})\mathbf{V}_L(\mathbf{X}_L, t; \mathbf{X}_0, t_0) \\ &= \mathbf{G}_L(\mathbf{X}_L, t; \mathbf{X}_0, t_0) + \nu \cdot \nabla_{\mathbf{x}_L}^2 \cdot \mathbf{V}_L(\mathbf{X}_L, t; \mathbf{X}_0, t_0) \end{aligned} \quad (2.6)$$

Here $\mathbf{G}_L(\mathbf{X}_L, t; \mathbf{X}_0, t_0)$ is the Lagrangian external mass-specific source strength of momentum exerted on the fluid particle X_0 at position \mathbf{X}_L at time t . ν is the molecular kinematic viscosity (or the molecular collision-transport coefficient for

momentum). $\nabla_{\mathbf{x}_L}^2$ is the Laplace operator with respect to \mathbf{X}_L .

The conservation of any other scalar of a fluid particle is then expressed as

$$\begin{aligned} \frac{d}{dt} C_L(\mathbf{X}_L, t; \mathbf{X}_0, t_0) &= \frac{\partial}{\partial t} C_L(\mathbf{X}_L, t; \mathbf{X}_0, t_0) + (\mathbf{V}_L(\mathbf{X}_L, t; \mathbf{X}_0, t_0) \cdot \nabla_{\mathbf{x}_L}) \cdot C_L(\mathbf{X}_L, t; \mathbf{X}_0, t_0) \\ &= S_L(\mathbf{X}_L, t; \mathbf{X}_0, t_0) + \kappa \cdot \nabla_{\mathbf{x}_L}^2 \cdot C_L(\mathbf{X}_L, t; \mathbf{X}_0, t_0) \end{aligned} \quad (2.7)$$

where $S_L(\mathbf{X}_L, t; \mathbf{X}_0, t_0)$ is the Lagrangian external mass-specific source strength of scalar exerted on the fluid particle \mathbf{X}_0 at position \mathbf{X}_L at time t , and κ is the molecular scalar viscosity (or the molecular collision-transport coefficient for scalar).

Combining (2.5) into (2.6) and (2.7), we have the following convenient forms of conservations of momentum and any other scalar of a fluid particle in an incompressible fluid:

$$\begin{aligned} \frac{\partial}{\partial t} \vartheta_L(\mathbf{X}_L, t; \mathbf{X}_0, t_0) + (\mathbf{V}_L(\mathbf{X}_L, t; \mathbf{X}_0, t_0) \cdot \nabla_{\mathbf{x}_L}) \cdot \vartheta_L(\mathbf{X}_L, t; \mathbf{X}_0, t_0) \\ = \mathbf{H}_L(\mathbf{X}_L, t; \mathbf{X}_0, t_0) + \nu \cdot \nabla_{\mathbf{x}_L}^2 \cdot \vartheta_L(\mathbf{X}_L, t; \mathbf{X}_0, t_0) \end{aligned} \quad (2.8)$$

$$\begin{aligned} \frac{\partial}{\partial t} \Psi_L(\mathbf{X}_L, t; \mathbf{X}_0, t_0) + (\mathbf{V}_L(\mathbf{X}_L, t; \mathbf{X}_0, t_0) \cdot \nabla_{\mathbf{x}_L}) \cdot \Psi_L(\mathbf{X}_L, t; \mathbf{X}_0, t_0) \\ = \mathbf{E}_L(\mathbf{X}_L, t; \mathbf{X}_0, t_0) + \kappa \cdot \nabla_{\mathbf{x}_L}^2 \cdot \Psi_L(\mathbf{X}_L, t; \mathbf{X}_0, t_0) \end{aligned} \quad (2.9)$$

In these two equations, the second order derivative of mass density $\rho_L(\mathbf{X}_L, t; \mathbf{X}_0, t_0)$ along the trajectory \mathbf{X}_L is negligible for ordinary fluids. $\vartheta_L(\mathbf{X}_L, t; \mathbf{X}_0, t_0)$, $\mathbf{H}_L(\mathbf{X}_L, t; \mathbf{X}_0, t_0)$, $\Psi_L(\mathbf{X}_L, t; \mathbf{X}_0, t_0)$ and $\mathbf{E}_L(\mathbf{X}_L, t; \mathbf{X}_0, t_0)$ are the corresponding volumetric measurements of the Lagrangian variables \mathbf{V}_L , \mathbf{G}_L , C_L and S_L , respectively, e.g.

$$\vartheta_L(\mathbf{x}_L, t; \mathbf{x}_o, t_o) = \rho_L(\mathbf{x}_L, t; \mathbf{x}_o, t_o) \cdot \mathbf{V}_L(\mathbf{x}_L, t; \mathbf{x}_o, t_o)$$

2.3. The potential limitation

When a real fluid, either a liquid or a gas, moves. Its constituent molecules may continuously change their positions relative to one another. In a liquid, although the forces of attraction between molecules are sufficient for macroscopic cohesion, the molecules can still move past one another to find new neighbours. In a gas, the forces of attraction between molecules are, in general, negligible so that the molecules are almost free to travel away from one another until collision (Batchelor 1967; Massey 1983). Therefore, both liquid and gas, cannot avoid mixing of molecules across the boundaries of different fluid elements during motion. This molecular mixing could contribute to the disintegration of the BMDFEs in turbulent flows (Durbin 1980a).

The structure of molecular mixing in turbulent fluids may have been implicitly described by the cascaded breakdown of eddies to small scales proposed by Richardson (1922) and developed by Kolmogorov (1941). According to their descriptions, a fully-developed turbulence at sufficiently large Reynolds number would be composed of eddies down to the molecular scale. Ultimately, the real mixing in turbulent fluids takes place through molecular mixing at fine scales, irrespective of the macroscopic flow character (Chatwin, Sullivan & Yip 1990, Chatwin & Sullivan 1991). Molecular mixing could occur, e.g. at the conduction cut-off length scale $(\kappa^3/\epsilon)^{1/4}$ (Batchelor 1959; Batchelor, Howells & Townsend 1959), which is of the order of $10^{-4} - 10^{-3}$ m in most flows, with ϵ the dissipation rate of turbulent kinetic energy.

Considering molecular mixing in real fluids, molecular diffusion in general should involve a mixing process through which individual molecules carrying physical properties are exchanged from one macroscopic fluid element to another. Unfortunately, this process has not so far been included in the fluid particle treatment according to its definition. This makes for an unsatisfactory description of molecular diffusion under the fluid particle treatment, as explained below.

With the second constraint of the fluid particle treatment met (see Section 2.1.), the term $\nu \cdot \nabla_{\mathbf{x}_L}^2 \cdot \phi_L(\mathbf{x}_L, t; \mathbf{x}_0, t_0)$ in (2.8) can only be interpreted as the molecular transport of momentum through surface collision between adjacent fluid particles of different velocities, without actual exchange of molecules between these fluid particles. Similarly, for any collision-transportable scalar such as heat, the term $\kappa \cdot \nabla_{\mathbf{x}_L}^2 \cdot \Psi_L(\mathbf{x}_L, t; \mathbf{x}_0, t_0)$ in (2.9) can only be interpreted as the molecular collision-transport of scalar through surface contact between adjacent fluid particles of different scalar concentrations. In these processes, however, the molecular collision-transport is by no means considered to cause exchange of molecules across the boundaries of different fluid particles. As shown in the mass conservation equation (2.5) of a fluid particle, where a fluid particle is assumed as a point-like system moving as a whole, exchange of molecules between this fluid particle and adjacent fluid particles is ignored in the first place. This is reflected by non-existence of a molecular mass transport term in the equation. Therefore, the classical fluid particle treatment could inherently suffer from a potential limitation of excluding the real physical process of molecular mixing (as opposed to collision-transport) between different BMDFEs in turbulent fluids.

The process of molecular collision-transport interacting with turbulent transport (generally referred to as "molecular diffusion" and "turbulent diffusion") has been studied by Saffman (1960) and many others (see Monin & Yaglom §10.1

and §10.2 1971), based on the diffusion equation similar to (2.9) in absence of the external source. According to their basically intuitive analyses, it has been suggested that the influence of molecular collision-transport on the evolution of the diffusion cloud is negligible in comparison with turbulent transport, for long diffusion times and sufficiently large Reynolds numbers. However, the parallel process of molecular mixing has not yet been given much attention.

3. The randomization supplement and the Lagrangian-Eulerian transformations

3.1. The randomization supplement

The randomization of fluid particles provides an important supplement to the fluid particle treatment in the statistical approach to turbulent diffusion in continuum framework. With this supplement, the Lagrangian trajectory $\mathbf{X}_L(\mathbf{x}_0, t)$, mass density $\rho_L(\mathbf{X}_L, t; \mathbf{x}_0, t_0)$, volumetric concentration of momentum $\vartheta_L(\mathbf{X}_L, t; \mathbf{x}_0, t_0)$ and volumetric concentration of scalar $\Psi_L(\mathbf{X}_L, t; \mathbf{x}_0, t_0)$ of a fluid particle in turbulent flows are treated as random processes. Correspondingly, the Eulerian mass density $\rho_E(\mathbf{x}, t)$, volumetric concentration of momentum $\vartheta_E(\mathbf{x}, t)$ and volumetric concentration of scalar $\Psi_E(\mathbf{x}, t)$ are treated as random fields. A turbulent flow is then statistically described as random motions of a group of fluid particles, where the observed values of either the Lagrangian or the Eulerian variables may differ in repeated experiments under the same conditions.

The complete set of values obtained in all repeated experiments is considered as an "ensemble" and each value obtained in one experiment is considered as a "realization" chosen under a certain probability from this ensemble (Taylor 1921, 1935; Von Kármán 1934; Millionshchikov 1939; Kampé de Fériet 1939). This random fluid particle treatment has, up to now, been generally used in the classical theory of turbulence (Kolmogorov 1942; Batchelor 1953; Obukhov 1954; Lin 1955;

Townsend 1956; Hinze 1959; Chandrasekhar 1961; Pasquill 1962; Lumley & Panofsky 1964; Longwell 1966; Monin & Yaglom 1971; Csanady 1973; Massey 1983; Lesieur 1987)

However, it should be born in mind that the above randomization supplement does not help to reduce the potential limitation of the fluid particle treatment in excluding molecular mixing between different BMDFEs in turbulent fluids, since it does not change the nature of the postulated fluid particle moving as an entity.

3.2. The Lagrangian–Eulerian transformations

In each realization of a turbulent flow, both Lagrangian and Eulerian variables can be regarded as single-valued ordinary variables under a certain probability. As such, they should satisfy the one-to-one Lagrangian–Eulerian transformations under the continuum hypotheses, i.e. the Lagrangian variables on the trajectory $X_L(\mathbf{x}_0, t)$ of a fluid particle at time t must be identical to the corresponding Eulerian variables at the fluid particle's position X_L at that time.

However, the exact determination of these variables in individual realizations of a real turbulent flow is practically impossible because they strongly depend on the details of initial and boundary conditions which may never be known with sufficient precision. Moreover, the structure of a turbulent flow may be so complex that the solution for any single realization, which may not always correspond to an actually observed flow, may be useless for practical application (Monin & Yaglom 1971).

Nevertheless, the random fluid particle treatment for a turbulent fluid implies the transition from the consideration of a single realization of a turbulent flow to the consideration of an ensemble of realizations of that turbulent flow. As a consequence, only the ensemble characteristics of the fluid dynamics are of interest,

instead of their exact values in individual realizations. With this implication, the relations between the random Lagrangian and Eulerian variables in a turbulent flow might be presented differently from the one used for a single realization, which is analyzed as follows.

Generally, the Lagrangian volumetric concentration of momentum $\vartheta_L(\mathbf{X}_L, t; \mathbf{X}_{o_i}, t_0)$ of the i th fluid particle \mathbf{X}_{o_i} is a random variable dependent on the random trajectory $\mathbf{X}_L(\mathbf{X}_{o_i}, t)$ of that fluid particle. (Here the subscript $i = 1, 2, 3 \dots$ reflects a discrete form chosen to explicitly label \mathbf{X}_o as the i th fluid particle in space, for convenience of expression only. It should not be interpreted as a violation of the continuum hypothesis.) The random trajectory $\mathbf{X}_L(\mathbf{X}_{o_i}, t)$ at a given time will choose the space positions as its realizations from an ensemble that could possibly cover the whole flow space:

$$\mathbf{X}_L(\mathbf{X}_{o_i}, t) \in \{\mathbf{X}_1, \mathbf{X}_2, \dots, \mathbf{X}_j \dots\} \quad (3.1)$$

Here the continuous space coordinates \mathbf{X} is again purposely written in the discrete form \mathbf{X}_j ($j = 1, 2, 3 \dots$) to explicitly label \mathbf{X} as the j th realization of $\mathbf{X}_L(\mathbf{X}_{o_i}, t)$ in its ensemble, for convenience of expression only.

To each realization position \mathbf{X}_j of the random trajectory $\mathbf{X}_L(\mathbf{X}_{o_i}, t)$ at a given time t , there corresponds a $\vartheta_L(\mathbf{X}_j, t; \mathbf{X}_{o_i}, t_0)$ in $\vartheta_L(\mathbf{X}_L, t; \mathbf{X}_{o_i}, t_0)$, which should also be a random variable of itself with its ensemble of realizations expressed as

$$\vartheta_L(\mathbf{X}_j, t; \mathbf{X}_{o_i}, t_0) \in \{\vartheta_{L_1}(\mathbf{X}_j, t; \mathbf{X}_{o_i}, t_0), \vartheta_{L_2}(\mathbf{X}_j, t; \mathbf{X}_{o_i}, t_0) \dots \vartheta_{L_k}(\mathbf{X}_j, t; \mathbf{X}_{o_i}, t_0) \dots\} \quad (3.2)$$

Here $\vartheta_{L_k}(\mathbf{X}_j, t; \mathbf{X}_{0_i}, t_0)$ is the k th realization of $\vartheta_L(\mathbf{X}_j, t; \mathbf{X}_{0_i}, t_0)$ in its ensemble, ($k = 1, 2, 3 \dots$).

Overall, the value of the random Lagrangian volumetric concentration of momentum $\vartheta_L(\mathbf{X}_L, t; \mathbf{X}_{0_i}, t_0)$ should be chosen from the following ensemble of realizations:

$$\vartheta_L(\mathbf{X}_L, t; \mathbf{X}_{0_i}, t_0) \in \left\{ \begin{aligned} & \{ \vartheta_{L_1}(\mathbf{X}_1, t; \mathbf{X}_{0_i}, t_0), \vartheta_{L_2}(\mathbf{X}_1, t; \mathbf{X}_{0_i}, t_0) \dots \vartheta_{L_k}(\mathbf{X}_1, t; \mathbf{X}_{0_i}, t_0) \dots \}, \\ & \{ \vartheta_{L_1}(\mathbf{X}_2, t; \mathbf{X}_{0_i}, t_0), \vartheta_{L_2}(\mathbf{X}_2, t; \mathbf{X}_{0_i}, t_0) \dots \vartheta_{L_k}(\mathbf{X}_2, t; \mathbf{X}_{0_i}, t_0) \dots \}, \\ & \dots \\ & \{ \vartheta_{L_1}(\mathbf{X}_j, t; \mathbf{X}_{0_i}, t_0), \vartheta_{L_2}(\mathbf{X}_j, t; \mathbf{X}_{0_i}, t_0) \dots \vartheta_{L_k}(\mathbf{X}_j, t; \mathbf{X}_{0_i}, t_0) \dots \}, \\ & \dots \end{aligned} \right\} \quad (3.3)$$

where its overall ensemble of realizations is composed of all the sub-ensembles for different realization positions of the random trajectory $\mathbf{X}_L(\mathbf{X}_{0_i}, t)$ of the given single fluid particle \mathbf{X}_{0_i} at a given time t .

For any combination of the realizations from ensembles (3.1) and (3.2), there should exist a joint probability density $P(\vartheta_{L_k}, \mathbf{X}_j, t | \mathbf{X}_{0_i}, t_0)$ for the unit volume fluid particle \mathbf{X}_{0_i} to appear at position \mathbf{X}_j at time t and have an unit value of the volumetric concentration of momentum ϑ_{L_k} .

All the joint probability density values for all realizations of the random variable $\vartheta_L(\mathbf{X}_L, t; \mathbf{X}_{0_i}, t_0)$, combined with the random trajectory $\mathbf{X}_L(\mathbf{X}_{0_i}, t)$ of the given fluid particle \mathbf{X}_{0_i} , should then be given in the following value set

$$\begin{aligned}
P_{\vartheta_L} \in \left\{ \right. & \{P(\vartheta_{L_1}, \mathbf{X}_1, t | \mathbf{X}_{0_1}, t_0), P(\vartheta_{L_2}, \mathbf{X}_1, t | \mathbf{X}_{0_1}, t_0) \dots P(\vartheta_{L_k}, \mathbf{X}_1, t | \mathbf{X}_{0_1}, t_0) \dots\}, \\
& \{P(\vartheta_{L_1}, \mathbf{X}_2, t | \mathbf{X}_{0_1}, t_0), P(\vartheta_{L_2}, \mathbf{X}_2, t | \mathbf{X}_{0_1}, t_0) \dots P(\vartheta_{L_k}, \mathbf{X}_2, t | \mathbf{X}_{0_1}, t_0) \dots\}, \\
& \dots\dots \\
& \{P(\vartheta_{L_1}, \mathbf{X}_j, t | \mathbf{X}_{0_1}, t_0), P(\vartheta_{L_2}, \mathbf{X}_j, t | \mathbf{X}_{0_1}, t_0) \dots P(\vartheta_{L_k}, \mathbf{X}_j, t | \mathbf{X}_{0_1}, t_0) \dots\}, \\
& \dots\dots
\end{aligned} \left. \right\} \tag{3.4}$$

Each value $P(\vartheta_{L_k}, \mathbf{X}_j, t | \mathbf{X}_{0_1}, t_0)$ in set (3.4) can be further presented in the form

$$P(\vartheta_{L_k}, \mathbf{X}_j, t | \mathbf{X}_{0_1}, t_0) = P(\vartheta_{L_k} | \mathbf{X}_j, t; \mathbf{X}_{0_1}, t_0) \cdot P(\mathbf{X}_j, t | \mathbf{X}_{0_1}, t_0) \tag{3.5a}$$

Here $P(\vartheta_{L_k} | \mathbf{X}_j, t; \mathbf{X}_{0_1}, t_0)$ is the conditional probability density for the fluid particle \mathbf{X}_{0_1} to have an unit value of the volumetric concentration of momentum ϑ_{L_k} when it appears at position \mathbf{X}_j at time t . $P(\mathbf{X}_j, t | \mathbf{X}_{0_1}, t_0)$ is the probability density for the unit volume fluid particle \mathbf{X}_{0_1} to appear at position \mathbf{X}_j at time t . They should satisfy the normal restrictions under the continuum hypothesis:

$$\sum_{i=1}^{\infty} P(\mathbf{X}_j, t | \mathbf{X}_{0_1}, t_0) \cdot d\mathbf{X}_{0_1} = 1 \tag{3.5b}$$

$$\sum_{j=1}^{\infty} P(\mathbf{X}_j, t | \mathbf{X}_{0_1}, t_0) \cdot d\mathbf{X}_j = 1 \tag{3.5c}$$

$$\sum_{k=1}^{\infty} P(\vartheta_{L_k} | X_j, t; X_{0_i}, t_0) \cdot d\vartheta_{L_k} = 1 \quad (3.5d)$$

$$\sum_{i=1}^{\infty} \sum_{k=1}^{\infty} P(\vartheta_{L_k}, X_j, t | X_{0_i}, t_0) \cdot d\vartheta_{L_k} \cdot dX_{0_i} = 1 \quad (3.5e)$$

where dX_{0_i} ($= dX_j$ in an incompressible fluid) is the volume of the fluid particle X_{0_i} , and $d\vartheta_{L_k}$ is the differential increment in the volumetric concentration of momentum of the fluid particle X_{0_i} at position X_j at time t . Here, we change the original notations δX_{0_i} and δX_j to dX_{0_i} and dX_j for technical convenience of expression. Hopefully, this would not confuse the fluid particle volume with the trajectory increment, in the remaining analysis.

By comparison, the Eulerian volumetric concentration of momentum $\vartheta_E(X_j, t)$ at a given space-time point (X_j, t) ($j = 1, 2, 3 \dots$) is simply a random variable at that given point, with its ensemble of realizations expressed as

$$\begin{aligned} \vartheta_E(X_j, t) \in \left\{ \begin{aligned} &\{ \vartheta_{E_{1,1}}(X_j, t), \vartheta_{E_{1,2}}(X_j, t) \dots \vartheta_{E_{1,k}}(X_j, t) \dots \}, \\ &\{ \vartheta_{E_{2,1}}(X_j, t), \vartheta_{E_{2,2}}(X_j, t) \dots \vartheta_{E_{2,k}}(X_j, t) \dots \}, \\ &\dots\dots \\ &\{ \vartheta_{E_{i,1}}(X_j, t), \vartheta_{E_{i,2}}(X_j, t) \dots \vartheta_{E_{i,k}}(X_j, t) \dots \}, \\ &\dots\dots \end{aligned} \right\} \end{aligned} \quad (3.6)$$

where $\vartheta_{E_{i,k}}(X_j, t)$ is the k th realization of $\vartheta_E(X_j, t)$ in its sub-ensemble at the given

space-time point (\mathbf{X}_j, t) contributed by the n th fluid particle \mathbf{X}_{o_i} , ($i, k = 1, 2, 3 \dots$). The overall ensemble of realizations of $\vartheta_E(\mathbf{X}_j, t)$ is then composed of all the sub-ensembles at the given space-time point (\mathbf{X}_j, t) contributed by different fluid particles \mathbf{X}_{o_i} in the flow.

As mentioned before, in each realization of a turbulent flow, the Lagrangian variable $\vartheta_{L_k}(\mathbf{X}_j, t; \mathbf{X}_{o_i}, t_0)$ and the Eulerian variable $\vartheta_{E_{i,k}}(\mathbf{X}_j(\mathbf{X}_{o_i}, t_0), t)$ must be identical to each other with one-to-one transformation under the continuum hypothesis, so that (3.6) can be further expressed as

$$\vartheta_E(\mathbf{X}_j, t) \in \left\{ \begin{aligned} & \{ \vartheta_{L_1}(\mathbf{X}_j, t; \mathbf{X}_{o_1}, t_0), \vartheta_{L_2}(\mathbf{X}_j, t; \mathbf{X}_{o_1}, t_0) \dots \vartheta_{L_k}(\mathbf{X}_j, t; \mathbf{X}_{o_1}, t_0) \dots \}, \\ & \{ \vartheta_{L_1}(\mathbf{X}_j, t; \mathbf{X}_{o_2}, t_0), \vartheta_{L_2}(\mathbf{X}_j, t; \mathbf{X}_{o_2}, t_0) \dots \vartheta_{L_k}(\mathbf{X}_j, t; \mathbf{X}_{o_2}, t_0) \dots \}, \\ & \dots \dots \dots \\ & \{ \vartheta_{L_1}(\mathbf{X}_j, t; \mathbf{X}_{o_i}, t_0), \vartheta_{L_2}(\mathbf{X}_j, t; \mathbf{X}_{o_i}, t_0) \dots \vartheta_{L_k}(\mathbf{X}_j, t; \mathbf{X}_{o_i}, t_0) \dots \}, \\ & \dots \dots \dots \end{aligned} \right\} \quad (3.7)$$

All the probability density values for all the realizations of the random Eulerian variable $\vartheta_E(\mathbf{X}_j, t)$ are then given in the following value set

$$P_{\vartheta_E} \in \left\{ \begin{aligned} & \{ P(\vartheta_{L_1}, \mathbf{X}_j, t | \mathbf{X}_{o_1}, t_0), P(\vartheta_{L_2}, \mathbf{X}_j, t | \mathbf{X}_{o_1}, t_0) \dots P(\vartheta_{L_k}, \mathbf{X}_j, t | \mathbf{X}_{o_1}, t_0) \dots \}, \\ & \{ P(\vartheta_{L_1}, \mathbf{X}_j, t | \mathbf{X}_{o_2}, t_0), P(\vartheta_{L_2}, \mathbf{X}_j, t | \mathbf{X}_{o_2}, t_0) \dots P(\vartheta_{L_k}, \mathbf{X}_j, t | \mathbf{X}_{o_2}, t_0) \dots \}, \\ & \dots \dots \dots \\ & \{ P(\vartheta_{L_1}, \mathbf{X}_j, t | \mathbf{X}_{o_i}, t_0), P(\vartheta_{L_2}, \mathbf{X}_j, t | \mathbf{X}_{o_i}, t_0) \dots P(\vartheta_{L_k}, \mathbf{X}_j, t | \mathbf{X}_{o_i}, t_0) \dots \}, \\ & \dots \dots \dots \end{aligned} \right\} \quad (3.8)$$

According to probability theory, two random variables are said to be statistically identical if and only if they have identical ensemble of realizations and identical probability distribution. Generally, the two conditions are not satisfied by the random Lagrangian variable $\vartheta_L(\mathbf{x}_L, t; \mathbf{x}_{o_i}, t_o)$ and the random Eulerian variable $\vartheta_E(\mathbf{x}_j, t)$. In fact, the two random variables have different ensembles of realizations and different probability density distributions if we compare (3.3) with (3.7) and (3.4) with (3.8). Therefore, although the instantaneous equivalence, expressed as one-to-one transformations between the Lagrangian and Eulerian variables in a single realization of a turbulent flow, should be maintained under the continuum hypothesis, the assumption of the statistical equivalence of the two variables in an ensemble of realizations of that turbulent flow is not generally satisfied. This assumption may have been expressed alternatively in terms of fluid particles moving at the local Eulerian velocity of the fluid (Thomson 1984, 1990).

The traditionally used Markovian approximation to the Lagrangian behaviour of individual fluid particles does not help to justify the above assumption either, because the "memory-losing" feature of a fluid particle does not assure that this fluid particle should be statistically identical to the other "memory-losing" fluid particles in the flow. The only exception may be the mathematical idealization of the stationary and homogeneous turbulence, where the statistical behaviour between different fluid particles cannot be discriminated (Taylor 1921; Batchelor 1949). However, this exception should not be regarded as invalidating the following statistical principle:

Equations (3.3), (3.4), (3.7) and (3.8) indicate that any fluid particle at a given time has a certain probability to appear at every space point in a turbulent flow in repeated experiments, and that any fixed space-time point of a turbulent flow is statistically linked to all fluid particles in the flow with certain

probabilities. This means that one Lagrangian fluid particle statistically occupies multiple Eulerian space points at any time and, conversely, one Eulerian space point statistically corresponds to multiple Lagrangian fluid particles at any instant. This statistical multi-to-one Lagrangian-Eulerian transformation can be expressed in the following calculation of the ensemble mean Eulerian volumetric concentration of momentum $\bar{\vartheta}_E(\mathbf{x}_j, t)$ according to (3.7) and (3.8):

$$\bar{\vartheta}_E(\mathbf{x}_j, t) = \sum_{i=1}^{\infty} \sum_{k=1}^{\infty} \vartheta_{L_k}(\mathbf{x}_j, t; \mathbf{x}_{o_i}, t_0) \cdot P(\vartheta_{L_k}, \mathbf{x}_j, t | \mathbf{x}_{o_i}, t_0) \cdot d\vartheta_{L_k} \cdot d\mathbf{X}_{o_i} \quad (3.9)$$

Considering (3.5a), (3.9) can be written as

$$\bar{\vartheta}_E(\mathbf{x}_j, t) = \sum_{i=1}^{\infty} \bar{\vartheta}_L(\mathbf{x}_j, t; \mathbf{x}_{o_i}, t_0) \cdot d\mathbf{X}_{o_i} \quad (3.10a)$$

with $\bar{\vartheta}_L$ defined as

$$\bar{\vartheta}_L(\mathbf{x}_j, t; \mathbf{x}_{o_i}, t_0) = \left(\sum_{k=1}^{\infty} \vartheta_{L_k}(\mathbf{x}_j, t; \mathbf{x}_{o_i}, t_0) \cdot P(\vartheta_{L_k} | \mathbf{x}_j, t; \mathbf{x}_{o_i}, t_0) \cdot d\vartheta_{L_k} \right) \cdot P(\mathbf{x}_j, t | \mathbf{x}_{o_i}, t_0) \quad (3.10b)$$

Here $\bar{\vartheta}_L(\mathbf{x}_j, t; \mathbf{x}_{o_i}, t_0)$ is the ensemble mean contribution to the Eulerian volumetric concentration of momentum at the space-time point (\mathbf{x}_j, t) from the unit volume fluid particle \mathbf{x}_{o_i} . $\sum_{k=1}^{\infty} \vartheta_{L_k}(\mathbf{x}_j, t; \mathbf{x}_{o_i}, t_0) \cdot P(\vartheta_{L_k} | \mathbf{x}_j, t; \mathbf{x}_{o_i}, t_0) \cdot d\vartheta_{L_k}$ is the ensemble mean evolution of the Lagrangian volumetric concentration of momentum of the

fluid particle X_{o_i} at position X_j at time t .

By returning to the continuous (rather than discrete) description of the ordinary variable X_o and random variables X_L and ϑ_L , equations (3.5)s are rewritten as

$$P(\vartheta_L, X, t | X_o, t_o) = P(\vartheta_L | X, t; X_o, t_o) \cdot P(X, t | X_o, t_o) \quad (3.11a)$$

$$\int P(X, t | X_o, t_o) \cdot dX_o = 1 \quad (3.11b)$$

$$\int P(X, t | X_o, t_o) \cdot dX = 1 \quad (3.11c)$$

$$\int P(\vartheta_L | X, t; X_o, t_o) \cdot d\vartheta_L = 1 \quad (3.11d)$$

$$\iint P(\vartheta_L, X, t | X_o, t_o) \cdot d\vartheta_L \cdot dX_o = 1 \quad (3.11e)$$

and (3.9) is rewritten as

$$\begin{aligned} \bar{\vartheta}_E(X, t) &= \iint \vartheta_L(X, t; X_o, t_o) \cdot P(\vartheta_L, X, t | X_o, t_o) \cdot d\vartheta_L \cdot dX_o \\ &= \int \bar{\vartheta}_L(X, t; X_o, t_o) \cdot dX_o \end{aligned} \quad (3.12a)$$

with $\bar{\vartheta}_L$ defined as

$$\bar{\vartheta}_L(X, t; X_o, t_o) = \left(\int \vartheta_L(X, t; X_o, t_o) \cdot P(\vartheta_L | X, t; X_o, t_o) \cdot d\vartheta_L \right) \cdot P(X, t | X_o, t_o) \quad (3.12b)$$

Similarly, for mass density in a turbulent flow, we have

$$P(\rho_L, \mathbf{X}, t | \mathbf{X}_0, t_0) = P(\rho_L | \mathbf{X}, t; \mathbf{X}_0, t_0) \cdot P(\mathbf{X}, t | \mathbf{X}_0, t_0) \quad (3.13)$$

$$\begin{aligned} \bar{\rho}_E(\mathbf{X}, t) &= \iint \rho_L(\mathbf{X}, t; \mathbf{X}_0, t_0) \cdot P(\rho_L, \mathbf{X}, t | \mathbf{X}_0, t_0) \cdot d\rho_L \cdot d\mathbf{X}_0 \\ &= \int \bar{\rho}_L(\mathbf{X}, t; \mathbf{X}_0, t_0) \cdot d\mathbf{X}_0 \end{aligned} \quad (3.14a)$$

with $\bar{\rho}_L$ defined as

$$\bar{\rho}_L(\mathbf{X}, t; \mathbf{X}_0, t_0) = \left(\int \rho_L(\mathbf{X}, t; \mathbf{X}_0, t_0) \cdot P(\rho_L | \mathbf{X}, t; \mathbf{X}_0, t_0) \cdot d\rho_L \right) \cdot P(\mathbf{X}, t | \mathbf{X}_0, t_0) \quad (3.14b)$$

In the above equations, $P(\rho_L, \mathbf{X}, t | \mathbf{X}_0, t_0)$ is the joint probability density for the unit volume fluid particle \mathbf{X}_0 to appear at position \mathbf{X} at time t and have an unit value of mass density ρ_L . $P(\rho_L | \mathbf{X}, t; \mathbf{X}_0, t_0)$ is the conditional probability density for the fluid particle \mathbf{X}_0 to have an unit value of mass density ρ_L when it appears at position \mathbf{X} at time t . $\rho_L(\mathbf{X}, t; \mathbf{X}_0, t_0)$ is the Lagrangian mass density of the fluid particle \mathbf{X}_0 at position \mathbf{X} at time t . $\bar{\rho}_E(\mathbf{X}, t)$ is the ensemble mean Eulerian mass density at the space-time point (\mathbf{X}, t) . $\bar{\rho}_L(\mathbf{X}, t; \mathbf{X}_0, t_0)$ is the ensemble mean contribution to the Eulerian mass density at the space-time point (\mathbf{X}, t) from the unit volume fluid particle \mathbf{X}_0 . $\int \rho_L(\mathbf{X}, t; \mathbf{X}_0, t_0) \cdot P(\rho_L | \mathbf{X}, t; \mathbf{X}_0, t_0) \cdot d\rho_L$ is the ensemble mean evolution of the Lagrangian mass density of the fluid particle \mathbf{X}_0 at position \mathbf{X} at time t .

For any other scalar in a turbulent flow, we have

$$P(\Psi_L, \mathbf{X}, t | \mathbf{X}_0, t_0) = P(\Psi_L | \mathbf{X}, t; \mathbf{X}_0, t_0) \cdot P(\mathbf{X}, t | \mathbf{X}_0, t_0) \quad (3.15)$$

$$\begin{aligned}\bar{\Psi}_E(\mathbf{x},t) &= \iint \Psi_L(\mathbf{x},t; \mathbf{x}_0,t_0) \cdot P(\Psi_L, \mathbf{x},t | \mathbf{x}_0,t_0) \cdot d\Psi_L \cdot d\mathbf{X}_0 \\ &= \int \bar{\Psi}_L(\mathbf{x},t; \mathbf{x}_0,t_0) \cdot d\mathbf{X}_0\end{aligned}\quad (3.16a)$$

with $\bar{\Psi}_L$ defined as

$$\bar{\Psi}_L(\mathbf{x},t; \mathbf{x}_0,t_0) = \left(\int \Psi_L(\mathbf{x},t; \mathbf{x}_0,t_0) \cdot P(\Psi_L | \mathbf{x},t; \mathbf{x}_0,t_0) \cdot d\Psi_L \right) \cdot P(\mathbf{x},t | \mathbf{x}_0,t_0) \quad (3.16b)$$

where symbols are defined in analogy to those in (3.13) and (3.14) for mass density, but here for the volumetric concentration of any other scalar.

4. The description of turbulent diffusion

Under the random fluid particle treatment, (3.12a), (3.14a) and (3.16a) define the basic problem of turbulent diffusion as finding the ensemble mean contributions $\bar{\rho}_L$, $\bar{\vartheta}_L$ and $\bar{\Psi}_L$ to the Eulerian physical properties from individual fluid particles in the flow. Credits should then be given to the long-practiced random-walk models in simulation of fluid particle dispersions, since by their nature they do address this problem.

4.1. Formulations of $\bar{\rho}_L$, $\bar{\vartheta}_L$ and $\bar{\Psi}_L$

As long as the random fluid particle is assumed to move as a whole, the conservation equations (2.5), (2.8) and (2.9) should be still applicable to individual fluid particles in turbulent flows. These equations in turbulent flows should be understood as random equations with respect to the random trajectory \mathbf{X}_L and random evolutions of the Lagrangian properties ρ_L , ϑ_L and Ψ_L , respectively. Based on these random equations, the ensemble mean contributions $\bar{\rho}_L(\mathbf{x},t; \mathbf{x}_0,t_0)$,

$\bar{\vartheta}_L(\mathbf{X}, t; \mathbf{X}_0, t_0)$ and $\bar{\Psi}_L(\mathbf{X}, t; \mathbf{X}_0, t_0)$ to the Eulerian properties from a single fluid particle can be statistically formulated as

$$\begin{aligned} \frac{\partial}{\partial t} \bar{\rho}_L(\mathbf{X}, t; \mathbf{X}_0, t_0) + (\bar{\mathbf{V}}_L(\mathbf{X}, t; \mathbf{X}_0, t_0) \cdot \nabla_{\mathbf{X}}) \cdot \bar{\rho}_L(\mathbf{X}, t; \mathbf{X}_0, t_0) \\ = - \overline{(\mathbf{V}_L'(\mathbf{X}, t; \mathbf{X}_0, t_0) \cdot \nabla_{\mathbf{X}}) \cdot \rho_L'(\mathbf{X}, t; \mathbf{X}_0, t_0)} \end{aligned} \quad (4.1)$$

$$\begin{aligned} \frac{\partial}{\partial t} \bar{\vartheta}_L(\mathbf{X}, t; \mathbf{X}_0, t_0) + (\bar{\mathbf{V}}_L(\mathbf{X}, t; \mathbf{X}_0, t_0) \cdot \nabla_{\mathbf{X}}) \cdot \bar{\vartheta}_L(\mathbf{X}, t; \mathbf{X}_0, t_0) \\ = \bar{\mathbf{H}}_L(\mathbf{X}, t; \mathbf{X}_0, t_0) + \nu \cdot \nabla_{\mathbf{X}}^2 \cdot \bar{\vartheta}_L(\mathbf{X}, t; \mathbf{X}_0, t_0) - \overline{(\mathbf{V}_L'(\mathbf{X}, t; \mathbf{X}_0, t_0) \cdot \nabla_{\mathbf{X}}) \cdot \vartheta_L'(\mathbf{X}, t; \mathbf{X}_0, t_0)} \end{aligned} \quad (4.2)$$

$$\begin{aligned} \frac{\partial}{\partial t} \bar{\Psi}_L(\mathbf{X}, t; \mathbf{X}_0, t_0) + (\bar{\mathbf{V}}_L(\mathbf{X}, t; \mathbf{X}_0, t_0) \cdot \nabla_{\mathbf{X}}) \cdot \bar{\Psi}_L(\mathbf{X}, t; \mathbf{X}_0, t_0) \\ = \bar{\mathbf{E}}_L(\mathbf{X}, t; \mathbf{X}_0, t_0) + \kappa \cdot \nabla_{\mathbf{X}}^2 \cdot \bar{\Psi}_L(\mathbf{X}, t; \mathbf{X}_0, t_0) - \overline{(\mathbf{V}_L'(\mathbf{X}, t; \mathbf{X}_0, t_0) \cdot \nabla_{\mathbf{X}}) \cdot \Psi_L'(\mathbf{X}, t; \mathbf{X}_0, t_0)} \end{aligned} \quad (4.3)$$

with the initial conditions:

when $t = t_0$ and $\mathbf{X} = \mathbf{X}_0$,

$$\bar{\rho}_L(\mathbf{X}, t; \mathbf{X}_0, t_0) = \rho_L(\mathbf{X}_0, t_0), \quad \bar{\vartheta}_L(\mathbf{X}, t; \mathbf{X}_0, t_0) = \vartheta_L(\mathbf{X}_0, t_0), \quad \bar{\Psi}_L(\mathbf{X}, t; \mathbf{X}_0, t_0) = \Psi_L(\mathbf{X}_0, t_0)$$

when $t = t_0$ and $\mathbf{X} \neq \mathbf{X}_0$,

$$\bar{\rho}_L(\mathbf{X}, t; \mathbf{X}_0, t_0) = 0, \quad \bar{\vartheta}_L(\mathbf{X}, t; \mathbf{X}_0, t_0) = 0, \quad \bar{\Psi}_L(\mathbf{X}, t; \mathbf{X}_0, t_0) = 0 \quad (4.4)$$

Here $\rho_L(\mathbf{X}_0, t_0)$, $\vartheta_L(\mathbf{X}_0, t_0)$ and $\Psi_L(\mathbf{X}_0, t_0)$ are the initial mass density, volumetric concentration of momentum and volumetric concentration of scalar of the fluid particle \mathbf{X}_0 , respectively. The ensemble means in the above equations are defined in the sense of (3.12b), (3.14b) and (3.16b), in which the random trajectory and random evolutions of the Lagrangian properties are jointly processed. "" indicates

the deviation from such ensemble mean.

According to (3.16b), $\bar{E}_L(\mathbf{X}, t; \mathbf{X}_0, t_0)$ should be defined as

$$\bar{E}_L(\mathbf{X}, t; \mathbf{X}_0, t_0) = \left(\int E_L(\mathbf{X}, t; \mathbf{X}_0, t_0) \cdot P(E_L | \mathbf{X}, t; \mathbf{X}_0, t_0) \cdot dE_L \right) \cdot P(\mathbf{X}, t | \mathbf{X}_0, t_0)$$

Here $E_L(\mathbf{X}, t; \mathbf{X}_0, t_0)$ is the Lagrangian external volumetric source strength of scalar exerted on the fluid particle \mathbf{X}_0 at position \mathbf{X} at time t . $P(E_L | \mathbf{X}, t; \mathbf{X}_0, t_0)$ is the conditional probability density for the fluid particle \mathbf{X}_0 to have an unit value of external source strength of scalar E_L when it appears at position \mathbf{X} at time t .

Since the existence of the external source may not depend on any specific fluid particle, $\int E_L(\mathbf{X}, t; \mathbf{X}_0, t_0) \cdot P(E_L | \mathbf{X}, t; \mathbf{X}_0, t_0) \cdot dE_L$ may be approximated by the ensemble mean Eulerian external volumetric source strength, i.e.

$$\bar{E}_E(\mathbf{X}, t) = \int E_E(\mathbf{X}, t) \cdot P(E_E | \mathbf{X}, t) \cdot dE_E$$

where $E_E(\mathbf{X}, t)$ is the Eulerian external volumetric source strength of scalar and $P(E_E | \mathbf{X}, t)$ is the probability density of $E_E(\mathbf{X}, t)$ at space-time point (\mathbf{X}, t) .

Then, $\bar{E}_L(\mathbf{X}, t; \mathbf{X}_0, t_0)$ can be regarded as the ensemble mean transport rate of scalar from the external source into the unit volume fluid particle \mathbf{X}_0 :

$$\bar{E}_L(\mathbf{X}, t; \mathbf{X}_0, t_0) \approx \bar{E}_E(\mathbf{X}, t) \cdot P(\mathbf{X}, t | \mathbf{X}_0, t_0)$$

Similarly, $\bar{H}_L(\mathbf{X}, t; \mathbf{X}_0, t_0)$ may be approximated as

$$\bar{H}_L(\mathbf{X}, t; \mathbf{X}_0, t_0) \approx \bar{H}_E(\mathbf{X}, t) \cdot P(\mathbf{X}, t | \mathbf{X}_0, t_0)$$

with \bar{H}_E defined as

$$\bar{H}_E(\mathbf{X}, t) = \int \mathbf{H}_E(\mathbf{X}, t) \cdot P(\mathbf{H}_E | \mathbf{X}, t) \cdot d\mathbf{H}_E \approx \int \mathbf{H}_L(\mathbf{X}, t; \mathbf{X}_0, t_0) \cdot P(\mathbf{H}_L | \mathbf{X}, t; \mathbf{X}_0, t_0) \cdot d\mathbf{H}_L$$

where symbols are defined in analogy to those for the scalar source, but here for the momentum source.

With the above approximations, (4.1), (4.2) and (4.3) combined with their initial conditions (4.4) are written as

$$\begin{aligned} \frac{\partial}{\partial t} \bar{\rho}_L(\mathbf{X}, t; \mathbf{X}_0, t_0) + (\bar{\mathbf{V}}_L(\mathbf{X}, t; \mathbf{X}_0, t_0) \cdot \nabla_{\mathbf{X}}) \cdot \bar{\rho}_L(\mathbf{X}, t; \mathbf{X}_0, t_0) \\ = - (\nabla_L^2(\mathbf{X}, t; \mathbf{X}_0, t_0) \cdot \nabla_{\mathbf{X}}) \cdot \bar{\rho}_L(\mathbf{X}, t; \mathbf{X}_0, t_0) + \rho_L(\mathbf{X}_0, t_0) \cdot \delta(\mathbf{X} - \mathbf{X}_0) \cdot \delta(t - t_0) \end{aligned} \quad (4.5)$$

$$\begin{aligned} \frac{\partial}{\partial t} \bar{\vartheta}_L(\mathbf{X}, t; \mathbf{X}_0, t_0) + (\bar{\mathbf{V}}_L(\mathbf{X}, t; \mathbf{X}_0, t_0) \cdot \nabla_{\mathbf{X}}) \cdot \bar{\vartheta}_L(\mathbf{X}, t; \mathbf{X}_0, t_0) \\ = \bar{H}_E(\mathbf{X}, t) \cdot P(\mathbf{X}, t | \mathbf{X}_0, t_0) + \nu \cdot \nabla_{\mathbf{X}}^2 \cdot \bar{\vartheta}_L(\mathbf{X}, t; \mathbf{X}_0, t_0) \\ - (\nabla_L^2(\mathbf{X}, t; \mathbf{X}_0, t_0) \cdot \nabla_{\mathbf{X}}) \cdot \bar{\vartheta}_L(\mathbf{X}, t; \mathbf{X}_0, t_0) + \vartheta_L(\mathbf{X}_0, t_0) \cdot \delta(\mathbf{X} - \mathbf{X}_0) \cdot \delta(t - t_0) \end{aligned} \quad (4.6)$$

$$\begin{aligned} \frac{\partial}{\partial t} \bar{\Psi}_L(\mathbf{X}, t; \mathbf{X}_0, t_0) + (\bar{\mathbf{V}}_L(\mathbf{X}, t; \mathbf{X}_0, t_0) \cdot \nabla_{\mathbf{X}}) \cdot \bar{\Psi}_L(\mathbf{X}, t; \mathbf{X}_0, t_0) \\ = \bar{E}_E(\mathbf{X}, t) \cdot P(\mathbf{X}, t | \mathbf{X}_0, t_0) + \kappa \cdot \nabla_{\mathbf{X}}^2 \cdot \bar{\Psi}_L(\mathbf{X}, t; \mathbf{X}_0, t_0) \\ - (\nabla_L^2(\mathbf{X}, t; \mathbf{X}_0, t_0) \cdot \nabla_{\mathbf{X}}) \cdot \bar{\Psi}_L(\mathbf{X}, t; \mathbf{X}_0, t_0) + \Psi_L(\mathbf{X}_0, t_0) \cdot \delta(\mathbf{X} - \mathbf{X}_0) \cdot \delta(t - t_0) \end{aligned} \quad (4.7)$$

where δ is the Dirac delta function indicating the combined initial conditions as instantaneous point "sources".

The probability density $P(\mathbf{X}, t | \mathbf{X}_0, t_0)$ of the fluid particle's trajectory can, in

principle, be determined from (2.3) and (2.6), given specified initial conditions. The modified Langevin equation may be considered to be an approximate approach in this case, which has been used implicitly or explicitly in most random-walk models to describe the motions of individual fluid particles in analogy with the description of Brownian motion (Durbin 1980b; Wilson, Thurtell & Kidd 1981; Lamb 1981; Legg & Raupach 1982; Gifford 1982; Pope 1983; Janicke 1983; Ley & Thomson 1983; Wilson, Legg & Thomson 1983; Thomson 1984; Sawford 1984; van Dop, Nieuwstadt & Hunt 1985; Haworth & Pope 1986; Sawford 1986; Novikov 1986; Raupach 1987; Thomson 1987; Pope 1987; Kaplan & Dinar 1988; Luhar & Britter 1989).

In order to solve equations (4.5), (4.6) and (4.7), some Lagrangian statistics must be specified. This may entail difficulties in practice, because the assumption of the statistical equivalence of the Lagrangian and Eulerian random variables is not generally satisfied, as shown in Section 3.2. Evaluating the Lagrangian statistics of a given fluid particle by the Eulerian statistics at a given spatial position, implicitly or explicitly based on this assumption, then becomes inappropriate.

Generally, the solutions of (4.5), (4.6) and (4.7) for individual fluid particles may involve technical difficulties in the nonlinearity of equations and the parameterization of the flow character with macroscopic inhomogeneity of both flow scale and turbulence intensity in complex systems. These difficulties are beyond the scope of this study.

In addition to the above-mentioned difficulties, the probability density distribution $P(\mathbf{x}, t | \mathbf{x}_0, t_0)$ of a fluid particle's trajectory would be modified by any change of the fluid particle's momentum. Such modification would influence the probability density distributions of other fluid particles in the flow if the restriction

(3.11b) is considered. As a result, equation (4.6) for a fluid particle would become dependent on the momentum of the other fluid particles in the flow. Similarly, equation (4.7) of a non-passive scalar for a fluid particle would become dependent on the scalar concentrations of the other fluid particles in the flow. Therefore, the solutions of $\bar{\psi}_L(\mathbf{x}, t; \mathbf{x}_0, t_0)$ and $\bar{\Psi}_L(\mathbf{x}, t; \mathbf{x}_0, t_0)$ may become practically complex.

For a passive scalar, the complexity of solution of $\bar{\Psi}_L(\mathbf{x}, t; \mathbf{x}_0, t_0)$ can be reduced. Because the change of the passive scalar concentration of a fluid particle does not influence fluid motion, and thus does not alter the dynamic behaviour of other fluid particles, equation (4.7) of the passive scalar for individual fluid particles can be independently solved. As will be discussed later, this has a practical importance in the final solution of the ensemble mean Eulerian concentration $\bar{\Psi}_E(\mathbf{x}, t)$.

If the passive scalar of individual fluid particles in the flow is also conservative in the sense of neglecting the external source influence and the molecular collision-transport between different fluid particles, the scalar would at all times remain in the same fluid particles as at the initial time, i.e. $\bar{\Psi}_L(\mathbf{x}, t; \mathbf{x}_0, t_0) \equiv \bar{\Psi}_L(\mathbf{x}_0, t_0)$. In this case, the solution of $\bar{\Psi}_L(\mathbf{x}, t; \mathbf{x}_0, t_0)$ is reduced to the solution of the probability density distribution $P(\mathbf{x}, t | \mathbf{x}_0, t_0)$ of the fluid particle's trajectory only. (e.g. Monin & Yaglom §10.1 1979; Thomson 1987).

4.2. The turbulent diffusion mechanism

In summary, turbulent diffusion under the random fluid particle treatment is formulated through the following equations:

$$\begin{aligned}
& \frac{\partial}{\partial t} \bar{\rho}_L(\mathbf{X}, t; \mathbf{X}_0, t_0) + (\bar{\mathbf{V}}_L(\mathbf{X}, t; \mathbf{X}_0, t_0) \cdot \nabla_{\mathbf{x}}) \cdot \bar{\rho}_L(\mathbf{X}, t; \mathbf{X}_0, t_0) \\
& = - \overline{(\mathbf{V}'_L(\mathbf{X}, t; \mathbf{X}_0, t_0) \cdot \nabla_{\mathbf{x}}) \cdot \rho'_L(\mathbf{X}, t; \mathbf{X}_0, t_0)} + \rho_L(\mathbf{X}_0, t_0) \cdot \delta(\mathbf{X} - \mathbf{X}_0) \cdot \delta(t - t_0)
\end{aligned} \tag{4.8}$$

$$\begin{aligned}
& \frac{\partial}{\partial t} \bar{\vartheta}_L(\mathbf{X}, t; \mathbf{X}_0, t_0) + (\bar{\mathbf{V}}_L(\mathbf{X}, t; \mathbf{X}_0, t_0) \cdot \nabla_{\mathbf{x}}) \cdot \bar{\vartheta}_L(\mathbf{X}, t; \mathbf{X}_0, t_0) \\
& = \bar{\mathbf{H}}_E(\mathbf{X}, t) \cdot \mathbf{P}(\mathbf{X}, t | \mathbf{X}_0, t_0) + \nu \cdot \nabla_{\mathbf{x}}^2 \cdot \bar{\vartheta}_L(\mathbf{X}, t; \mathbf{X}_0, t_0) \\
& \quad - \overline{(\mathbf{V}'_L(\mathbf{X}, t; \mathbf{X}_0, t_0) \cdot \nabla_{\mathbf{x}}) \cdot \vartheta'_L(\mathbf{X}, t; \mathbf{X}_0, t_0)} + \vartheta_L(\mathbf{X}_0, t_0) \cdot \delta(\mathbf{X} - \mathbf{X}_0) \cdot \delta(t - t_0)
\end{aligned} \tag{4.9}$$

$$\begin{aligned}
& \frac{\partial}{\partial t} \bar{\Psi}_L(\mathbf{X}, t; \mathbf{X}_0, t_0) + (\bar{\mathbf{V}}_L(\mathbf{X}, t; \mathbf{X}_0, t_0) \cdot \nabla_{\mathbf{x}}) \cdot \bar{\Psi}_L(\mathbf{X}, t; \mathbf{X}_0, t_0) \\
& = \bar{\mathbf{E}}_E(\mathbf{X}, t) \cdot \mathbf{P}(\mathbf{X}, t | \mathbf{X}_0, t_0) + \kappa \cdot \nabla_{\mathbf{x}}^2 \cdot \bar{\Psi}_L(\mathbf{X}, t; \mathbf{X}_0, t_0) \\
& \quad - \overline{(\mathbf{V}'_L(\mathbf{X}, t; \mathbf{X}_0, t_0) \cdot \nabla_{\mathbf{x}}) \cdot \Psi'_L(\mathbf{X}, t; \mathbf{X}_0, t_0)} + \Psi_L(\mathbf{X}_0, t_0) \cdot \delta(\mathbf{X} - \mathbf{X}_0) \cdot \delta(t - t_0)
\end{aligned} \tag{4.10}$$

$$\bar{\rho}_E(\mathbf{X}, t) = \int \bar{\rho}_L(\mathbf{X}, t; \mathbf{X}_0, t_0) \cdot d\mathbf{X}_0 \tag{4.11}$$

$$\bar{\vartheta}_E(\mathbf{X}, t) = \int \bar{\vartheta}_L(\mathbf{X}, t; \mathbf{X}_0, t_0) \cdot d\mathbf{X}_0 \tag{4.12}$$

$$\bar{\Psi}_E(\mathbf{X}, t) = \int \bar{\Psi}_L(\mathbf{X}, t; \mathbf{X}_0, t_0) \cdot d\mathbf{X}_0 \tag{4.13}$$

Here, turbulent diffusion is described in terms of random fluid particle dispersions through which the ensemble mean Eulerian mass density $\bar{\rho}_E(\mathbf{X}, t)$, volumetric concentration $\bar{\vartheta}_E(\mathbf{X}, t)$ of momentum and volumetric concentration $\bar{\Psi}_E(\mathbf{X}, t)$ of any other scalar are respectively calculated as the statistical superimpositions of the ensemble mean contributions from all the individual fluid particles in the flow.

In the process of statistical superimposition, each ensemble mean contribution

from a single fluid particle is individually solved from (4.8), (4.9) and (4.10). It could be essentially viewed as a statistical "shadow" in physical properties of that fluid particle, which is assumed to be developed as if the "shadows" of the other fluid particles did not exist. Therefore, it is a consequence of the fact that the fluid particle treatment excludes molecular mixing between the BMDFEs, that turbulent diffusion under the random fluid particle treatment can only be described by superimposing the "shadows" of individual fluid particles. It is the conjecture of our study that this limitation has been inherently embodied in the described turbulent diffusion mechanism, which lacks a description for feeding back the superimposed "shadows" in terms of $\bar{\rho}_E(\mathbf{X},t)$, $\bar{\vartheta}_E(\mathbf{X},t)$ and $\bar{\Psi}_E(\mathbf{X},t)$ into the diffusion process. Any further joint development of the superimposed fluid particle "shadows" then becomes physically meaningless.

It might thus be said that the mixing between the BMDFEs of real turbulent fluids, caused by molecular mixing, does not lend itself to the concept of superimposition of the fluid particle "shadows". The lack of a feedback mechanism in this description may suggest the possibility of error when it is applied to real turbulent flows. In real turbulent flows, molecular mixing between different BMDFEs requires that the mixed BMDFEs should be physically described in their further joint development. Therefore, the description of turbulent diffusion under the random fluid particle treatment may lead to a potential mathematical-physical inconsistency in the understanding of turbulent diffusion in real turbulent fluids.

According to the discussion in Section 4.1., the statistical superimposition (4.12) or (4.13), for momentum or non-passive scalar, should be dependent in the sense that their ensemble mean contributions from different fluid particles in the flow are mutually dependent. This adds an additional practical complexity to solutions of turbulent diffusion. For a passive scalar, however, the contributions to

the statistical superimposition (4.13) from different fluid particles become mutually independent. The practical importance of this independence is that the overall diffusion of a passive scalar from distributed sources (assigned to different fluid particles at the initial time) can be reduced to an independent summation of separate diffusions from individual point sources.

Finally, it should be emphasized that the statistical superimposition is conceptually different from the standard technique of linear superposition. The statistical superimposition is an expression of the statistical summation (or ensemble average) of all the realization values of a random variable weighted by certain probabilities from the ensemble of realizations. The standard technique of linear superposition, on the other hand, is an expression of the non-statistical linear summation (or linearity) of non-random values. Therefore, the statistical superimposition is not conceptually related to linearity and the standard technique of linear superposition is not conceptually related to statistics.

5. Conclusion

This study points out that with the constraint that individual BMDFEs maintain their integrities in motion, the classical fluid particle treatment of the BMDFE excludes molecular mixing between different BMDFEs in turbulent fluids. The randomization of the fluid particle does not alleviate this fact since it does not change the nature of the postulated fluid particle moving as an entity.

It is demonstrated that the statistical equivalence of the random Lagrangian and Eulerian variables in turbulent flows under the random fluid particle treatment is not generally satisfied. Instead, the one-to-one Lagrangian-Eulerian transformations for a single realization of a turbulent flow are shown to be replaced by the statistical multi-to-one Lagrangian-Eulerian transformations for the

ensemble of realizations of that turbulent flow. This leads to the following consequence:

Turbulent diffusion under the random fluid particle treatment can only be described as random fluid particle dispersions in process of the statistical superimposition of the shadow-like ensemble mean contributions from individual fluid particles in the flow. The lack of a feedback mechanism in this description suggests the possibility of error when it is applied to real turbulent flows, because the physical process of mixing between real fluid elements, caused by molecular mixing, does not lend itself to such superimposition. As a result, this description may lead to a potential mathematical-physical inconsistency in the understanding of turbulent diffusion in real turbulent fluids.

This analysis suggests, therefore, that the description of turbulent diffusion might be improved by extending the fluid particle treatment to incorporate molecular mixing. This suggestion will be further explored in the following study (Part 2).

REFERENCES

- Batchelor, G.K. 1949 Diffusion in a field of homogeneous turbulence. *Austr. J. Sci. Res.*, A2, 4, 437-450.
- Batchelor, G.K. 1953 *The Theory of Homogeneous Turbulence*. Cambridge Univ. Press, Cambridge, England.
- Batchelor, G.K. 1959 Small-scale variation of convected quantities like temperature in turbulent fluid. Part 1. General discussion and the case of small conductivity. *J. Fluid Mech.* 5, 113-133.
- Batchelor, G.K., Howells, I.D. & Townsend, A.A. 1959 Small-scale variation of convected quantities like temperature in turbulent fluid. Part 2. The case of large conductivity. *J. Fluid Mech.* 5, 134-139.
- Batchelor, G.K. 1967 *An Introduction to Fluid Dynamics*. Cambridge, The University Press, England.
- Chandrasekhar, S. 1961 *Hydrodynamic and Hydromagnetic Stability*. Clarendon Press, Oxford.
- Chatwin, P.C. & Sullivan, P.J. 1979 The relative diffusion of a cloud of passive contaminant in incompressible turbulent flow. *J. Fluid Mech.* 91, 337-355.
- Chatwin, P.C., Sullivan, P.J. & Yip 1990 Dilution and marked fluid particle analysis. *Proceedings of International Conference on Physical Modeling of Turbulent and Dispersion*, MIT, 6B3-6B8.
- Chatwin, P.C. & Sullivan, P.J. 1991 The use of exact but idealized results in turbulent diffusion problems. Submitted to *Combustion Conference on Fluid Mechanics*, Trinidad.
- Csanady, G.T. 1973 *Turbulent diffusion in the environment*. D. Reidel Publ. Co., Dordrecht.
- Durbin, P.A. 1980a A stochastic model of two-particle dispersion and concentration fluctuations in homogeneous turbulence. *J. Fluid Mech.* 100, 279-302.
- Durbin, P.A. 1980b A random flight model of inhomogeneous turbulent dispersion. *Phys. Fluids* 23, 2151-2153.
- Gifford, F.A. 1982 Horizontal diffusion in the atmosphere: a Lagrangian dynamical theory. *Atmos. Environ.* 16, 505-515.
- Haworth, D.C. & Pope, S.B. 1986 A generalized Langevin model for turbulent flows. *Phys. Fluids* 29, 387-405.
- Hinze, J.O. 1959 *Turbulence. An Introduction to Its Mechanism and Theory*. McGraw-Hill Book Co., New York.

- Hunt, J.C.R. 1985 Turbulent diffusion from sources in complex flows. *Ann Rev. Fluid Mech.* **17**, 447-485.
- Janicke, L. 1983 Particle simulation of inhomogeneous turbulent diffusion. In *Air Pollution Modeling and Its Application*, II, pp.527-535. Plenum Press, New York.
- John, J.E.A. & Haberman, W.L. 1988 *Introduction to Fluid Mechanics*. Prentice Hall, Englewood Cliffs, New Jersey.
- Kaplan, H. & Dinar, N. 1988 A stochastic model for dispersion and concentration distribution in homogeneous turbulence. *J. Fluid Mech.* **190**, 121-140.
- Kampé de Fériet, J. 1939 Les fonctions aléatoires stationnaires et la théorie statistique de la turbulence homogène. *Ann. Soc. Sci. Bruxelles* **59**, 145-194.
- Kármán, T. von 1934 Some aspects of the theory of turbulent motion. *Proc. Intern. Congr. Appl. Mech.*, Cambridge.
- Kolmogorov, A.N. 1941 Local structure of turbulence in an incompressible fluid at very high Reynolds Numbers. *Doklady AN SSSR*, **30**, 299-303.
- Kolmogorov, A.N. 1942 Equations of turbulent motion of an incompressible fluid. *Izvestiya AN SSSR, Ser.Fiz.*, **6**, 56-58.
- Lamb, H. 1932 *Hydrodynamics*, 6th edition. Dover Publications Inc., New York.
- Lamb, R.G. 1981 A scheme for simulating particle pair motions in turbulent fluid. *J. Comput. Phys.* **39**, 329-346.
- Legg, B.J. & Raupach, M.R. 1982 Markov-chain simulation of particle diffusion in inhomogeneous flows: the mean drift velocity induced by a gradient in Eulerian velocity variance. *Bound.-Layer Meteor.* **24**, 3-13.
- Lesieur, M. 1987 *Turbulence in Fluids*. Martinus Nijhoff Publ., Dordrecht, The Netherlands.
- Ley, A.J. & Thomson, D.J. 1983 A random walk model of dispersion in the diabatic surface layer. *Q. J. R. Met. Soc.* **109**, 867-880.
- Lin, C.C. 1955 *The Theory of Hydrodynamic Stability*. Cambridge, The University Press.
- Longwell, P.A. 1966 *Mechanics of Fluid Flow*. McGraw-Hill Book Co., New York.
- Lu Pau-Chang 1979 *Fluid Mechanics, An Introductory Course*. The Iowa State University Press, Ames, Iowa.
- Luhar, A.K. & Britter, R.E. 1989: A random walk model for dispersion in inhomogeneous turbulence in a convective boundary layer. *Atmos. Environ.* **23**, 1911-1924.

- Lumley, J.L. & Panofsky, H.A. 1964 *The Structure of Atmospheric Turbulence*. Interscience Publ., New York.
- Massey, B.S. 1983 *Mechanics of Fluids*, 5th edition. van Nostrand Reinhold (UK) Co. Ltd. Berkshire, England.
- Millionshchikov M.D. 1939 Decay of homogeneous isotropic turbulence in viscous incompressible fluids. *Doklady AN SSSR*, **22**, 236-240.
- Mironer, A. 1979 *Engineering Fluid Mechanics*. McGraw-Hill Book Com., New York.
- Monin, A.S. & Yaglom, A.M. 1971 *Statistical Fluid Mechanics: Mechanics of Turbulence*, vol. I. MIT Press, Cambridge, Mass.
- Novikov, E.A. 1986 The Lagrangian-Eulerian probability relations and the random force method for nonhomogeneous turbulence. *Phys. Fluids* **29**, 3907-3909.
- Obukhov, A.M. 1954 Statistical description of continuous fields. *Trudy Geofiz. In-ta AN SSSR*, **151**, 3-42.
- Owczarek, J.A. 1968 *Introduction to Fluid Mechanics*. International Textbook Com., Scranton, Pennsylvania.
- Pao, R.H.F. 1966 *Fluid Dynamics*. Charles E. Merrill Books Inc., Columbus, Ohio.
- Pasquill, F. 1962 *Atmospheric Diffusion. A Study of the Dispersion of Windborne Material from Industrial and Other Sources*. D. van Nostrand Publ., London.
- Pope, S.B. 1979 The statistical theory of turbulent flames. *Phil. Trans. R. Soc. Lond.* **A291**, 529-568.
- Pope, S.B. 1983 Consistent modeling of scalars in turbulent flows. *Phys. Fluids* **26**, 404-408.
- Pope, S.B. 1987 Consistency conditions for random-walk models of turbulent dispersion. *Phys. Fluids* **30**, 2374-2379.
- Raupach, M.R. 1987 A Lagrangian analysis of scalar transfer in vegetation canopies. *Q. J. R. Met. Soc.* **113**, 107-120.
- Richardson, L.F. 1922 *Weather Prediction by Numerical Process*. Cambridge, The University Press.
- Richardson, S.M. 1989 *Fluid Mechanics*. Hemisphere Publ. Co., New York.
- Saffman, P.G. 1960 On the effect of the molecular diffusivity in turbulent diffusion. *J. Fluid Mech.* **8**, 273-283.
- Sawford, B.L. 1984 The basic for, and some limitations of, the Langevin equation in atmospheric relative dispersion modeling. *Atmos. Environ.* **18**, 2405-2411.

Sawford, B.L. 1986 Generalized random forcing in random-walk turbulent dispersion models. *Phys. Fluids* **29**, 3582-3585.

Sawford, B.L. & Hunt, J.C.R. 1986 Effects of turbulence structure, molecular diffusion and source size on scalar fluctuations in homogeneous turbulence. *J. Fluid Mech.* **165**, 373-400.

Stapountzis, H., Sawford, B.L., Hunt, J.C.R. and Britter, R.E. 1986 Structure of the temperature field downwind of a line source in grid turbulence. *J. Fluid Mech.* **165**, 401-424.

Taylor, G.I. 1921 Diffusion by continuous movements. *Proc. Lond. Math. Soc.* (2), **20**, 196-211.

Taylor, G.I. 1935 Statistical theory of turbulence, I-III. *Proc. Roy. Soc.* **a151**, 421-464.

Thomson, D.J. 1984 Random walk modeling of diffusion in inhomogeneous turbulence. *Q. J. R. Met. Soc.* **110**, 1107-1120.

Thomson, D.J. 1987 Criteria for the selection of stochastic models of particle trajectories in turbulent flows. *J. Fluid Mech.* **180**, 529-556.

Thomson, D.J. 1990 A stochastic model for the motion of particle pairs in isotropic high-Reynolds-number turbulence and its application to the problem of concentration variance. *J. Fluid Mech.* **210**, 113-153.

Townsend, A.A. 1956 *The Structure of Turbulent Shear Flow* Cambridge Univ. Press, Cambridge, England.

van Dop, H., Nieuwstadt, F.T.M. & Hunt, J.C.R. 1985 Random walk models for particle displacements in inhomogeneous unsteady turbulent flows. *Phys. Fluids* **28**, 1639-1653.

Wilson, J.D., Thurtell, G.W. & Kidd, G.E. 1981 Numerical simulation of particle trajectories in inhomogeneous turbulence, II: system with variable turbulent velocity scale. *Bound.-Layer Meteor.* **21**, 423-441.

Wilson, J.D., Legg, B.J. & Thomson, D.J. 1983 Calculation of particle trajectories in the presence of a gradient in turbulent velocity variance. *Bound.-Layer Meteor.* **27**, 163-169.

Part 2 (attached Y. Guo, 1991): The role of molecular mixing in the description of turbulent diffusion in fluid continuum. Part 2. The virtual fluid parcel treatment.

Part 2. The Virtual Fluid Parcel Treatment

Abstract

A new "virtual fluid parcel" treatment of the BMDFE (Basic Macroscopically Describable Fluid Element) in continuum framework is proposed to extend the classical fluid particle treatment. This new treatment conceptually incorporates molecular mixing between different BMDFEs by permitting disintegration of individual BMDFEs. It is found to simplify the description of the fluid dynamic variables in turbulent flows by not tracing the Lagrangian characteristics of the BMDFEs. It gives the description only in the Eulerian framework, so that additional concerns about the transformation between Lagrangian and Eulerian variables can be avoided.

The main improvement made by the virtual fluid parcel treatment in the description of turbulent diffusion lies in the introduction of a feedback mechanism in the form of physically coupled disintegration and integration of the BMDFEs. This improvement might reduce the potential mathematical-physical inconsistency in the understanding of turbulent diffusion in real turbulent fluids, when compared to the non-feedback mechanism of the statistical superimpositions under the classical random fluid particle treatment. It suggests that molecular mixing is a controlling agent of the mixing mechanism in every time-step of turbulent diffusion, whose significance could be cumulatively increased.

1. Introduction

As pointed out in the first part (Part 1), molecular mixing between macroscopic fluid elements has been conceptually excluded by the classical fluid particle treatment of the BMDFE (Basic Macroscopically Describable Fluid Element) in continuum framework. This may cause difficulties in the interpretation of turbulent diffusion mechanism in real turbulent fluids. The randomization of the fluid particle does not alleviate this fact because it does not change the nature of the postulated fluid particle moving as an entity. Instead, it leads to the statistical multi-to-one Lagrangian-Eulerian transformations, resulting in the non-feedback mechanism of statistical superimpositions in the description of turbulent diffusion. This non-feedback mechanism may be perceived as a potential mathematical-physical inconsistency in the understanding of turbulent diffusion.

In order to improve the situation, molecular mixing needs to be conceptually considered. The idea has been addressed by Chatwin and Sullivan (1979) and developed by Durbin (1980), who pointed out that "blobs", as the BMDFEs, undergo disintegration in turbulent flows through molecular mixing.

To account for details of molecular mixing we should, in principle, focus on individual molecules that exhibit Brownian motion relative to the fluid continuum, rather than on the BMDFEs (Sawford & Hunt 1986; Stapountzis et al. 1986; Kaplan & Dinar 1988). This approach, however, may go beyond continuum mechanics. Its success requires detailed specification and prescription of individual molecular behaviour, which may not generally be accessible under the present state of knowledge and technology.

In the interim, this study attempts to explore an alternative as an extension of the fluid particle treatment of the BMDFE. By developing Durbin's (1980) idea, a new "virtual fluid parcel" treatment of the BMDFE is proposed, which

conceptually incorporate molecular mixing between different BMDFEs. This new treatment is then applied to the description of turbulent diffusion problem. For reason of simplicity, and without jeopardizing general validity, the discussion is limited to incompressible fluids.

2. The virtual fluid parcel treatment

2.1. Concept

The classical fluid particle treatment defines the BMDFE subject to two assumed constraints: First, it is considered as a finite, macroscopically significant fluid element in which macroscopic physical properties (such as density, velocity, temperature etc.) can be reasonably defined and measured by averaging molecular properties within that element. Second, it is nevertheless regarded as a point-like "particle" of uniform state in space, relative to the macroscopic flow scale, moving as a whole in motion (Pao 7pp 1966; Owczarek 3pp 1968; Monin & Yaglom 528pp 1971; Lu 11pp 1979; Mironer 10pp 1979; Richardson 3-4pp 1989).

Except for some extreme situations, such as a gas at low pressure, where the intermolecular distances may be comparable to the characteristic dimensions of the problem, the first constraint should be acceptable for studies of macroscopic phenomena of fluid motion within continuum framework.

Before commenting on the second constraint, we may consider that a real fluid is a moving medium whose constituent molecules may continuously change their positions relative to one another (Batchelor 1967; Massey 1983). During motion, a real fluid cannot avoid mixing of molecules from one macroscopic fluid element to another. In turbulent flows, this molecular mixing could break the integrity of the BMDFE (Durbin 1980). Ultimately, the real mixing in turbulent fluids takes place through molecular mixing at fine scales, such as the conduction cut-off length scale

$(\kappa^3/\epsilon)^{1/4}$, irrespective of the macroscopic flow character (Chatwin, Sullivan & Yip 1990, Chatwin & Sullivan 1991). The latter is of the order of $10^{-4} - 10^{-3}$ m in most flows, where κ is the molecular scalar viscosity (or the molecular collision-transport coefficient for scalar) and ϵ is the dissipation rate of turbulent kinetic energy (Batchelor 1959; Batchelor, Howells & Townsend 1959).

When the process of molecular mixing has had a significant cumulative effect, it becomes meaningless to refer to the classical concept of the fluid particle (Chatwin & Sullivan 1979). Instead, any real BMDFE may physically exist or maintain its integrity only briefly before it is disintegrated in turbulent flows. We may refer to this more realistic BMDFE as the "virtual fluid parcel", to distinguish it from the classical "fluid particle". In fact, the new concept of the virtual fluid parcel extends the classical concept of the fluid particle by relaxing its second constraint to permit disintegration of the BMDFE. Therefore, the virtual fluid parcel is not distinguished from the classical fluid particle by its size, but by the fact that it is not necessarily perceived as moving as an entity. With this extension, molecular mixing between different BMDFEs in turbulent fluids can be naturally incorporated. A turbulent fluid under the continuum hypothesis may then be viewed as being continuously composed of virtual fluid parcels which are subject to potential disintegration at any time.

2.2. The description of the fluid dynamic variables

The virtual fluid parcel treatment can simplify the description of the fluid dynamic variables in turbulent flows in a way not permitted by the random fluid particle treatment, by giving the description only in the Eulerian framework. Because the virtual fluid parcel may not, in general, maintain integrity in turbulent flow, its

trajectory and Lagrangian variables of physical properties cannot be properly defined. Therefore, additional concerns about the transformation between the Lagrangian and Eulerian variables are eliminated.

Under the virtual fluid parcel treatment, any space point in a turbulent fluid can at any time be macroscopically considered as being occupied by only one virtual fluid parcel. Its composition, originating from different parts of the fluid, may sooner or later disintegrate. The (Eulerian) macroscopic physical properties at that point and at that time should be uniquely measurable by averaging the molecular properties within that virtual fluid parcel, which can be defined as follows:

Suppose that in the neighbourhood of an given space-time point (\mathbf{X}, t) of a turbulent fluid, an existing volume $d\tau$ contains a number N of molecules. Each molecule is located at position (\mathbf{X}_i, t) , with microscopic mass $m(\mathbf{X}_i, t)$, velocity $\mathbf{v}(\mathbf{X}_i, t)$ and mass-specific concentration $c(\mathbf{X}_i, t)$ of any other scalar. We can then always find a virtual fluid parcel, with volume $d\mathbf{X}$ and a number N_0 of molecules, whose center of gravity coincides with the spatial position \mathbf{X}

$$\mathbf{X} = \lim_{\substack{d\tau \rightarrow d\mathbf{x} \\ N \rightarrow N_0}} \frac{\sum_{i=1}^N m(\mathbf{X}_i, t) \cdot \mathbf{X}_i}{\sum_{i=1}^N m(\mathbf{X}_i, t)} \quad (2.1)$$

and whose mass $dM(\mathbf{X}, t)$, momentum $dM\mathbf{V}(\mathbf{X}, t)$, and amount of scalar $dA(\mathbf{X}, t)$ are

$$dM(\mathbf{X}, t) = \lim_{\substack{d\tau \rightarrow d\mathbf{x} \\ N \rightarrow N_0}} \sum_{i=1}^N m(\mathbf{X}_i, t) \quad (2.2)$$

$$d\mathbf{M}\mathbf{V}(\mathbf{x},t) = \lim_{\substack{d\tau \rightarrow 0 \\ N \rightarrow N_0}} \sum_{i=1}^N m(\mathbf{x}_i,t) \cdot \mathbf{v}(\mathbf{x}_i,t) \quad (2.3)$$

$$dA(\mathbf{x},t) = \lim_{\substack{d\tau \rightarrow 0 \\ N \rightarrow N_0}} \sum_{i=1}^N m(\mathbf{x}_i,t) \cdot c(\mathbf{x}_i,t) \quad (2.4)$$

Then, the (Eulerian) macroscopic mass density $\rho(\mathbf{x},t)$, velocity $\mathbf{V}(\mathbf{x},t)$ and mass-specific concentration $C(\mathbf{x},t)$ of any other scalar at the space-time point (\mathbf{x},t) can be defined as

$$\rho(\mathbf{x},t) = \lim_{\substack{d\tau \rightarrow 0 \\ N \rightarrow N_0}} \frac{dM(\mathbf{x},t)}{d\tau} = \lim_{\substack{d\tau \rightarrow 0 \\ N \rightarrow N_0}} \frac{\sum_{i=1}^N m(\mathbf{x}_i,t)}{d\tau} \quad (2.5)$$

$$\mathbf{V}(\mathbf{x},t) = \lim_{\substack{d\tau \rightarrow 0 \\ N \rightarrow N_0}} \frac{d\mathbf{M}\mathbf{V}(\mathbf{x},t)}{dM(\mathbf{x},t)} = \lim_{\substack{d\tau \rightarrow 0 \\ N \rightarrow N_0}} \frac{\sum_{i=1}^N m(\mathbf{x}_i,t) \cdot \mathbf{v}(\mathbf{x}_i,t)}{\sum_{i=1}^N m(\mathbf{x}_i,t)} \quad (2.6)$$

$$C(\mathbf{x},t) = \lim_{\substack{d\tau \rightarrow 0 \\ N \rightarrow N_0}} \frac{dA(\mathbf{x},t)}{dM(\mathbf{x},t)} = \lim_{\substack{d\tau \rightarrow 0 \\ N \rightarrow N_0}} \frac{\sum_{i=1}^N m(\mathbf{x}_i,t) \cdot c(\mathbf{x}_i,t)}{\sum_{i=1}^N m(\mathbf{x}_i,t)} \quad (2.7)$$

For incompressible fluids, the convenient volumetric concentration $\phi(\mathbf{x},t)$ of

momentum and volumetric concentration $\Psi(\mathbf{X},t)$ of scalar at point (\mathbf{X},t) are given by

$$\boldsymbol{\sigma}(\mathbf{X},t) = \rho(\mathbf{X},t) \cdot \mathbf{V}(\mathbf{X},t) = \lim_{\substack{d\tau \rightarrow d\mathbf{x} \\ N \rightarrow N_0}} \frac{\sum_{i=1}^N m(\mathbf{X}_i,t) \cdot \mathbf{v}(\mathbf{X}_i,t)}{d\tau} \quad (2.8)$$

$$\Psi(\mathbf{X},t) = \rho(\mathbf{X},t) \cdot C(\mathbf{X},t) = \lim_{\substack{d\tau \rightarrow d\mathbf{x} \\ N \rightarrow N_0}} \frac{\sum_{i=1}^N m(\mathbf{X}_i,t) \cdot c(\mathbf{X}_i,t)}{d\tau} \quad (2.9)$$

In the above definitions, the space-time point (\mathbf{X},t) is arbitrarily and continuously chosen in the fluid, so that any change of spatial position \mathbf{X} or time t could result in composition changes in $d\mathbf{X}$ and, consequently, change of the identity of the virtual fluid parcel. Therefore, the virtual fluid parcel treatment is truly compatible with the continuum hypothesis.

According to the above concept and definitions, the following three points need to be emphasized.

1). Earlier, Durbin's (1980) "outer limit" two-particle relative dispersion model may have implied an adaptation similar to the virtual fluid parcel treatment. By arguing that the small-scale structure of the scalar field is eliminated by molecular mixing between fluid elements with different concentrations, his model has already implicitly incorporated the effect of molecular mixing. In this sense, his fluid particle concept has already differed from

the classical one. The virtual fluid parcel treatment presented here may be considered as a development of his idea, but more direct in incorporation of molecular mixing.

2). The virtual fluid parcel treatment incorporates molecular mixing into the definitions of the macroscopic physical properties without necessarily considering the details of how the molecular mixing occurs. In each small time interval we could, in principle, prescribe the motion of a single molecule as the sum of a macroscopic component (the motion of the center-of-mass of the virtual fluid parcel containing the molecule at that time) and a Brownian component (similar to that used by Sawford & Hunt 1986, and Kaplan & Dinar 1988). However, doing so would expect difficulties in practice, as mentioned in the Introduction. In any case, when individual molecules with detailed prescriptions are used to calculate macroscopic physical properties in continuum framework, an averaging process (such as that used by Sawford & Hunt 1986) is required. This averaging should have a proper macroscopic scale resolution matching the fluid continuum in order to make the macroscopic physical properties meaningful. The virtual fluid parcel treatment provides a theoretical base for such averaging. Beyond the continuum framework, however, only the description of individual molecules is capable of gaining insight into the details of molecular mixing. It is not our concern at this stage of the study.

3). The local Eulerian fluid velocity at a space-time point (\mathbf{X}, t) in a turbulent flow should be measured as macroscopic momentum by averaging the molecular momentum within the fluid element at (\mathbf{X}, t) . However, due to molecular mixing, all the molecules in the fluid element at (\mathbf{X}, t) in a real turbulent fluid are not guaranteed to originate from the same group in the previous time interval and subsequently to move as an entity to another spatial point during the next time

interval. Therefore, strictly speaking, fluid elements assumed to move at the local Eulerian fluid velocity (such as Thomson 1990) in turbulent flow can only be regarded as virtual fluid parcels. The assumption that classical fluid particles move at the local Eulerian velocity may be inappropriate. In the previous study (Part 1), it has been shown that under the random fluid particle treatment the assumption of statistical equivalence between the Lagrangian variables of a single fluid particle and the Eulerian variables at one space-time point is not generally satisfied.

3. The mixing processes

The virtual fluid parcel treatment can naturally access to the description of molecular mixing in a way not accessible to the random fluid particle treatment. In their life cycles, the virtual fluid parcels undergo two mixing processes: One is disintegration through which they are fragmented, and the other is integration through which the disintegrated fragments come together to form "new" virtual fluid parcels, whose integrities will again be broken in subsequent disintegration.

3.1. Disintegration

For the given times t and $t+\Delta t$, where Δt is a small time interval, we can arbitrarily choose two virtual fluid parcels, located at (\mathbf{X},t) with volume $d\mathbf{X}$ and at $(\mathbf{Y},t+\Delta t)$ with volume $d\mathbf{Y}$, respectively. During Δt , the disintegration of parcel (\mathbf{X},t) may occur in such a way that each molecule with its mass $m(\mathbf{X}_i,t)$ in parcel (\mathbf{X},t) has a potential to mix into parcel $(\mathbf{Y},t+\Delta t)$, with a mass contribution $m(\mathbf{Y}_i,t+\Delta t; \mathbf{X}_i,t)$

$$m(\mathbf{Y}_i,t+\Delta t; \mathbf{X}_i,t) = m(\mathbf{X}_i,t) \cdot r(\mathbf{Y}_i,t+\Delta t | \mathbf{X}_i,t) \quad (3.1)$$

Here $r(Y_i, t+\Delta t | X_i, t)$ is the molecular mixing coefficient for a single molecule, which is defined as $r = 1$ if this molecule in parcel (X, t) mixes into parcel $(Y, t+\Delta t)$ in Δt , and $r = 0$ if it does not.

The fractional contribution $dM(Y, t+\Delta t; X, t)$ to mass of parcel $(Y, t+\Delta t)$ by disintegration of parcel (X, t) is then

$$dM(Y, t+\Delta t; X, t) = \sum_{i=1}^{N_0} m(X_i, t) \cdot r(Y_i, t+\Delta t | X_i, t) \quad (3.2)$$

where N_0 is the number of molecules in parcel (X, t) .

Considering (2.2), (3.2) can be written as

$$dM(Y, t+\Delta t; X, t) = dM(X, t) \cdot R_M(Y, t+\Delta t | X, t) \quad (3.3a)$$

with R_M defined as

$$R_M(Y, t+\Delta t | X, t) = \frac{\sum_{i=1}^{N_0} m(X_i, t) \cdot r(Y_i, t+\Delta t | X_i, t)}{\sum_{i=1}^{N_0} m(X_i, t)} \quad (3.3b)$$

$R_M(Y, t+\Delta t | X, t)$ represents the portion of mass disintegrated from parcel (X, t) and then mixed into parcel $(Y, t+\Delta t)$ in Δt . It can be defined as the fractional redistribution coefficient for mass disintegrated from parcel (X, t) and then mixed into parcel $(Y, t+\Delta t)$.

Dividing both sides of (3.3a) by dX and dY , multiplying both sides by dX and

considering (2.5), we have

$$\tilde{\rho}(\mathbf{Y}, t + \Delta t; \mathbf{X}, t) \cdot d\mathbf{X} = \rho(\mathbf{X}, t) \cdot F_M(\mathbf{Y}, t + \Delta t | \mathbf{X}, t) \cdot d\mathbf{X} \quad (3.4a)$$

with $\tilde{\rho}$ defined as

$$\tilde{\rho}(\mathbf{Y}, t + \Delta t; \mathbf{X}, t) = \frac{dM(\mathbf{Y}, t + \Delta t; \mathbf{X}, t)}{d\mathbf{X} \cdot d\mathbf{Y}} \quad (3.4b)$$

and F_M defined as

$$F_M(\mathbf{Y}, t + \Delta t | \mathbf{X}, t) = \frac{R_M(\mathbf{Y}, t + \Delta t | \mathbf{X}, t)}{d\mathbf{Y}} \quad (3.4c)$$

Here $\rho(\mathbf{X}, t)$ is the (Eulerian) mass density at (\mathbf{X}, t) . $\tilde{\rho}(\mathbf{Y}, t + \Delta t; \mathbf{X}, t)$ is the fractional contribution to the mass density of parcel $(\mathbf{Y}, t + \Delta t)$ from the unit volume of parcel (\mathbf{X}, t) . $F_M(\mathbf{Y}, t + \Delta t | \mathbf{X}, t)$ is the fractional redistribution density coefficient for mass disintegrated from parcel (\mathbf{X}, t) and then mixed into the unit volume of parcel $(\mathbf{Y}, t + \Delta t)$, which represents the portion of mass disintegrated from parcel (\mathbf{X}, t) and then mixed into the unit volume of parcel $(\mathbf{Y}, t + \Delta t)$ in Δt .

Similarly, the fractional contribution $dMV(\mathbf{Y}, t + \Delta t; \mathbf{X}, t)$ to momentum of parcel $(\mathbf{Y}, t + \Delta t)$ by disintegration of parcel (\mathbf{X}, t) would be

$$\begin{aligned} dMV(\mathbf{Y}, t + \Delta t; \mathbf{X}, t) &= \sum_{i=1}^{N_0} m(\mathbf{X}_i, t) \cdot \mathbf{v}(\mathbf{Y}_i, t + \Delta t; \mathbf{X}_i, t) \cdot \Gamma(\mathbf{Y}_i, t + \Delta t | \mathbf{X}_i, t) \\ &= dMV(\mathbf{X}, t) \cdot R_V(\mathbf{Y}, t + \Delta t | \mathbf{X}, t) \end{aligned} \quad (3.5a)$$

with $R_{\mathbf{v}}$ defined as

$$R_{\mathbf{v}}(\mathbf{Y}, t + \Delta t | \mathbf{X}, t) = \frac{\sum_{i=1}^{N_0} m(\mathbf{X}_i, t) \cdot \mathbf{v}(\mathbf{Y}_i, t + \Delta t; \mathbf{X}_i, t) \cdot \Gamma(\mathbf{Y}_i, t + \Delta t | \mathbf{X}_i, t)}{\sum_{i=1}^{N_0} m(\mathbf{X}_i, t) \cdot \mathbf{v}(\mathbf{X}_i, t)} \quad (3.5b)$$

Here $\mathbf{v}(\mathbf{Y}_i, t + \Delta t; \mathbf{X}_i, t)$ is the velocity of a molecule found in parcel $(\mathbf{Y}, t + \Delta t)$ which comes from parcel (\mathbf{X}, t) (considering the molecular collision-transport, $\mathbf{v}(\mathbf{Y}_i, t + \Delta t; \mathbf{X}_i, t)$ may be different from its previous value $\mathbf{v}(\mathbf{X}_i, t)$ in parcel (\mathbf{X}, t)). $R_{\mathbf{v}}(\mathbf{Y}, t + \Delta t | \mathbf{X}, t)$ is the fractional redistribution coefficient for momentum disintegrated from parcel (\mathbf{X}, t) and then mixed into parcel $(\mathbf{Y}, t + \Delta t)$.

Multiplying both sides of (3.5a) by $\frac{d\mathbf{X}}{d\mathbf{X} \cdot d\mathbf{Y}}$ and considering (2.8), we have

$$\tilde{\vartheta}(\mathbf{Y}, t + \Delta t; \mathbf{X}, t) \cdot d\mathbf{X} = \vartheta(\mathbf{X}, t) \cdot F_{\mathbf{v}}(\mathbf{Y}, t + \Delta t | \mathbf{X}, t) \cdot d\mathbf{X} \quad (3.6a)$$

with $\tilde{\vartheta}$ defined as

$$\tilde{\vartheta}(\mathbf{Y}, t + \Delta t; \mathbf{X}, t) = \frac{dM\mathbf{V}(\mathbf{Y}, t + \Delta t; \mathbf{X}, t)}{d\mathbf{X} \cdot d\mathbf{Y}} \quad (3.6b)$$

and $F_{\mathbf{v}}$ defined as

$$F_{\mathbf{v}}(\mathbf{Y}, t + \Delta t | \mathbf{X}, t) = \frac{R_{\mathbf{v}}(\mathbf{Y}, t + \Delta t | \mathbf{X}, t)}{d\mathbf{Y}} \quad (3.6c)$$

Here $\bar{\rho}(\mathbf{X},t)$ is the (Eulerian) volumetric concentration of momentum at (\mathbf{X},t) . $\bar{\rho}(\mathbf{Y},t+\Delta t; \mathbf{X},t)$ is the fractional contribution to the volumetric concentration of momentum of parcel $(\mathbf{Y},t+\Delta t)$ from the unit volume of parcel (\mathbf{X},t) . $F_{\mathbf{V}}(\mathbf{Y},t+\Delta t | \mathbf{X},t)$ is the fractional redistribution density coefficient for momentum disintegrated from parcel (\mathbf{X},t) and then mixed into the unit volume of parcel $(\mathbf{Y},t+\Delta t)$.

For any other scalar, the fractional contribution $dA(\mathbf{Y},t+\Delta t; \mathbf{X},t)$ to scalar of parcel $(\mathbf{Y},t+\Delta t)$ by disintegration of parcel (\mathbf{X},t) would be

$$\begin{aligned} dA(\mathbf{Y},t+\Delta t; \mathbf{X},t) &= \sum_{i=1}^{N_0} m(\mathbf{X}_i,t) \cdot c(\mathbf{Y}_i,t+\Delta t; \mathbf{X}_i,t) \cdot r(\mathbf{Y}_i,t+\Delta t | \mathbf{X}_i,t) \\ &= dA(\mathbf{X},t) \cdot R_C(\mathbf{Y},t+\Delta t | \mathbf{X},t) \end{aligned} \quad (3.7a)$$

with R_C defined as

$$R_C(\mathbf{Y},t+\Delta t | \mathbf{X},t) = \frac{\sum_{i=1}^{N_0} m(\mathbf{X}_i,t) \cdot c(\mathbf{Y}_i,t+\Delta t; \mathbf{X}_i,t) \cdot r(\mathbf{Y}_i,t+\Delta t | \mathbf{X}_i,t)}{\sum_{i=1}^{N_0} m(\mathbf{X}_i,t) \cdot c(\mathbf{X}_i,t)} \quad (3.7b)$$

Here $c(\mathbf{Y}_i,t+\Delta t; \mathbf{X}_i,t)$ is the mass-specific concentration of scalar of a molecule found in parcel $(\mathbf{Y},t+\Delta t)$ which comes from parcel (\mathbf{X},t) (considering the molecular collision-transport, $c(\mathbf{Y}_i,t+\Delta t; \mathbf{X}_i,t)$ may be different from its previous value $c(\mathbf{X}_i,t)$ in parcel (\mathbf{X},t)). $R_C(\mathbf{Y},t+\Delta t | \mathbf{X},t)$ is the fractional redistribution coefficient for scalar disintegrated from parcel (\mathbf{X},t) and then mixed into parcel $(\mathbf{Y},t+\Delta t)$.

Multiplying both sides of (3.7a) by $\frac{d\mathbf{X}}{d\mathbf{X} \cdot d\mathbf{Y}}$ and considering (2.9), we have

$$\tilde{\Psi}(\mathbf{Y}, t+\Delta t; \mathbf{X}, t) \cdot d\mathbf{X} = \Psi(\mathbf{X}, t) \cdot F_{\mathbf{C}}(\mathbf{Y}, t+\Delta t | \mathbf{X}, t) \cdot d\mathbf{X} \quad (3.8a)$$

with $\tilde{\Psi}$ defined as

$$\tilde{\Psi}(\mathbf{Y}, t+\Delta t; \mathbf{X}, t) = \frac{dA(\mathbf{Y}, t+\Delta t; \mathbf{X}, t)}{d\mathbf{X} \cdot d\mathbf{Y}} \quad (3.8b)$$

and $F_{\mathbf{C}}$ defined as

$$F_{\mathbf{C}}(\mathbf{Y}, t+\Delta t | \mathbf{X}, t) = \frac{R_{\mathbf{C}}(\mathbf{Y}, t+\Delta t | \mathbf{X}, t)}{d\mathbf{Y}} \quad (3.8c)$$

Here $\Psi(\mathbf{X}, t)$ is the (Eulerian) volumetric concentration of scalar at (\mathbf{X}, t) . $\tilde{\Psi}(\mathbf{Y}, t+\Delta t; \mathbf{X}, t)$ is the fractional contribution to the volumetric concentration of scalar of parcel $(\mathbf{Y}, t+\Delta t)$ from the unit volume of parcel (\mathbf{X}, t) . $F_{\mathbf{C}}(\mathbf{Y}, t+\Delta t | \mathbf{X}, t)$ is the fractional redistribution density coefficient for scalar disintegrated from parcel (\mathbf{X}, t) and then mixed into the unit volume of parcel $(\mathbf{Y}, t+\Delta t)$.

Generally, there may exist, at (\mathbf{X}, t) , external sources for momentum and scalar, with volumetric source strengths $\mathbf{H}(\mathbf{X}, t)$ and $E(\mathbf{X}, t)$, respectively. Thus the general forms of (3.6a) and (3.8a) should become

$$\tilde{\boldsymbol{\sigma}}(\mathbf{Y}, t+\Delta t; \mathbf{X}, t) \cdot d\mathbf{X} = (\boldsymbol{\sigma}(\mathbf{X}, t) + \mathbf{H}(\mathbf{X}, t) \cdot \Delta t) \cdot F_{\mathbf{V}}(\mathbf{Y}, t+\Delta t | \mathbf{X}, t) \cdot d\mathbf{X} \quad (3.9)$$

$$\tilde{\Psi}(\mathbf{Y}, t+\Delta t; \mathbf{X}, t) \cdot d\mathbf{X} = (\Psi(\mathbf{X}, t) + E(\mathbf{X}, t) \cdot \Delta t) \cdot F_{\mathbf{C}}(\mathbf{Y}, t+\Delta t | \mathbf{X}, t) \cdot d\mathbf{X} \quad (3.10)$$

If mass, momentum and scalar are conservative during disintegration, the following constraints must be satisfied

$$\int F_M(\mathbf{Y}, t + \Delta t | \mathbf{X}, t) \cdot d\mathbf{Y} = 1 \quad (3.11)$$

$$\int F_V(\mathbf{Y}, t + \Delta t | \mathbf{X}, t) \cdot d\mathbf{Y} = 1 \quad (3.12)$$

$$\int F_C(\mathbf{Y}, t + \Delta t | \mathbf{X}, t) \cdot d\mathbf{Y} = 1 \quad (3.13)$$

3.2. Integration

In each time interval Δt , the virtual fluid parcel at every point (\mathbf{X}, t) in a turbulent fluid can be regarded as a potential source of disintegration which redistributes its disintegrated fragments $\tilde{\rho}(\mathbf{Y}, t + \Delta t; \mathbf{X}, t) \cdot d\mathbf{X}$, $\tilde{\boldsymbol{\sigma}}(\mathbf{Y}, t + \Delta t; \mathbf{X}, t) \cdot d\mathbf{X}$ and $\tilde{\Psi}(\mathbf{Y}, t + \Delta t; \mathbf{X}, t) \cdot d\mathbf{X}$ to the parcel at $(\mathbf{Y}, t + \Delta t)$. Therefore, at the end of the time interval, the (Eulerian) mass density $\rho(\mathbf{Y}, t + \Delta t)$, volumetric concentration of momentum $\boldsymbol{\sigma}(\mathbf{Y}, t + \Delta t)$ and volumetric concentration of scalar $\Psi(\mathbf{Y}, t + \Delta t)$ in the "new" virtual fluid parcel at $(\mathbf{Y}, t + \Delta t)$ would be constituted of the disintegrated fragments from all the "old" virtual fluid parcels in the turbulent fluid. They are expressed as the integration of (3.4a), (3.9) and (3.10), respectively, over the space of the flow

$$\begin{aligned} \rho(\mathbf{Y}, t + \Delta t) &= \int \tilde{\rho}(\mathbf{Y}, t + \Delta t; \mathbf{X}, t) \cdot d\mathbf{X} \\ &= \int \rho(\mathbf{X}, t) \cdot F_M(\mathbf{Y}, t + \Delta t | \mathbf{X}, t) \cdot d\mathbf{X} \end{aligned} \quad (3.14)$$

$$\begin{aligned} \boldsymbol{\sigma}(\mathbf{Y}, t + \Delta t) &= \int \tilde{\boldsymbol{\sigma}}(\mathbf{Y}, t + \Delta t; \mathbf{X}, t) \cdot d\mathbf{X} \\ &= \int (\boldsymbol{\sigma}(\mathbf{X}, t) + \mathbf{H}(\mathbf{X}, t) \cdot \Delta t) \cdot F_V(\mathbf{Y}, t + \Delta t | \mathbf{X}, t) \cdot d\mathbf{X} \end{aligned} \quad (3.15)$$

$$\begin{aligned}\Psi(\mathbf{Y}, t+\Delta t) &= \int \tilde{\Psi}(\mathbf{Y}, t+\Delta t; \mathbf{X}, t) \cdot d\mathbf{X} \\ &= \int (\Psi(\mathbf{X}, t) + \mathbf{E}(\mathbf{X}, t) \cdot \Delta t) \cdot F_{\mathbf{C}}(\mathbf{Y}, t+\Delta t | \mathbf{X}, t) \cdot d\mathbf{X}\end{aligned}\quad (3.16)$$

The results of the above integration then become the new sources for the next disintegration described again by (3.4a), (3.9) and (3.10) in the next time interval.

4. The description of turbulent diffusion

Under the virtual fluid parcel treatment, (3.14), (3.15) and (3.16) define the basic problem of turbulent diffusion as finding the fractional redistribution density coefficients $F_{\mathbf{M}}$, $F_{\mathbf{V}}$ and $F_{\mathbf{C}}$, or the fractional contributions $\tilde{\rho}$, $\tilde{\boldsymbol{\theta}}$ and $\tilde{\Psi}$, from the "old" virtual fluid parcels in space (\mathbf{X}, t) to the "new" virtual fluid parcels in space $(\mathbf{Y}, t+\Delta t)$ in each time interval Δt .

4.1. Approximations of $F_{\mathbf{M}}$, $F_{\mathbf{V}}$ and $F_{\mathbf{C}}$, or $\tilde{\rho}$, $\tilde{\boldsymbol{\theta}}$ and $\tilde{\Psi}$

If the time interval Δt is sufficiently small for the virtual fluid parcel at (\mathbf{X}, t) to be still recognized by its center of gravity in Δt , it may be acceptable, as an approximation, to assume that the virtual fluid parcel moves as a whole during Δt , with its possible disintegration taking place at the end of the time interval. In this case, the virtual fluid parcel at (\mathbf{X}, t) can be temporarily treated as a "pseudo-fluid-particle" during Δt , with its mass, momentum and any other scalar, including the parts coming from external source, regarded as an instantaneous point source. Its fractional contributions to the (Eulerian) mass density, volumetric concentrations of momentum and scalar at $(\mathbf{Y}, t+\Delta t)$ during Δt may then be approximated in the following:

According to our previous study (Part 1), the conservation equations for the mass, momentum and any other scalar of such "pseudo-fluid-particle" can be

expressed as

$$\begin{aligned} \frac{\partial}{\partial s} \bar{\rho}(\mathbf{Y}, t+s; \mathbf{X}, t) + (\bar{\mathbf{V}}(\mathbf{Y}, t+s; \mathbf{X}, t) \cdot \nabla_{\mathbf{y}}) \cdot \bar{\rho}(\mathbf{Y}, t+s; \mathbf{X}, t) \\ = - \overline{(\mathbf{V}'(\mathbf{Y}, t+s; \mathbf{X}, t) \cdot \nabla_{\mathbf{y}}) \cdot \rho'(\mathbf{Y}, t+s; \mathbf{X}, t)} + \rho(\mathbf{X}, t) \cdot \delta(\mathbf{Y}-\mathbf{X}) \cdot \delta(s) \end{aligned} \quad (4.1)$$

$$\begin{aligned} \frac{\partial}{\partial s} \bar{\vartheta}(\mathbf{Y}, t+s; \mathbf{X}, t) + (\bar{\mathbf{V}}(\mathbf{Y}, t+s; \mathbf{X}, t) \cdot \nabla_{\mathbf{y}}) \cdot \bar{\vartheta}(\mathbf{Y}, t+s; \mathbf{X}, t) \\ = \nu \cdot \nabla_{\mathbf{y}}^2 \cdot \bar{\vartheta}(\mathbf{Y}, t+s; \mathbf{X}, t) - \overline{(\mathbf{V}'(\mathbf{Y}, t+s; \mathbf{X}, t) \cdot \nabla_{\mathbf{y}}) \cdot \vartheta'(\mathbf{Y}, t+s; \mathbf{X}, t)} \\ + (\bar{\vartheta}(\mathbf{X}, t) + \mathbf{H}(\mathbf{X}, t) \cdot \Delta t) \cdot \delta(\mathbf{Y}-\mathbf{X}) \cdot \delta(s) \end{aligned} \quad (4.2)$$

$$\begin{aligned} \frac{\partial}{\partial s} \bar{\Psi}(\mathbf{Y}, t+s; \mathbf{X}, t) + (\bar{\mathbf{V}}(\mathbf{Y}, t+s; \mathbf{X}, t) \cdot \nabla_{\mathbf{y}}) \cdot \bar{\Psi}(\mathbf{Y}, t+s; \mathbf{X}, t) \\ = \kappa \cdot \nabla_{\mathbf{y}}^2 \cdot \bar{\Psi}(\mathbf{Y}, t+s; \mathbf{X}, t) - \overline{(\mathbf{V}'(\mathbf{Y}, t+s; \mathbf{X}, t) \cdot \nabla_{\mathbf{y}}) \cdot \Psi'(\mathbf{Y}, t+s; \mathbf{X}, t)} \\ + (\bar{\Psi}(\mathbf{X}, t) + \mathbf{E}(\mathbf{X}, t) \cdot \Delta t) \cdot \delta(\mathbf{Y}-\mathbf{X}) \cdot \delta(s) \end{aligned} \quad (4.3)$$

$$(0 \leq s \leq \Delta t)$$

Here the original subscript L, indicating the Lagrangian properties, is omitted in order to distinguish the present, assumed "pseudo-Lagrangian" approximations from the original, true Lagrangian descriptions. The statistical mean contributions are defined as

$$\begin{aligned} \bar{\rho}(\mathbf{Y}, t+s; \mathbf{X}, t) &= \int \rho(\mathbf{Y}, t+s; \mathbf{X}, t) \cdot \mathbf{P}(\rho, \mathbf{Y}, t+s | \mathbf{X}, t) \cdot d\rho \\ &= \left(\int \rho(\mathbf{Y}, t+s; \mathbf{X}, t) \cdot \mathbf{P}(\rho | \mathbf{Y}, t+s; \mathbf{X}, t) \cdot d\rho \right) \cdot \mathbf{P}(\mathbf{Y}, t+s | \mathbf{X}, t) \end{aligned} \quad (4.4)$$

$$\begin{aligned}\bar{\boldsymbol{\theta}}(\mathbf{Y}, t+s; \mathbf{X}, t) &= \int \boldsymbol{\theta}(\mathbf{Y}, t+s; \mathbf{X}, t) \cdot P(\boldsymbol{\theta}, \mathbf{Y}, t+s | \mathbf{X}, t) \cdot d\boldsymbol{\theta} \\ &= \left(\int \boldsymbol{\theta}(\mathbf{Y}, t+s; \mathbf{X}, t) \cdot P(\boldsymbol{\theta} | \mathbf{Y}, t+s; \mathbf{X}, t) \cdot d\boldsymbol{\theta} \right) \cdot P(\mathbf{Y}, t+s | \mathbf{X}, t)\end{aligned}\quad (4.5)$$

$$\begin{aligned}\bar{\Psi}(\mathbf{Y}, t+s; \mathbf{X}, t) &= \int \Psi(\mathbf{Y}, t+s; \mathbf{X}, t) \cdot P(\Psi, \mathbf{Y}, t+s | \mathbf{X}, t) \cdot d\Psi \\ &= \left(\int \Psi(\mathbf{Y}, t+s; \mathbf{X}, t) \cdot P(\Psi | \mathbf{Y}, t+s; \mathbf{X}, t) \cdot d\Psi \right) \cdot P(\mathbf{Y}, t+s | \mathbf{X}, t)\end{aligned}\quad (4.6)$$

$$(0 \leq s \leq \Delta t)$$

Terms in the above equations are defined as following: $\mathbf{V}(\mathbf{Y}, t+s; \mathbf{X}, t) = \boldsymbol{\theta}(\mathbf{Y}, t+s; \mathbf{X}, t) / \rho(\mathbf{Y}, t+s; \mathbf{X}, t)$ is the pseudo-Lagrangian velocity of the pseudo-fluid-particle arriving at $(\mathbf{Y}, t+s)$ from (\mathbf{X}, t) . $\rho(\mathbf{Y}, t+s; \mathbf{X}, t)$, $\boldsymbol{\theta}(\mathbf{Y}, t+s; \mathbf{X}, t)$, $\Psi(\mathbf{Y}, t+s; \mathbf{X}, t)$ are the pseudo-Lagrangian mass density, volumetric concentrations of momentum and scalar of the pseudo-fluid-particle arriving at $(\mathbf{Y}, t+s)$ from (\mathbf{X}, t) , respectively. $\bar{\rho}(\mathbf{Y}, t+s; \mathbf{X}, t)$, $\bar{\boldsymbol{\theta}}(\mathbf{Y}, t+s; \mathbf{X}, t)$, $\bar{\Psi}(\mathbf{Y}, t+s; \mathbf{X}, t)$ are the ensemble mean contributions to the (Eulerian) mass density, volumetric concentrations of momentum and scalar at $(\mathbf{Y}, t+s)$ by the unit volume pseudo-fluid-particle from (\mathbf{X}, t) , respectively. $\rho'(\mathbf{Y}, t+s; \mathbf{X}, t)$, $\boldsymbol{\theta}'(\mathbf{Y}, t+s; \mathbf{X}, t)$, and $\Psi'(\mathbf{Y}, t+s; \mathbf{X}, t)$ are the deviations from $\bar{\rho}$, $\bar{\boldsymbol{\theta}}$, $\bar{\Psi}$, respectively. $P(\rho, \mathbf{Y}, t+s | \mathbf{X}, t)$, $P(\boldsymbol{\theta}, \mathbf{Y}, t+s | \mathbf{X}, t)$ and $P(\Psi, \mathbf{Y}, t+s | \mathbf{X}, t)$ are the joint probability densities for the unit volume pseudo-fluid-particle from (\mathbf{X}, t) to appear at position \mathbf{Y} at time $t+s$, and to have unit mass density, unit volumetric concentration of momentum and unit volumetric concentration of scalar, respectively. $P(\rho | \mathbf{Y}, t+s; \mathbf{X}, t)$, $P(\boldsymbol{\theta} | \mathbf{Y}, t+s; \mathbf{X}, t)$ and $P(\Psi | \mathbf{Y}, t+s; \mathbf{X}, t)$ are the conditional probability densities for the pseudo-fluid-particle from (\mathbf{X}, t) to have unit mass density, unit volumetric concentration of momentum and unit volumetric concentration of scalar when it appears at position \mathbf{Y} at time $t+s$, respectively.

$P(\mathbf{Y}, t+s | \mathbf{X}, t)$ is the probability density for the unit volume pseudo-fluid-particle from (\mathbf{X}, t) to appear at position \mathbf{Y} at time $t+s$. ν and κ are the molecular kinematic and scalar viscosities (or the molecular collision-transport coefficients for momentum and scalar), respectively. $\nabla_{\mathbf{y}}$ and $\nabla_{\mathbf{y}}^2$ are del and Laplace operators with respect to \mathbf{Y} , and δ is the Dirac delta function.

With solutions from (4.1), (4.2) and (4.3) at the end of the time interval Δt , the fractional redistribution density coefficients F_M , F_V and F_C could be approximately estimated by the following ratios:

$$F_M(\mathbf{Y}, t+\Delta t | \mathbf{X}, t) \approx \frac{\bar{\rho}(\mathbf{Y}, t+\Delta t; \mathbf{X}, t)}{\rho(\mathbf{X}, t)} \quad (4.7)$$

$$F_V(\mathbf{Y}, t+\Delta t | \mathbf{X}, t) \approx \frac{\bar{\theta}(\mathbf{Y}, t+\Delta t; \mathbf{X}, t)}{(\theta(\mathbf{X}, t) + \mathbf{H}(\mathbf{X}, t) \cdot \Delta t)} \quad (4.8)$$

$$F_C(\mathbf{Y}, t+\Delta t | \mathbf{X}, t) \approx \frac{\bar{\Psi}(\mathbf{Y}, t+\Delta t; \mathbf{X}, t)}{(\Psi(\mathbf{X}, t) + \mathbf{E}(\mathbf{X}, t) \cdot \Delta t)} \quad (4.9)$$

Comparing (4.7) with (3.4a), (4.8) with (3.9), (4.9) with (3.10), we have

$$\tilde{\rho}(\mathbf{Y}, t+\Delta t; \mathbf{X}, t) \approx \bar{\rho}(\mathbf{Y}, t+\Delta t; \mathbf{X}, t) \quad (4.10)$$

$$\tilde{\theta}(\mathbf{Y}, t+\Delta t; \mathbf{X}, t) \approx \bar{\theta}(\mathbf{Y}, t+\Delta t; \mathbf{X}, t) \quad (4.11)$$

$$\tilde{\Psi}(\mathbf{Y}, t+\Delta t; \mathbf{X}, t) \approx \bar{\Psi}(\mathbf{Y}, t+\Delta t; \mathbf{X}, t) \quad (4.12)$$

Strictly speaking, the above estimations of F_M , F_V and F_C , or $\tilde{\rho}$, $\tilde{\theta}$ and $\tilde{\Psi}$,

should approach their exact values only for the vanishing time interval Δt when the assumed pseudo-Lagrangian statistics may not significantly differ from the local Eulerian statistics. In practice, however, these estimations may be justified when Δt is comparable to the minimum period of the significant fluctuations of $\rho(\mathbf{x},t)$, $\vartheta(\mathbf{x},t)$ and $\Psi(\mathbf{x},t)$.

In order to solve equations (4.1), (4.2) and (4.3), some local Eulerian statistics and the molecular collision-transport properties (such as ν and κ) must be specified. The values of ν and κ may have to be specified because, if a virtual fluid parcel at any time is regarded as a small point source, the effect of ν and κ should be considered for small time intervals Δt according to Saffman (1960).

Generally, the solutions of (4.1), (4.2) and (4.3) may involve technical difficulties in the nonlinearity of equations and the parameterization of the flow character with macroscopic inhomogeneity of both flow scale and turbulence intensity in complex systems. Solutions of these difficulties are not pursued at this stage of the study. However, according to the above approximations, the fractional redistribution density coefficients F_M , F_V and F_C , or the fractional contributions $\tilde{\rho}$, $\tilde{\vartheta}$ and $\tilde{\Psi}$ should be, in general, solved as functions of flow scale, turbulence intensity and distributions of physical properties, with their dependence on the molecular collision-transport properties.

4.2. The turbulent diffusion mechanism

In summary, turbulent diffusion under the virtual fluid parcel treatment is formulated in the following recurring joint equations:

$$\begin{aligned}
& \frac{\partial}{\partial s} \bar{\rho}(\mathbf{Y}, t_i + s; \mathbf{X}, t_i) + (\bar{\mathbf{V}}(\mathbf{Y}, t_i + s; \mathbf{X}, t_i) \cdot \nabla_{\mathbf{y}}) \cdot \bar{\rho}(\mathbf{Y}, t_i + s; \mathbf{X}, t_i) \\
& = - \overline{(\mathbf{V}'(\mathbf{Y}, t_i + s; \mathbf{X}, t_i) \cdot \nabla_{\mathbf{y}}) \cdot \rho'(\mathbf{Y}, t_i + s; \mathbf{X}, t_i)} + \rho(\mathbf{X}, t_i) \cdot \delta(\mathbf{Y} - \mathbf{X}) \cdot \delta(s)
\end{aligned} \tag{4.13}$$

$$\begin{aligned}
& \frac{\partial}{\partial s} \bar{\vartheta}(\mathbf{Y}, t_i + s; \mathbf{X}, t_i) + (\bar{\mathbf{V}}(\mathbf{Y}, t_i + s; \mathbf{X}, t_i) \cdot \nabla_{\mathbf{y}}) \cdot \bar{\vartheta}(\mathbf{Y}, t_i + s; \mathbf{X}, t_i) \\
& = \nu \cdot \nabla_{\mathbf{y}}^2 \cdot \bar{\vartheta}(\mathbf{Y}, t_i + s; \mathbf{X}, t_i) - \overline{(\mathbf{V}'(\mathbf{Y}, t_i + s; \mathbf{X}, t_i) \cdot \nabla_{\mathbf{y}}) \cdot \vartheta'(\mathbf{Y}, t_i + s; \mathbf{X}, t_i)} \\
& \quad + (\bar{\vartheta}(\mathbf{X}, t_i) + \mathbf{H}(\mathbf{X}, t_i) \cdot \Delta t) \cdot \delta(\mathbf{Y} - \mathbf{X}) \cdot \delta(s)
\end{aligned} \tag{4.14}$$

$$\begin{aligned}
& \frac{\partial}{\partial s} \bar{\Psi}(\mathbf{Y}, t_i + s; \mathbf{X}, t_i) + (\bar{\mathbf{V}}(\mathbf{Y}, t_i + s; \mathbf{X}, t_i) \cdot \nabla_{\mathbf{y}}) \cdot \bar{\Psi}(\mathbf{Y}, t_i + s; \mathbf{X}, t_i) \\
& = \kappa \cdot \nabla_{\mathbf{y}}^2 \cdot \bar{\Psi}(\mathbf{Y}, t_i + s; \mathbf{X}, t_i) - \overline{(\mathbf{V}'(\mathbf{Y}, t_i + s; \mathbf{X}, t_i) \cdot \nabla_{\mathbf{y}}) \cdot \Psi'(\mathbf{Y}, t_i + s; \mathbf{X}, t_i)} \\
& \quad + (\bar{\Psi}(\mathbf{X}, t_i) + \mathbf{E}(\mathbf{X}, t_i) \cdot \Delta t) \cdot \delta(\mathbf{Y} - \mathbf{X}) \cdot \delta(s)
\end{aligned} \tag{4.15}$$

$$(0 \leq s \leq \Delta t)$$

$$\rho(\mathbf{Y}, t_{i+1}) = \int \bar{\rho}(\mathbf{Y}, t_{i+1}; \mathbf{X}, t_i) \cdot d\mathbf{X} \tag{4.16}$$

$$\vartheta(\mathbf{Y}, t_{i+1}) = \int \bar{\vartheta}(\mathbf{Y}, t_{i+1}; \mathbf{X}, t_i) \cdot d\mathbf{X} \tag{4.17}$$

$$\Psi(\mathbf{Y}, t_{i+1}) = \int \bar{\Psi}(\mathbf{Y}, t_{i+1}; \mathbf{X}, t_i) \cdot d\mathbf{X} \tag{4.18}$$

$$t_{i+1} = t_i + \Delta t, \quad i = 0, 1, 2, \dots$$

Here, turbulent diffusion is described as a succession of physically coupled disintegration and integration of the virtual fluid parcels. Through them, the (Eulerian) mass density $\rho(\mathbf{Y}, t_{i+1})$, volumetric concentration $\vartheta(\mathbf{Y}, t_{i+1})$ of momentum

and volumetric concentration $\Psi(\mathbf{Y}, t_{i+1})$ of any other scalar are solved, in successive time steps, through cascaded integrations of the fractional contributions in physical properties from continuous disintegration of the previous virtual fluid parcels in the flow.

This description differs from the description under the classical random fluid particle treatment, which is formulated in the following equations (Part 1):

$$\begin{aligned} \frac{\partial}{\partial t} \bar{\rho}_L(\mathbf{X}, t; \mathbf{X}_0, t_0) + (\bar{\mathbf{V}}_L(\mathbf{X}, t; \mathbf{X}_0, t_0) \cdot \nabla_{\mathbf{X}}) \cdot \bar{\rho}_L(\mathbf{X}, t; \mathbf{X}_0, t_0) \\ = - \overline{(\mathbf{V}_L^2(\mathbf{X}, t; \mathbf{X}_0, t_0) \cdot \nabla_{\mathbf{X}}) \cdot \rho_L^2(\mathbf{X}, t; \mathbf{X}_0, t_0)} + \rho_L(\mathbf{X}_0, t_0) \cdot \delta(\mathbf{X} - \mathbf{X}_0) \cdot \delta(t - t_0) \end{aligned} \quad (4.19)$$

$$\begin{aligned} \frac{\partial}{\partial t} \bar{\vartheta}_L(\mathbf{X}, t; \mathbf{X}_0, t_0) + (\bar{\mathbf{V}}_L(\mathbf{X}, t; \mathbf{X}_0, t_0) \cdot \nabla_{\mathbf{X}}) \cdot \bar{\vartheta}_L(\mathbf{X}, t; \mathbf{X}_0, t_0) \\ = \bar{\mathbf{H}}(\mathbf{X}, t) \cdot \mathbf{P}(\mathbf{X}, t | \mathbf{X}_0, t_0) + \nu \cdot \nabla_{\mathbf{X}}^2 \cdot \bar{\vartheta}_L(\mathbf{X}, t; \mathbf{X}_0, t_0) \\ - \overline{(\mathbf{V}_L^2(\mathbf{X}, t; \mathbf{X}_0, t_0) \cdot \nabla_{\mathbf{X}}) \cdot \vartheta_L^2(\mathbf{X}, t; \mathbf{X}_0, t_0)} + \vartheta_L(\mathbf{X}_0, t_0) \cdot \delta(\mathbf{X} - \mathbf{X}_0) \cdot \delta(t - t_0) \end{aligned} \quad (4.20)$$

$$\begin{aligned} \frac{\partial}{\partial t} \bar{\Psi}_L(\mathbf{X}, t; \mathbf{X}_0, t_0) + (\bar{\mathbf{V}}_L(\mathbf{X}, t; \mathbf{X}_0, t_0) \cdot \nabla_{\mathbf{X}}) \cdot \bar{\Psi}_L(\mathbf{X}, t; \mathbf{X}_0, t_0) \\ = \bar{\mathbf{E}}(\mathbf{X}, t) \cdot \mathbf{P}(\mathbf{X}, t | \mathbf{X}_0, t_0) + \kappa \cdot \nabla_{\mathbf{X}}^2 \cdot \bar{\Psi}_L(\mathbf{X}, t; \mathbf{X}_0, t_0) \\ - \overline{(\mathbf{V}_L^2(\mathbf{X}, t; \mathbf{X}_0, t_0) \cdot \nabla_{\mathbf{X}}) \cdot \Psi_L^2(\mathbf{X}, t; \mathbf{X}_0, t_0)} + \Psi_L(\mathbf{X}_0, t_0) \cdot \delta(\mathbf{X} - \mathbf{X}_0) \cdot \delta(t - t_0) \end{aligned} \quad (4.21)$$

$$\bar{\rho}(\mathbf{X}, t) = \int \bar{\rho}_L(\mathbf{X}, t; \mathbf{X}_0, t_0) \cdot d\mathbf{X}_0 \quad (4.22)$$

$$\bar{\vartheta}(\mathbf{X}, t) = \int \bar{\vartheta}_L(\mathbf{X}, t; \mathbf{X}_0, t_0) \cdot d\mathbf{X}_0 \quad (4.23)$$

$$\bar{\Psi}(\mathbf{X}, t) = \int \bar{\Psi}_L(\mathbf{X}, t; \mathbf{X}_0, t_0) \cdot d\mathbf{X}_0 \quad (4.24)$$

Here $\mathbf{V}_L(\mathbf{X},t; \mathbf{X}_0,t_0) = \boldsymbol{\vartheta}_L(\mathbf{X},t; \mathbf{X}_0,t_0)/\rho_L(\mathbf{X},t; \mathbf{X}_0,t_0)$ is the Lagrangian velocity of the fluid particle \mathbf{X}_0 at position \mathbf{X} at time t . $\bar{\rho}_L(\mathbf{X},t; \mathbf{X}_0,t_0)$, $\bar{\boldsymbol{\vartheta}}_L(\mathbf{X},t; \mathbf{X}_0,t_0)$ and $\bar{\Psi}_L(\mathbf{X},t; \mathbf{X}_0,t_0)$ are the ensemble mean contributions to the Eulerian mass density, volumetric concentrations of momentum and scalar at (\mathbf{X},t) from the unit volume fluid particle \mathbf{X}_0 , respectively. $\rho_L'(\mathbf{X},t; \mathbf{X}_0,t_0)$, $\boldsymbol{\vartheta}_L'(\mathbf{X},t; \mathbf{X}_0,t_0)$ and $\Psi_L'(\mathbf{X},t; \mathbf{X}_0,t_0)$ are the deviations from $\bar{\rho}_L$, $\bar{\boldsymbol{\vartheta}}_L$ and $\bar{\Psi}_L$, respectively. $\rho_L(\mathbf{X}_0,t_0)$, $\boldsymbol{\vartheta}_L(\mathbf{X}_0,t_0)$ and $\Psi_L(\mathbf{X}_0,t_0)$ are the initial mass density, volumetric concentrations of momentum and scalar of the fluid particle \mathbf{X}_0 , respectively. $\bar{\mathbf{H}}(\mathbf{X},t)$ and $\bar{\mathbf{E}}(\mathbf{X},t)$ are the ensemble mean Eulerian external volumetric source strengths of momentum and scalar, respectively. $P(\mathbf{X},t|\mathbf{X}_0,t_0)$ is the probability density for the unit volume fluid particle \mathbf{X}_0 to appear at position \mathbf{X} at time t . $\bar{\rho}(\mathbf{X},t)$, $\bar{\boldsymbol{\vartheta}}(\mathbf{X},t)$ and $\bar{\Psi}(\mathbf{X},t)$ are the ensemble mean Eulerian mass density, volumetric concentrations of momentum and scalar at (\mathbf{X},t) , respectively.

Under the classical random fluid particle treatment, turbulent diffusion can only be described as random fluid particle dispersions. Through them, the ensemble mean Eulerian physical properties $\bar{\rho}(\mathbf{X},t)$, $\bar{\boldsymbol{\vartheta}}(\mathbf{X},t)$ and $\bar{\Psi}(\mathbf{X},t)$ are calculated as the statistical superimpositions of the "shadow-like" ensemble mean contributions from individual fluid particles in the flow. The non-feedback mechanism of the statistical superimpositions in this description reflects the exclusion of molecular mixing between different BMDFEs.

By comparison, the introduction of the feedback mechanism through physically coupled disintegration and integration of the BMDFEs under the virtual fluid parcel treatment would be seen as a major improvement in the description of turbulent diffusion. This improvement might reduce the potential mathematical-physical inconsistency in the understanding of turbulent diffusion in real turbulent fluids, when compared to the non-feedback mechanism of the

statistical superimpositions under the classical random fluid particle treatment. It is exclusively attributed to the incorporation of molecular mixing.

According to (4.13)–(4.18), in each time step, the disintegration of the "old" virtual fluid parcels will trigger the integration of the "new" virtual fluid parcels, which are then potentially subject to subsequent disintegration. At the end of each time step, the integrated solutions of $\rho(\mathbf{Y}, t_{i+1})$, $\theta(\mathbf{Y}, t_{i+1})$ and $\Psi(\mathbf{Y}, t_{i+1})$ must be fed back, as "new" source terms, into the conservation equations (4.13), (4.14) and (4.15). In the process of this feedback, each fractional contribution from a "old" virtual fluid parcel must be physically considered as an integral part of the "new" virtual fluid parcel, whose existence physically interferes with the other parts of the "new" virtual fluid parcel due to molecular mixing. This suggests, then, that molecular mixing is a controlling agent of the mixing mechanism in every time-step of turbulent diffusion, whose significance could be cumulatively increased.

5. Conclusion

By permitting disintegration of individual BMDFEs, this study extends the classical fluid particle treatment to a new virtual fluid parcel treatment of the BMDFE where molecular mixing between different BMDFEs in turbulent fluids is conceptually incorporated. Improvements over the classical fluid particle treatment are embodied in the following two aspects:

First, it simplifies the description of the fluid dynamic variables in turbulent flows by not tracing the Lagrangian characteristics of the BMDFEs, but rather by restricting the description to the Eulerian framework. As a result, additional concerns about the transformations between Lagrangian and Eulerian variables are eliminated.

Second, it introduces a feedback mechanism in the description of turbulent diffusion through physically coupled disintegration and integration of the BMDFEs. In comparison with the non-feedback mechanism of the statistical superimpositions under the classical random fluid particle treatment, this feedback mechanism might reduce a potential mathematical-physical inconsistency in our understanding of turbulent diffusion in real turbulent fluids. This feedback mechanism suggests that molecular mixing is a controlling agent of the mixing mechanism in every time-step of turbulent diffusion, whose effect could be cumulatively important.

According to these improvements, we may infer that the new virtual fluid parcel treatment of the BMDFE in continuum framework would be more realistic, from a physical viewpoint, in its description of turbulent diffusion than the classical random fluid particle treatment. Confirmation of this inference will be attempted in the next study (Part 3).

REFERENCES

- Batchelor, G.K. 1959 Small-scale variation of convected quantities like temperature in turbulent fluid. Part 1. General discussion and the case of small conductivity. *J. Fluid Mech.* **5**, 113-133.
- Batchelor, G.K., Howells, I.D. & Townsend, A.A. 1959 Small-scale variation of convected quantities like temperature in turbulent fluid. Part 2. The case of large conductivity. *J. Fluid Mech.* **5**, 134-179.
- Batchelor, G.K. 1967 *An Introduction to Fluid Dynamics*. Cambridge, The University Press, England.
- Chatwin, P.C. & Sullivan, P.J. 1979 The relative diffusion of a cloud of passive contaminant in incompressible turbulent flow. *J. Fluid Mech.* **91**, 337-355.
- Chatwin, P.C., Sullivan, P.J. & Yip 1990 Dilution and marked fluid particle analysis. *Proceedings of International Conference on Physical Modeling of Turbulent and Dispersion*, MIT, 633-638.
- Chatwin, P.C. & Sullivan, P.J. 1991 The use of exact but idealized results in turbulent diffusion problems. Submitted to *Combustion Conference on Fluid Mechanics*, Trinidad.
- Durbin, P.A. 1980 A stochastic model of two-particle dispersion and concentration fluctuations in homogeneous turbulence. *J. Fluid Mech.* **100**, 279-302.
- Kaplan, H. & Dinar, N. 1988 A stochastic model for dispersion and concentration distribution in homogeneous turbulence. *J. Fluid Mech.* **190**, 121-140.
- Lu, Pau-Chang 1979 *Fluid Mechanics, An Introductory Course*. The Iowa State University Press, Ames, Iowa.
- Massey, B.S. 1983 *Mechanics of Fluids*, 5th edition. Van Nostrand Reinhold (UK) Co. Ltd. Berkshire, England.
- Mironer, A. 1979 *Engineering Fluid Mechanics*. McGraw-Hill Book Company, New York.
- Moin, A.S. & Yaglom, A.M. 1971 *Statistical Fluid Mechanics. Mechanics of Turbulence*, vol. I. MIT Press, Cambridge, Mass.
- Owczarek, J.A. 1968 *Introduction to Fluid Mechanics*. International Textbook Company, Scranton, Pennsylvania.
- Pao, R.H.F. 1966 *Fluid Dynamics*. Charles E. Merrill Books Inc., Columbus, Ohio.
- Richardson, S.M. 1989 *Fluid Mechanics*. Hemisphere Publishing Co., New York.

Saffman, P.G. 1960 On the effect of the molecular diffusivity in turbulent diffusion *J. Fluid Mech* **8**, 273-283.

Sawford, B.L. & Hunt, J.C.R. 1986 Effects of turbulence structure, molecular diffusion and source size on scalar fluctuations in homogeneous turbulence. *J. Fluid Mech.* **165**, 373-400

Stapountzis, H , Sawford, B.L , Hunt, J.C.R. and Britter, R.E. 1986 Structure of the temperature field downwind of a line source in grid turbulence. *J. Fluid Mech.* **165**, 401-424.

Thomson, D J 1990 A stochastic model for the motion of particle pairs in isotropic high-Reynolds-number turbulence and its application to the problem of concentration variance *J. Fluid Mech.* **210**, 113-153.

Part 1 (attached Y. Guo, 1991): The role of molecular mixing in the description of turbulent diffusion in fluid continuum Part 1. The limitation of the fluid particle treatment.

Part 3 (attached Y. Guo, 1991): The role of molecular mixing in the description of turbulent diffusion in fluid continuum. Part 3. Application to the diffusion cloud.

Part 3. Application to the Diffusion Cloud.

Abstract

The influence of molecular mixing on turbulent diffusion is qualitatively examined by comparing the virtual fluid parcel treatment with the random fluid particle treatment of the BMDFE (Basic Macroscopically Describable Fluid Element) in continuum framework. The evolution of the diffusion cloud is analyzed by both treatments on the level of single time-step diffusion redistributions. The analytical results suggest a persistent and cumulative influence of molecular mixing on the evolution of the diffusion cloud, and thus on the evolution of the mean concentration field, by reducing the diffusion distribution variance. This suggestion would mean that the random fluid particle treatment, by excluding molecular mixing, may lead to a potential mathematical-physical inconsistency in the description of turbulent diffusion by exaggerating the diffusion distribution variance. Supporting evidence is presented from water flow diffusion experiments which appear to confirm that the virtual fluid parcel treatment is more realistic in its description of turbulent diffusion than the classical random fluid particle treatment.

1. Introduction

Our previous study (Part 2) has outlined differences between the classical random fluid particle treatment and a new virtual fluid parcel treatment of the BMDFE (Basic Macroscopically Describable Fluid Element) in continuum framework. The main difference lies in the fact that the new treatment incorporates molecular mixing between different BMDFEs by permitting disintegration of individual BMDFEs, while the classical treatment excludes such molecular mixing by restricting individual BMDFEs to move as entities. This difference leads to different descriptions of turbulent diffusion.

Under the classical random fluid particle treatment, turbulent diffusion is described as random fluid particle dispersions, in process of statistical superimpositions of the "shadow-like" ensemble mean contributions from individual fluid particles in the flow (Part 1):

$$\begin{aligned} \frac{\partial}{\partial t} \bar{\rho}_L(\mathbf{x}, t; \mathbf{x}_0, t_0) + (\bar{\mathbf{V}}_L(\mathbf{x}, t; \mathbf{x}_0, t_0) \cdot \nabla_{\mathbf{x}}) \cdot \bar{\rho}_L(\mathbf{x}, t; \mathbf{x}_0, t_0) \\ = - \overline{(\mathbf{V}_L^2(\mathbf{x}, t; \mathbf{x}_0, t_0) \cdot \nabla_{\mathbf{x}}) \cdot \rho_L^2(\mathbf{x}, t; \mathbf{x}_0, t_0)} + \rho_L(\mathbf{x}_0, t_0) \cdot \delta(\mathbf{x} - \mathbf{x}_0) \cdot \delta(t - t_0) \end{aligned} \quad (1.1)$$

$$\begin{aligned} \frac{\partial}{\partial t} \bar{\vartheta}_L(\mathbf{x}, t; \mathbf{x}_0, t_0) + (\bar{\mathbf{V}}_L(\mathbf{x}, t; \mathbf{x}_0, t_0) \cdot \nabla_{\mathbf{x}}) \cdot \bar{\vartheta}_L(\mathbf{x}, t; \mathbf{x}_0, t_0) \\ = \bar{\mathbf{H}}(\mathbf{x}, t) \cdot \mathbf{P}(\mathbf{x}, t | \mathbf{x}_0, t_0) + \nu \cdot \nabla_{\mathbf{x}}^2 \cdot \bar{\vartheta}_L(\mathbf{x}, t; \mathbf{x}_0, t_0) \\ - \overline{(\mathbf{V}_L^2(\mathbf{x}, t; \mathbf{x}_0, t_0) \cdot \nabla_{\mathbf{x}}) \cdot \vartheta_L^2(\mathbf{x}, t; \mathbf{x}_0, t_0)} + \vartheta_L(\mathbf{x}_0, t_0) \cdot \delta(\mathbf{x} - \mathbf{x}_0) \cdot \delta(t - t_0) \end{aligned} \quad (1.2)$$

$$\begin{aligned}
 & \frac{\partial}{\partial t} \bar{\Psi}_L(\mathbf{X}, t; \mathbf{X}_0, t_0) + (\bar{\mathbf{V}}_L(\mathbf{X}, t; \mathbf{X}_0, t_0) \cdot \nabla_{\mathbf{X}}) \cdot \bar{\Psi}_L(\mathbf{X}, t; \mathbf{X}_0, t_0) \\
 & = \bar{\mathbf{E}}(\mathbf{X}, t) \cdot \mathbf{P}(\mathbf{X}, t | \mathbf{X}_0, t_0) + \kappa \cdot \nabla_{\mathbf{X}}^2 \cdot \bar{\Psi}_L(\mathbf{X}, t; \mathbf{X}_0, t_0) \\
 & \quad - \overline{(\nabla_{\mathbf{L}}'(\mathbf{X}, t; \mathbf{X}_0, t_0) \cdot \nabla_{\mathbf{X}}) \cdot \Psi_{\mathbf{L}}'(\mathbf{X}, t, \mathbf{X}_0, t_0)} + \Psi_{\mathbf{L}}(\mathbf{X}_0, t_0) \cdot \delta(\mathbf{X} - \mathbf{X}_0) \cdot \delta(t - t_0)
 \end{aligned} \tag{1.3}$$

$$\bar{\rho}(\mathbf{X}, t) = \int \bar{\rho}_L(\mathbf{X}, t; \mathbf{X}_0, t_0) \cdot d\mathbf{X}_0 \tag{1.4}$$

$$\bar{\boldsymbol{\theta}}(\mathbf{X}, t) = \int \bar{\boldsymbol{\theta}}_L(\mathbf{X}, t; \mathbf{X}_0, t_0) \cdot d\mathbf{X}_0 \tag{1.5}$$

$$\bar{\Psi}(\mathbf{X}, t) = \int \bar{\Psi}_L(\mathbf{X}, t; \mathbf{X}_0, t_0) \cdot d\mathbf{X}_0 \tag{1.6}$$

Terms in these equations are defined as follows $\mathbf{V}_L(\mathbf{X}, t; \mathbf{X}_0, t_0) = \boldsymbol{\theta}'_L(\mathbf{X}, t; \mathbf{X}_0, t_0) / \rho'_L(\mathbf{X}, t; \mathbf{X}_0, t_0)$ is the Lagrangian velocity of the fluid particle \mathbf{X}_0 at position \mathbf{X} at time t . $\bar{\rho}_L(\mathbf{X}, t; \mathbf{X}_0, t_0)$, $\bar{\boldsymbol{\theta}}_L(\mathbf{X}, t, \mathbf{X}_0, t_0)$ and $\bar{\Psi}_L(\mathbf{X}, t, \mathbf{X}_0, t_0)$ are the ensemble mean contributions to the Eulerian mass density, volumetric concentrations of momentum and scalar at (\mathbf{X}, t) from the unit volume fluid particle \mathbf{X}_0 , respectively. $\rho'_L(\mathbf{X}, t, \mathbf{X}_0, t_0)$, $\boldsymbol{\theta}'_L(\mathbf{X}, t, \mathbf{X}_0, t_0)$ and $\Psi'_L(\mathbf{X}, t, \mathbf{X}_0, t_0)$ are the deviations from $\bar{\rho}_L$, $\bar{\boldsymbol{\theta}}_L$ and $\bar{\Psi}_L$, respectively. $\rho_L(\mathbf{X}_0, t_0)$, $\boldsymbol{\theta}_L(\mathbf{X}_0, t_0)$ and $\Psi_L(\mathbf{X}_0, t_0)$ are the initial mass density, volumetric concentrations of momentum and scalar of the fluid particle \mathbf{X}_0 , respectively. $\bar{\mathbf{H}}(\mathbf{X}, t)$ and $\bar{\mathbf{E}}(\mathbf{X}, t)$ are the ensemble mean Eulerian external volumetric source strengths of momentum and scalar, respectively. $\mathbf{P}(\mathbf{X}, t | \mathbf{X}_0, t_0)$ is the probability density for the unit volume fluid particle \mathbf{X}_0 to appear at position \mathbf{X} at time t . $\bar{\rho}(\mathbf{X}, t)$, $\bar{\boldsymbol{\theta}}(\mathbf{X}, t)$ and $\bar{\Psi}(\mathbf{X}, t)$ are the ensemble mean Eulerian mass density, volumetric concentrations of momentum and scalar at (\mathbf{X}, t) , respectively. ν and κ are the molecular kinematic and scalar viscosities (or the molecular collision-transport coefficients for momentum and scalar), respectively. $\nabla_{\mathbf{X}}$ and $\nabla_{\mathbf{X}}^2$

are del and Laplace operators with respect to \mathbf{X} , and δ is the Dirac delta function.

Under the new virtual fluid parcel treatment, turbulent diffusion is described as physically coupled disintegration and integration of the virtual fluid parcels, in process of cascaded integration of the fractional contributions from the continuously disintegrated virtual fluid parcels in the flow (Part 2).

$$\begin{aligned} \frac{\partial}{\partial s} \bar{\rho}(\mathbf{Y}, t_1+s; \mathbf{X}, t_1) + (\bar{\mathbf{V}}(\mathbf{Y}, t_1+s; \mathbf{X}, t_1) \cdot \nabla_{\mathbf{y}}) \cdot \bar{\rho}(\mathbf{Y}, t_1+s; \mathbf{X}, t_1) \\ = - \overline{(\mathbf{V}'(\mathbf{Y}, t_1+s; \mathbf{X}, t_1) \cdot \nabla_{\mathbf{y}}) \cdot \rho'(\mathbf{Y}, t_1+s; \mathbf{X}, t_1)} + \rho(\mathbf{X}, t_1) \cdot \delta(\mathbf{Y}-\mathbf{X}) \cdot \delta(s) \end{aligned} \quad (1.7)$$

$$\begin{aligned} \frac{\partial}{\partial s} \bar{\theta}(\mathbf{Y}, t_1+s; \mathbf{X}, t_1) + (\bar{\mathbf{V}}(\mathbf{Y}, t_1+s; \mathbf{X}, t_1) \cdot \nabla_{\mathbf{y}}) \cdot \bar{\theta}(\mathbf{Y}, t_1+s; \mathbf{X}, t_1) \\ = \nu \cdot \nabla_{\mathbf{y}}^2 \cdot \bar{\theta}(\mathbf{Y}, t_1+s; \mathbf{X}, t_1) - \overline{(\mathbf{V}'(\mathbf{Y}, t_1+s; \mathbf{X}, t_1) \cdot \nabla_{\mathbf{y}}) \cdot \theta'(\mathbf{Y}, t_1+s; \mathbf{X}, t_1)} \\ + (\bar{\theta}(\mathbf{X}, t_1) + \mathbf{H}(\mathbf{X}, t_1) \cdot \Delta t) \cdot \delta(\mathbf{Y}-\mathbf{X}) \cdot \delta(s) \end{aligned} \quad (1.8)$$

$$\begin{aligned} \frac{\partial}{\partial s} \bar{\Psi}(\mathbf{Y}, t_1+s; \mathbf{X}, t_1) + (\bar{\mathbf{V}}(\mathbf{Y}, t_1+s; \mathbf{X}, t_1) \cdot \nabla_{\mathbf{y}}) \cdot \bar{\Psi}(\mathbf{Y}, t_1+s; \mathbf{X}, t_1) \\ = \kappa \cdot \nabla_{\mathbf{y}}^2 \cdot \bar{\Psi}(\mathbf{Y}, t_1+s; \mathbf{X}, t_1) - \overline{(\mathbf{V}'(\mathbf{Y}, t_1+s; \mathbf{X}, t_1) \cdot \nabla_{\mathbf{y}}) \cdot \Psi'(\mathbf{Y}, t_1+s; \mathbf{X}, t_1)} \\ + (\bar{\Psi}(\mathbf{X}, t_1) + \mathbf{E}(\mathbf{X}, t_1) \cdot \Delta t) \cdot \delta(\mathbf{Y}-\mathbf{X}) \cdot \delta(s) \end{aligned} \quad (1.9)$$

$$(0 \leq s \leq \Delta t)$$

$$\rho(\mathbf{Y}, t_{i+1}) = \int \bar{\rho}(\mathbf{Y}, t_{i+1}; \mathbf{X}, t_i) \cdot d\mathbf{X} \quad (1.10)$$

$$\bar{\theta}(\mathbf{Y}, t_{i+1}) = \int \bar{\theta}(\mathbf{Y}, t_{i+1}; \mathbf{X}, t_i) \cdot d\mathbf{X} \quad (1.11)$$

$$\Psi(\mathbf{Y}, t_{i+1}) = \int \bar{\Psi}(\mathbf{Y}, t_{i+1}; \mathbf{X}, t_i) \cdot d\mathbf{X} \quad (1.12)$$

$$t_{i+1} = t_i + \Delta t, \quad i = 0, 1, 2, \dots$$

Terms in these equations are defined as follows. $\mathbf{V}(\mathbf{Y}, t_1+s; \mathbf{X}, t_1) = \boldsymbol{\phi}(\mathbf{Y}, t_1+s; \mathbf{X}, t_1) / \rho(\mathbf{Y}, t_1+s; \mathbf{X}, t_1)$ is the pseudo-Lagrangian velocity of the center of the virtual fluid parcel arriving at (\mathbf{Y}, t_1+s) from (\mathbf{X}, t_1) . $\bar{\rho}(\mathbf{Y}, t_1+s, \mathbf{X}, t_1)$, $\bar{\boldsymbol{\phi}}(\mathbf{Y}, t_1+s, \mathbf{X}, t_1)$ and $\bar{\Psi}(\mathbf{Y}, t_1+s, \mathbf{X}, t_1)$ are the approximate fractional contributions to the mass density, volumetric concentrations of momentum and scalar of the virtual fluid parcel at (\mathbf{Y}, t_1+s) from the unit volume virtual fluid parcel at (\mathbf{X}, t_1) , respectively. $\rho'(\mathbf{Y}, t_1+s; \mathbf{X}, t_1)$, $\boldsymbol{\phi}'(\mathbf{Y}, t_1+s, \mathbf{X}, t_1)$ and $\Psi'(\mathbf{Y}, t_1+s, \mathbf{X}, t_1)$ are the deviations from $\bar{\rho}$, $\bar{\boldsymbol{\phi}}$ and $\bar{\Psi}$, respectively. $\mathbf{H}(\mathbf{X}, t_1)$ and $\mathbf{E}(\mathbf{X}, t_1)$ are the (Eulerian) external volumetric source strengths of momentum and scalar at (\mathbf{X}, t_1) , respectively. $\rho(\mathbf{Y}, t_{i+1})$, $\boldsymbol{\phi}(\mathbf{Y}, t_{i+1})$ and $\Psi(\mathbf{Y}, t_{i+1})$ are the (Eulerian) mass density, volumetric concentrations of momentum and scalar at (\mathbf{Y}, t_{i+1}) , respectively. Δt is the time interval comparable to the minimum period of the significant fluctuations of $\rho(\mathbf{X}, t_1)$, $\boldsymbol{\phi}(\mathbf{X}, t_1)$ and $\Psi(\mathbf{X}, t_1)$.

The main improvement by the new virtual fluid parcel treatment in the description of turbulent diffusion is embodied in the introduction of a feedback mechanism through physically coupled disintegration and integration of the BMDFEs. This might reduce a potential mathematical-physical inconsistency in the understanding of turbulent diffusion in real turbulent fluids, when contrasted to the non-feedback mechanism of the statistical superimpositions under the classical random fluid particle treatment. The feedback mechanism suggests that, as a controlling agent of the mixing mechanism, molecular mixing could be cumulatively important in every time-step of turbulent diffusion. The conclusion is then that molecular mixing should not generally be neglected in the description of

turbulent diffusion, which was also realized by the previous studies (Chatwin & Sullivan 1979, Durbin 1980; Sawford & Hunt 1986; Stapountzis et al. 1986; Kaplan & Dinar 1988).

According to the above improvement, we may infer that the new virtual fluid parcel treatment is more realistic in its description of turbulent diffusion than the classical random fluid particle treatment

To clarify the effect of molecular mixing, and thereby to confirm the above inference, this study tries to apply the new and classical treatments to the description of the diffusion cloud evolution on the level of single time-step diffusion redistribution analysis. The analytical results are then compared and experimentally tested.

Earlier, the effect of molecular collision-transport interacting with turbulent transport (generally referred to as "molecular diffusion" and "turbulent diffusion") has been studied by Saffman (1960) and many others (see Monin & Yaglom §10.1 and §10.2 1971) based on the classical scalar diffusion equation. According to their basically intuitive analyses, it has been suggested that the influence on the evolution of the diffusion cloud by molecular collision-transport is negligible when the diffusion time is long and the Reynolds number is sufficiently large. However, the effect of molecular mixing in such situation remains an open question.

For reason of simplicity, a passive scalar will be used as a tracer in the subsequent analysis. It is assumed to be conservative in the sense that the influence from external sources and from molecular collision-transport between different BMDFEs are neglected.

2. Diffusion redistributions and the effect of molecular mixing

2.1. Formal description of redistributions

Suppose, for the sake of argument, a scalar located at positions $\mathbf{X}_{o_1}, \mathbf{X}_{o_2} \dots \mathbf{X}_{o_n}$, at initial time t_o , with volumetric concentrations $\Psi(\mathbf{X}_{o_1}, t_o), \Psi(\mathbf{X}_{o_2}, t_o) \dots \Psi(\mathbf{X}_{o_n}, t_o)$, respectively. In the first small time interval $\Delta t_1 = t_1 - t_o$, the scalar at initial positions in \mathbf{X}_o is diffused into \mathbf{X}_1 . At time t_1 , we may arbitrarily choose a point (\mathbf{X}_1, t_1) where the volumetric concentration $\Psi(\mathbf{X}_1, t_1)$ of the scalar is measured as the sum of contributions from all initial locations. In the second small time interval $\Delta t_2 = t_2 - t_1$, the scalar property at (\mathbf{X}_1, t_1) is re-diffused into \mathbf{X}_2 , with redistribution density $P(\mathbf{X}_2, t_2 | \mathbf{X}_1, t_1)$. It will be shown below that different solutions for $P(\mathbf{X}_2, t_2 | \mathbf{X}_1, t_1)$ would be obtained under the random fluid particle treatment and the virtual fluid parcel treatment, respectively.

Under the random fluid particle treatment, each initial location of the scalar is assumed to be occupied by a fluid particle with volume $d\mathbf{X}_{o_i}$ ($i = 1, 2 \dots n$) which subsequently moves randomly as an entity, statistically described by the probability density distribution of its trajectory in repeated experiments.

In the first time interval $\Delta t_1 = t_1 - t_o$, each fluid particle has a probability density $P(\mathbf{X}_1, t_1 | \mathbf{X}_{o_i}, t_o)$ for its unit volume to move from the initial location (\mathbf{X}_{o_i}, t_o) to point (\mathbf{X}_1, t_1) . At time t_1 , each fluid particle should have a "shadow-like" ensemble mean (Lagrangian) contribution density $\bar{\Psi}_L(\mathbf{X}_1, t_1, \mathbf{X}_{o_i}, t_o)$ to the ensemble mean (Eulerian) volumetric concentration $\bar{\Psi}(\mathbf{X}_1, t_1)$ of the scalar at point (\mathbf{X}_1, t_1) in repeated experiments:

$$\bar{\Psi}_L(\mathbf{X}_1, t_1; \mathbf{X}_{o_i}, t_o) = \Psi(\mathbf{X}_{o_i}, t_o) \cdot P(\mathbf{X}_1, t_1 | \mathbf{X}_{o_i}, t_o) \quad (2.1)$$

According to (1.3) and (1.6), the ensemble mean (Eulerian) volumetric concentration $\bar{\Psi}(\mathbf{X}_1, t_1)$ at (\mathbf{X}_1, t_1) should be calculated as the statistical superimposition of the ensemble mean (Lagrangian) contributions from all the individual fluid particles in the flow:

$$\begin{aligned}\bar{\Psi}(\mathbf{X}_1, t_1) &= \sum_{i=1}^n \bar{\Psi}_L(\mathbf{X}_1, t_1, \mathbf{X}_{0i}, t_0) \cdot d\mathbf{X}_{0i} \\ &= \sum_{i=1}^n \Psi(\mathbf{X}_{0i}, t_0) \cdot P(\mathbf{X}_1, t_1 | \mathbf{X}_{0i}, t_0) \cdot d\mathbf{X}_{0i}\end{aligned}\quad (2.2)$$

Since molecular mixing between fluid particles is excluded by the fluid particle treatment (Part 1), the shadow-like ensemble mean contributions to point (\mathbf{X}_1, t_1) from different fluid particles are not allowed to be physically linked. In this process, each ensemble mean contribution $\Psi(\mathbf{X}_{0i}, t_0) \cdot P(\mathbf{X}_1, t_1 | \mathbf{X}_{0i}, t_0) \cdot d\mathbf{X}_{0i}$ from a single fluid particle is assumed to be developed as if the ensemble mean contributions from other fluid particles did not exist. This means that different fluid particles only come to point (\mathbf{X}_1, t_1) in different realizations in repeated experiments since more than one fluid particle cannot physically occupy a given space-time point in a single realization. In the next time interval, the overall shadow-like ensemble mean contributions at point (\mathbf{X}_1, t_1) cannot then be jointly considered in their further re-diffusion.

In the second time interval $\Delta t_2 = t_2 - t_1$, each fluid particle has a further probability density $P(\mathbf{X}_2, t_2 | \mathbf{X}_1, t_1, \mathbf{X}_{0i}, t_0)$ for its unit volume to re-diffuse from (\mathbf{X}_1, t_1) to (\mathbf{X}_2, t_2) . At time t_2 , each fluid particle via (\mathbf{X}_1, t_1) , or each shadow-like contribution at (\mathbf{X}_1, t_1) , should have a further shadow-like ensemble mean (Lagrangian) contribution density $\Psi(\mathbf{X}_{0i}, t_0) \cdot P(\mathbf{X}_1, t_1 | \mathbf{X}_{0i}, t_0) \cdot P(\mathbf{X}_2, t_2 | \mathbf{X}_1, t_1, \mathbf{X}_{0i}, t_0) \cdot d\mathbf{X}_{0i}$ to the ensemble mean (Eulerian) volumetric concentration $\bar{\Psi}(\mathbf{X}_2, t_2)$ of the scalar at

point (\mathbf{X}_2, t_2) in repeated experiments. The overall further ensemble mean contribution density to $\bar{\Psi}(\mathbf{X}_2, t_2)$ from all the fluid particles via (\mathbf{X}_1, t_1) , or from all their shadow-like contributions at (\mathbf{X}_1, t_1) , should then be calculated as

$$\bar{\Psi}_L(\mathbf{X}_2, t_2 | \mathbf{X}_1, t_1) = \sum_{i=1}^n \Psi(\mathbf{X}_{0i}, t_0) \cdot P(\mathbf{X}_1, t_1 | \mathbf{X}_{0i}, t_0) \cdot P(\mathbf{X}_2, t_2 | \mathbf{X}_1, t_1; \mathbf{X}_{0i}, t_0) \cdot d\mathbf{X}_{0i} \quad (2.3)$$

This means that, under the random fluid particle treatment, the redistribution density $P_r(\mathbf{X}_2, t_2 | \mathbf{X}_1, t_1)$ of the scalar for all the fluid particles via (\mathbf{X}_1, t_1) , or for all their shadow-like contributions at (\mathbf{X}_1, t_1) , to appear at (\mathbf{X}_2, t_2) is described as

$$\begin{aligned} P_r(\mathbf{X}_2, t_2 | \mathbf{X}_1, t_1) &= \frac{\bar{\Psi}_L(\mathbf{X}_2, t_2 | \mathbf{X}_1, t_1)}{\bar{\Psi}(\mathbf{X}_1, t_1)} \\ &= \frac{\sum_{i=1}^n \Psi(\mathbf{X}_{0i}, t_0) \cdot P(\mathbf{X}_1, t_1 | \mathbf{X}_{0i}, t_0) \cdot P(\mathbf{X}_2, t_2 | \mathbf{X}_1, t_1; \mathbf{X}_{0i}, t_0) \cdot d\mathbf{X}_{0i}}{\sum_{i=1}^n \Psi(\mathbf{X}_{0i}, t_0) \cdot P(\mathbf{X}_1, t_1 | \mathbf{X}_{0i}, t_0) \cdot d\mathbf{X}_{0i}} \end{aligned} \quad (2.4)$$

where the subscript r denotes the random fluid particle treatment

The appropriateness of (2.4) can be tested as follows: If we statistically consider that every point (\mathbf{X}_1, t_1) in \mathbf{X}_1 is occupied by an "imaginary fluid particle" with volume $d\mathbf{X}_1$, the ensemble mean (Eulerian) volumetric concentration $\bar{\Psi}(\mathbf{X}_2, t_2)$ of the scalar at point (\mathbf{X}_2, t_2) should then be calculated as the statistical superimposition of the shadow-like ensemble mean contributions from all such "imaginary fluid particles" in \mathbf{X}_1 :

$$\begin{aligned}
\bar{\Psi}(\mathbf{X}_2, t_2) &= \sum_{\mathbf{X}_1} \bar{\Psi}(\mathbf{X}_1, t_1) \cdot P_f(\mathbf{X}_2, t_2 | \mathbf{X}_1, t_1) \cdot d\mathbf{X}_1 \\
&= \sum_{i=1}^n \sum_{\mathbf{X}_{0_i}} \Psi(\mathbf{X}_{0_i}, t_0) \cdot P(\mathbf{X}_1, t_1 | \mathbf{X}_{0_i}, t_0) \cdot P(\mathbf{X}_2, t_2 | \mathbf{X}_1, t_1; \mathbf{X}_{0_i}, t_0) \cdot d\mathbf{X}_{0_i} \cdot d\mathbf{X}_1
\end{aligned}
\tag{2.5}$$

Considering that the probability density for each fluid particle to move from its initial location (\mathbf{X}_{0_i}, t_0) to (\mathbf{X}_2, t_2) is

$$P(\mathbf{X}_2, t_2 | \mathbf{X}_{0_i}, t_0) = \sum_{\mathbf{X}_1} P(\mathbf{X}_1, t_1 | \mathbf{X}_{0_i}, t_0) \cdot P(\mathbf{X}_2, t_2 | \mathbf{X}_1, t_1; \mathbf{X}_{0_i}, t_0) \cdot d\mathbf{X}_1$$

(2.5) can be written as

$$\bar{\Psi}(\mathbf{X}_2, t_2) = \sum_{i=1}^n \Psi(\mathbf{X}_{0_i}, t_0) \cdot P(\mathbf{X}_2, t_2 | \mathbf{X}_{0_i}, t_0) \cdot d\mathbf{X}_{0_i}$$

which complies with (1.6).

By contrast, under the virtual fluid parcel treatment, each initial location of the scalar is assumed to be occupied by a virtual fluid parcel with volume $d\mathbf{X}_{0_i}$ ($i = 1, 2 \dots n$), subject to disintegration as described by the fractional redistribution density.

In the first time interval $\Delta t_1 = t_1 - t_0$, each virtual fluid parcel in \mathbf{X}_0 has a fractional redistribution density $F(\mathbf{X}_1, t_1 | \mathbf{X}_{0_i}, t_0)$ for its disintegrated scalar fragment to diffuse into the unit volume virtual fluid parcel at (\mathbf{X}_1, t_1) . If Δt_1 is sufficiently small for the virtual fluid parcel at (\mathbf{X}_{0_i}, t_0) to be still recognized by its center of gravity, it may be acceptable, as an approximation, to assume that the virtual

fluid parcel moves as a whole during Δt_1 with disintegration taking place at the end of the time interval. In this case, the virtual fluid parcel at (\mathbf{X}_{o_i}, t_0) can be temporarily treated as a "pseudo-fluid-particle" during Δt_1 . $F(\mathbf{X}_{1,t_1} | \mathbf{X}_{o_i}, t_0)$ can then be approximately estimated by the probability density $P(\mathbf{X}_{1,t_1} | \mathbf{X}_{o_i}, t_0)$ for such a "pseudo-fluid-particle" to diffuse from the initial location (\mathbf{X}_{o_i}, t_0) to point (\mathbf{X}_{1,t_1}) . At time t_1 , due to disintegration, each virtual fluid parcel in \mathbf{X}_0 should have a fractional contribution density $\tilde{\Psi}$ to the (Eulerian) volumetric concentration $\Psi(\mathbf{X}_{1,t_1})$ of the scalar of the newly formed virtual fluid parcel at (\mathbf{X}_{1,t_1})

$$\begin{aligned}\tilde{\Psi}(\mathbf{X}_{1,t_1}; \mathbf{X}_{o_i}, t_0) &= \Psi(\mathbf{X}_{o_i}, t_0) \cdot F(\mathbf{X}_{1,t_1} | \mathbf{X}_{o_i}, t_0) \\ &\approx \bar{\Psi}(\mathbf{X}_{1,t_1}, \mathbf{X}_{o_i}, t_0) \\ &\approx \Psi(\mathbf{X}_{o_i}, t_0) \cdot P(\mathbf{X}_{1,t_1} | \mathbf{X}_{o_i}, t_0)\end{aligned}\quad (2.6)$$

According to (1.9) and (1.12), the (Eulerian) volumetric concentration $\Psi(\mathbf{X}_{1,t_1})$ should be calculated as the integration of the fractional contributions disintegrated from all the previous virtual fluid parcels in \mathbf{X}_0 :

$$\begin{aligned}\Psi(\mathbf{X}_{1,t_1}) &= \sum_{i=1}^n \tilde{\Psi}(\mathbf{X}_{1,t_1}; \mathbf{X}_{o_i}, t_0) \cdot d\mathbf{X}_{o_i} \\ &= \sum_{i=1}^n \Psi(\mathbf{X}_{o_i}, t_0) \cdot F(\mathbf{X}_{1,t_1} | \mathbf{X}_{o_i}, t_0) \cdot d\mathbf{X}_{o_i} \\ &\approx \sum_{i=1}^n \Psi(\mathbf{X}_{o_i}, t_0) \cdot P(\mathbf{X}_{1,t_1} | \mathbf{X}_{o_i}, t_0) \cdot d\mathbf{X}_{o_i}\end{aligned}\quad (2.7)$$

Since molecular mixing between fluid elements is considered under the virtual fluid parcel treatment, the fractional contributions to point (\mathbf{X}_{1,t_1}) disintegrated from the different previous virtual fluid parcels in \mathbf{X}_0 should be physically linked.

In this process, each fractional contribution $\Psi(\mathbf{X}_{0_i}, t_0) \cdot F(\mathbf{X}_1, t_1 | \mathbf{X}_{0_i}, t_0) \cdot d\mathbf{X}_{0_i}$ from a previous virtual fluid parcel is regarded as an integral part of the newly formed virtual fluid parcel at (\mathbf{X}_1, t_1) . In the next time interval, the overall fractional contributions at (\mathbf{X}_1, t_1) should then be jointly considered in their further re-diffusion, which is described by the joint disintegration of the new virtual fluid parcel at (\mathbf{X}_1, t_1) .

In the second time interval $\Delta t_2 = t_2 - t_1$, the new virtual fluid parcel at (\mathbf{X}_1, t_1) has a further joint fractional redistribution density $F(\mathbf{X}_2(\mathbf{X}_{0_1}), \mathbf{X}_2(\mathbf{X}_{0_2}) \dots \mathbf{X}_2(\mathbf{X}_{0_n}), t_2 | \mathbf{X}_1, t_1)$ for all its constituent scalar parts, arrived at (\mathbf{X}_1, t_1) from all the previous virtual fluid parcels in \mathbf{X}_0 , to jointly disintegrate and then re-diffuse into the unit volume newer virtual fluid parcel at (\mathbf{X}_2, t_2) . In addition, each constituent scalar part of the virtual fluid parcel at (\mathbf{X}_1, t_1) , coming from one previous virtual fluid parcel in \mathbf{X}_0 , has a further individual fractional redistribution density $F(\mathbf{X}_2, t_2 | \mathbf{X}_1, t_1; \mathbf{X}_{0_i}, t_0)$ to re-diffuse into the unit volume newer virtual fluid parcel at (\mathbf{X}_2, t_2) . If Δt_2 is sufficiently small for the new virtual fluid parcel at (\mathbf{X}_1, t_1) to be still recognized by its center of gravity, it may again be acceptable, as an approximation, to assume that the new virtual fluid parcel moves as a whole during Δt_2 , with disintegration taking place at the end of the time interval. As discussed above, the new virtual fluid parcel at (\mathbf{X}_1, t_1) becomes a temporary "pseudo-fluid-particle" during Δt_2 . $F(\mathbf{X}_2(\mathbf{X}_{0_1}), \mathbf{X}_2(\mathbf{X}_{0_2}) \dots \mathbf{X}_2(\mathbf{X}_{0_n}), t_2 | \mathbf{X}_1, t_1)$ can then be approximately estimated by the joint probability density $P(\mathbf{X}_2(\mathbf{X}_{0_1}), \mathbf{X}_2(\mathbf{X}_{0_2}) \dots \mathbf{X}_2(\mathbf{X}_{0_n}), t_2 | \mathbf{X}_1, t_1)$ for all the fluid particles in \mathbf{X}_0 to jointly appear at (\mathbf{X}_2, t_2) via (\mathbf{X}_1, t_1) . $F(\mathbf{X}_2, t_2 | \mathbf{X}_1, t_1; \mathbf{X}_{0_i}, t_0)$ can then be approximately estimated by the probability density $P(\mathbf{X}_2, t_2 | \mathbf{X}_1, t_1; \mathbf{X}_{0_i}, t_0)$ for each of the fluid particles in \mathbf{X}_0 to jointly appear at (\mathbf{X}_2, t_2) via (\mathbf{X}_1, t_1) . At time t_2 , due to disintegration of the virtual fluid parcel at (\mathbf{X}_1, t_1) , each of its constituent scalar

parts should have a subsequent fractional contribution to the newer virtual fluid parcel at (\mathbf{X}_2, t_2) , with a contribution to the center of gravity (with respect to the scalar) of the newer virtual fluid parcel estimated as

$$\frac{\tilde{\Psi}(\mathbf{X}_1, t_1; \mathbf{X}_{o_i}, t_0) \cdot \mathbf{X}_2(\mathbf{X}_{o_i}) \cdot d\mathbf{X}_{o_i}}{\Psi(\mathbf{X}_1, t_1)}$$

As a consequence, the overall contributions to the center of gravity of the newer virtual fluid parcel at (\mathbf{X}_2, t_2) from all the constituent fractions of the virtual fluid parcel at (\mathbf{X}_1, t_1) should be estimated as

$$\begin{aligned} \mathbf{X}_2(\mathbf{X}_1) &= \frac{\sum_{i=1}^n \tilde{\Psi}(\mathbf{X}_1, t_1; \mathbf{X}_{o_i}, t_0) \cdot \mathbf{X}_2(\mathbf{X}_{o_i}) \cdot d\mathbf{X}_{o_i}}{\Psi(\mathbf{X}_1, t_1)} \\ &= \frac{\sum_{i=1}^n \Psi(\mathbf{X}_{o_i}, t_0) \cdot F(\mathbf{X}_1, t_1 | \mathbf{X}_{o_i}, t_0) \cdot \mathbf{X}_2(\mathbf{X}_{o_i}) \cdot d\mathbf{X}_{o_i}}{\sum_{i=1}^n \Psi(\mathbf{X}_{o_i}, t_0) \cdot F(\mathbf{X}_1, t_1 | \mathbf{X}_{o_i}, t_0) \cdot d\mathbf{X}_{o_i}} \\ &\approx \frac{\sum_{i=1}^n \Psi(\mathbf{X}_{o_i}, t_0) \cdot P(\mathbf{X}_1, t_1 | \mathbf{X}_{o_i}, t_0) \cdot \mathbf{X}_2(\mathbf{X}_{o_i}) \cdot d\mathbf{X}_{o_i}}{\sum_{i=1}^n \Psi(\mathbf{X}_{o_i}, t_0) \cdot P(\mathbf{X}_1, t_1 | \mathbf{X}_{o_i}, t_0) \cdot d\mathbf{X}_{o_i}} \end{aligned} \quad (2.8)$$

This means that, under the virtual fluid parcel treatment, the redistribution density $P_v(\mathbf{X}_2, t_2 | \mathbf{X}_1, t_1)$ of the scalar for all the constituent fractions to diffuse from (\mathbf{X}_1, t_1) to (\mathbf{X}_2, t_2) is determined according to (2.8). Here the subscript v denotes the virtual fluid parcel treatment.

In practice, the determination of $P_v(\mathbf{X}_2, t_2 | \mathbf{X}_1, t_1)$ according to (2.8) is often

complicated. One possible approach is through the concept of the characteristic function $\hat{P}_v(\theta_2)$, which is defined as the Fourier integral transform:

$$\hat{P}_v(\theta_2) = \int_{-\infty}^{\infty} P_v(\mathbf{X}_2, t_2 | \mathbf{X}_1, t_1) \cdot e^{k \cdot \theta_2 \cdot \mathbf{X}_2} \cdot d\mathbf{X}_2$$

$$(k = \sqrt{-1}) \quad (2.9)$$

Assuming $\mathbf{X}_2(\mathbf{X}_{0_1})$, $\mathbf{X}_2(\mathbf{X}_{0_2})$... $\mathbf{X}_2(\mathbf{X}_{0_n})$ in (2.8) are mutually statistically independent, we can expect (Derman, Gleser & Olkin 1973) that

$$\hat{P}_v(\theta_2) = \hat{p}_1(\theta_2) \cdot \hat{p}_2(\theta_2) \cdots \hat{p}_n(\theta_2) \quad (2.10)$$

where the characteristic functions $\hat{p}_i(\theta_2)$ are defined as

$$\hat{p}_i(\theta_2) = \int_{-\infty}^{\infty} \left(\int_{-\infty}^{\infty} \frac{\mathbf{X}_2(\mathbf{X}_{0_i})}{b} P(\mathbf{Y}(\mathbf{X}_{0_i}), t_2 | \mathbf{X}_1, t_1; \mathbf{X}_{0_i}, t_0) \cdot d\mathbf{Y} \right) \cdot e^{k \cdot \theta_2 \cdot \mathbf{X}_2(\mathbf{X}_{0_i})} \cdot d\mathbf{X}_2$$

$$(2.11)$$

with

$$b = \frac{\tilde{\Psi}(\mathbf{X}_1, t_1; \mathbf{X}_{0_i}, t_0) \cdot d\mathbf{X}_{0_i}}{\Psi(\mathbf{X}_1, t_1)}$$

$$= \frac{\Psi(\mathbf{X}_{0_i}, t_0) \cdot P(\mathbf{X}_1, t_1 | \mathbf{X}_{0_i}, t_0) \cdot d\mathbf{X}_{0_i}}{\sum_{i=1}^n \Psi(\mathbf{X}_{0_i}, t_0) \cdot P(\mathbf{X}_1, t_1 | \mathbf{X}_{0_i}, t_0) \cdot d\mathbf{X}_{0_i}}$$

$$(i = 1, 2 \dots n)$$

Here $\int_{-\infty}^{\infty} \frac{X_2(X_{0i})}{b} P(Y(X_{0i}), t_2 | X_1, t_1; X_{0i}, t_0) \cdot dY$ is the individual probability density of $b \cdot X_2(X_{0i})$.

Then the redistribution density $P_v(X_2, t_2 | X_1, t_1)$ can be calculated as the inversion of the Fourier integral transform:

$$\begin{aligned} P_v(X_2, t_2 | X_1, t_1) &= \frac{1}{2\pi} \int_{-\infty}^{\infty} \hat{P}_v(\theta_2) \cdot e^{-k \cdot \theta_2 \cdot X_2} \cdot d\theta_2 \\ &= \frac{1}{2\pi} \int_{-\infty}^{\infty} (\hat{p}_1(\theta_2) \cdot \hat{p}_2(\theta_2) \cdots \hat{p}_n(\theta_2)) \cdot e^{-k \cdot \theta_2 \cdot X_2} \cdot d\theta_2 \end{aligned} \quad (2.12)$$

The distinct forms of (2.4) and (2.12) suggests that the redistribution density $P_v(X_2, t_2 | X_1, t_1)$ under the virtual fluid parcel treatment differs from the redistribution density $P_r(X_2, t_2 | X_1, t_1)$ under the random fluid particle treatment. The nature of this difference will be further explored in the following section.

2.2. The means and variances of the redistributions

For convenience of illustration, we may assume a simple situation where a scalar is initially located at two positions X_{0_1} and X_{0_2} in a turbulent fluid, with initial volumetric concentrations $\Psi(X_{0_1}, t_0)$ and $\Psi(X_{0_2}, t_0)$, respectively. In the first time interval $\Delta t_1 = t_1 - t_0$, the individual probability densities for each of the unit volumes of fluid at (X_{0_1}, t_0) and (X_{0_2}, t_0) to diffuse into point (X_1, t_1) are $P(X_1, t_1 | X_{0_1}, t_0)$ and $P(X_1, t_1 | X_{0_2}, t_0)$, respectively. In the second time interval $\Delta t_2 = t_2 - t_1$, the individual probability densities for each of the contributions at (X_1, t_1) from (X_{0_1}, t_0) and (X_{0_2}, t_0) to re-diffuse into point (X_2, t_2) are $P(X_2, t_2 | X_1, t_1; X_{0_1}, t_0)$ and $P(X_2, t_2 | X_1, t_1; X_{0_2}, t_0)$, respectively, with their joint

probability density being $P(\mathbf{X}_2(\mathbf{X}_{0_1}), \mathbf{X}_2(\mathbf{X}_{0_2}), t_2 | \mathbf{X}_1, t_1)$.

Under the random fluid particle treatment, according to (2.4), the redistribution density $P_r(\mathbf{X}_2, t_2 | \mathbf{X}_1, t_1)$ of the scalar from (\mathbf{X}_1, t_1) to (\mathbf{X}_2, t_2) is determined as

$$P_r(\mathbf{X}_2, t_2 | \mathbf{X}_1, t_1) = \frac{\Psi(\mathbf{X}_{0_1}, t_0) \cdot P(\mathbf{X}_1, t_1 | \mathbf{X}_{0_1}, t_0) \cdot P(\mathbf{X}_2, t_2 | \mathbf{X}_1, t_1; \mathbf{X}_{0_1}, t_0) \cdot d\mathbf{X}_{0_1}}{\sum_{i=1}^2 \Psi(\mathbf{X}_{0_i}, t_0) \cdot P(\mathbf{X}_1, t_1 | \mathbf{X}_{0_i}, t_0) \cdot d\mathbf{X}_{0_i}} + \frac{\Psi(\mathbf{X}_{0_2}, t_0) \cdot P(\mathbf{X}_1, t_1 | \mathbf{X}_{0_2}, t_0) \cdot P(\mathbf{X}_2, t_2 | \mathbf{X}_1, t_1; \mathbf{X}_{0_2}, t_0) \cdot d\mathbf{X}_{0_2}}{\sum_{i=1}^2 \Psi(\mathbf{X}_{0_i}, t_0) \cdot P(\mathbf{X}_1, t_1 | \mathbf{X}_{0_i}, t_0) \cdot d\mathbf{X}_{0_i}} \quad (2.13)$$

If we let

$$\Psi_1 = \Psi(\mathbf{X}_{0_1}, t_0) \cdot P(\mathbf{X}_1, t_1 | \mathbf{X}_{0_1}, t_0) \cdot d\mathbf{X}_{0_1}$$

$$\Psi_2 = \Psi(\mathbf{X}_{0_2}, t_0) \cdot P(\mathbf{X}_1, t_1 | \mathbf{X}_{0_2}, t_0) \cdot d\mathbf{X}_{0_2}$$

$$\Psi = \Psi_1 + \Psi_2 = \sum_{i=1}^2 \Psi(\mathbf{X}_{0_i}, t_0) \cdot P(\mathbf{X}_1, t_1 | \mathbf{X}_{0_i}, t_0) \cdot d\mathbf{X}_{0_i}$$

(2.13) can then be written as

$$P_r(\mathbf{X}_2, t_2 | \mathbf{X}_1, t_1) = \frac{\Psi_1}{\Psi} \cdot P(\mathbf{X}_2, t_2 | \mathbf{X}_1, t_1; \mathbf{X}_{0_1}, t_0) + \frac{\Psi_2}{\Psi} \cdot P(\mathbf{X}_2, t_2 | \mathbf{X}_1, t_1; \mathbf{X}_{0_2}, t_0) \quad (2.14)$$

By definition, the mean vector E_r of the redistribution $P_r(\mathbf{X}_2, t_2 | \mathbf{X}_1, t_1)$ is calculated as

$$\begin{aligned}
\mathbf{E}_r &= \int_{-\infty}^{\infty} \mathbf{X}_2 \cdot P_r(\mathbf{X}_2, t_2 | \mathbf{X}_1, t_1) \cdot d\mathbf{X}_2 \\
&= \int_{-\infty}^{\infty} \mathbf{X}_2 \cdot \left(\frac{\Psi_1}{\Psi} \cdot P(\mathbf{X}_2, t_2 | \mathbf{X}_1, t_1; \mathbf{X}_{0_1}, t_0) + \frac{\Psi_2}{\Psi} \cdot P(\mathbf{X}_2, t_2 | \mathbf{X}_1, t_1; \mathbf{X}_{0_2}, t_0) \right) \cdot d\mathbf{X}_2 \\
&= \frac{\Psi_1 \cdot \mathbf{e}_1 + \Psi_2 \cdot \mathbf{e}_2}{\Psi} \tag{2.15}
\end{aligned}$$

with the individual mean vectors \mathbf{e}_1 and \mathbf{e}_2 defined as

$$\begin{aligned}
\mathbf{e}_1 &= \int_{-\infty}^{\infty} \mathbf{X}_2 \cdot P(\mathbf{X}_2, t_2 | \mathbf{X}_1, t_1; \mathbf{X}_{0_1}, t_0) \cdot d\mathbf{X}_2 \\
\mathbf{e}_2 &= \int_{-\infty}^{\infty} \mathbf{X}_2 \cdot P(\mathbf{X}_2, t_2 | \mathbf{X}_1, t_1; \mathbf{X}_{0_2}, t_0) \cdot d\mathbf{X}_2
\end{aligned}$$

The variance Ω_r^2 of $P_r(\mathbf{X}_2, t_2 | \mathbf{X}_1, t_1)$ is calculated as

$$\begin{aligned}
\Omega_r^2 &= \int_{-\infty}^{\infty} (\mathbf{X}_2 - \mathbf{E}_r)^2 \cdot P_r(\mathbf{X}_2, t_2 | \mathbf{X}_1, t_1) \cdot d\mathbf{X}_2 \\
&= \int_{-\infty}^{\infty} \left(\mathbf{X}_2 - \frac{\Psi_1 \cdot \mathbf{e}_1 + \Psi_2 \cdot \mathbf{e}_2}{\Psi} \right)^2 \cdot \frac{\Psi_1}{\Psi} \cdot P(\mathbf{X}_2, t_2 | \mathbf{X}_1, t_1; \mathbf{X}_{0_1}, t_0) \cdot d\mathbf{X}_2 \\
&\quad + \int_{-\infty}^{\infty} \left(\mathbf{X}_2 - \frac{\Psi_1 \cdot \mathbf{e}_1 + \Psi_2 \cdot \mathbf{e}_2}{\Psi} \right)^2 \cdot \frac{\Psi_2}{\Psi} \cdot P(\mathbf{X}_2, t_2 | \mathbf{X}_1, t_1; \mathbf{X}_{0_2}, t_0) \cdot d\mathbf{X}_2 \\
&= \frac{1}{\Psi^3} (\Psi_1^3 \cdot \sigma_1^2 + \Psi_2^3 \cdot \sigma_2^2) + \frac{\Psi_1 \cdot \Psi_2^2}{\Psi^3} \cdot \int_{-\infty}^{\infty} (\mathbf{X}_2 - \mathbf{e}_2)^2 \cdot P(\mathbf{X}_2, t_2 | \mathbf{X}_1, t_1; \mathbf{X}_{0_1}, t_0) \cdot d\mathbf{X}_2 \\
&\quad + \frac{\Psi_1^2 \cdot \Psi_2}{\Psi^3} \cdot \int_{-\infty}^{\infty} (\mathbf{X}_2 - \mathbf{e}_1)^2 \cdot P(\mathbf{X}_2, t_2 | \mathbf{X}_1, t_1; \mathbf{X}_{0_2}, t_0) \cdot d\mathbf{X}_2 \\
&\quad + \frac{2\Psi_1^2 \cdot \Psi_2}{\Psi^3} \cdot \int_{-\infty}^{\infty} (\mathbf{X}_2 - \mathbf{e}_1) \cdot (\mathbf{X}_2 - \mathbf{e}_2) \cdot P(\mathbf{X}_2, t_2 | \mathbf{X}_1, t_1; \mathbf{X}_{0_1}, t_0) \cdot d\mathbf{X}_2 \\
&\quad + \frac{2\Psi_1 \cdot \Psi_2^2}{\Psi^3} \cdot \int_{-\infty}^{\infty} (\mathbf{X}_2 - \mathbf{e}_1) \cdot (\mathbf{X}_2 - \mathbf{e}_2) \cdot P(\mathbf{X}_2, t_2 | \mathbf{X}_1, t_1; \mathbf{X}_{0_2}, t_0) \cdot d\mathbf{X}_2 \tag{2.16}
\end{aligned}$$

with the individual variances σ_1^2 and σ_2^2 defined as

$$\sigma_1^2 = \int_{-\infty}^{\infty} (\mathbf{X}_2 - \mathbf{e}_1)^2 \cdot P(\mathbf{X}_2, t_2 | \mathbf{X}_1, t_1; \mathbf{X}_{0_1}, t_0) \cdot d\mathbf{X}_2$$

$$\sigma_2^2 = \int_{-\infty}^{\infty} (\mathbf{X}_2 - \mathbf{e}_2)^2 \cdot P(\mathbf{X}_2, t_2 | \mathbf{X}_1, t_1; \mathbf{X}_{0_2}, t_0) \cdot d\mathbf{X}_2$$

By contrast, under the virtual fluid parcel treatment, the contribution to the center of gravity with respect to the scalar from (\mathbf{X}_1, t_1) to (\mathbf{X}_2, t_2) is determined according to (2.8) as

$$\mathbf{X}_2(\mathbf{X}_1) = \frac{\Psi_1}{\Psi} \cdot \mathbf{X}_2(\mathbf{X}_{0_1}) + \frac{\Psi_2}{\Psi} \cdot \mathbf{X}_2(\mathbf{X}_{0_2}) \quad (2.17)$$

If the marginal distribution densities of the joint distribution density $P(\mathbf{X}_2(\mathbf{X}_{0_1}), \mathbf{X}_2(\mathbf{X}_{0_2}), t_2 | \mathbf{X}_1, t_1)$ are approximated by $P(\mathbf{X}_2, t_2 | \mathbf{X}_1, t_1; \mathbf{X}_{0_1}, t_0)$ and $P(\mathbf{X}_2, t_2 | \mathbf{X}_1, t_1; \mathbf{X}_{0_2}, t_0)$ respectively, the mean vector \mathbf{E}_v and variance Ω_v^2 of the redistribution $P_v(\mathbf{X}_2, t_2 | \mathbf{X}_1, t_1)$ of (2.17) are calculated as (Derman, Gleser & Olkin 1973):

$$\mathbf{E}_v = \frac{\Psi_1 \cdot \mathbf{e}_1 + \Psi_2 \cdot \mathbf{e}_2}{\Psi} \quad (2.18)$$

$$\Omega_v^2 = \frac{\Psi_1^2 \cdot \sigma_1^2 + 2\Psi_1 \cdot \Psi_2 \cdot \sigma_{1,2} + \Psi_2^2 \cdot \sigma_2^2}{\Psi^2} \quad (2.19)$$

Here, the covariance $\sigma_{1,2}$ is defined as

$$\sigma_{1,2} = \int_{-\infty}^{\infty} \int_{-\infty}^{\infty} (\mathbf{X}_2(\mathbf{X}_{0_1}) - \mathbf{e}_1) \cdot (\mathbf{X}_2(\mathbf{X}_{0_2}) - \mathbf{e}_2) \cdot P(\mathbf{X}_2(\mathbf{X}_{0_1}), \mathbf{X}_2(\mathbf{X}_{0_2}), t_2 | \mathbf{X}_1, t_1) \cdot d\mathbf{X}_2(\mathbf{X}_{0_1}) \cdot d\mathbf{X}_2(\mathbf{X}_{0_2})$$

Comparing (2.15) with (2.18) and (2.16) with (2.19), we have

$$\mathbf{E}_v = \mathbf{E}_r \quad (2.20)$$

and

$$\Omega_v^2 \leq \Omega_r^2 \quad (2.21)$$

This indicates that, although both redistributions $P_v(\mathbf{X}_2, t_2 | \mathbf{X}_1, t_1)$ and $P_r(\mathbf{X}_2, t_2 | \mathbf{X}_1, t_1)$ have the same mean, the redistribution $P_v(\mathbf{X}_2, t_2 | \mathbf{X}_1, t_1)$ under the virtual fluid parcel treatment may generally have "narrower" distribution, with smaller variance, than the redistribution $P_r(\mathbf{X}_2, t_2 | \mathbf{X}_1, t_1)$ under the random fluid particle treatment

The direct comparison between (2.16) and (2.19) is structurally complex. It can be simplified by assuming

$$P(\mathbf{X}_2, t_2 | \mathbf{X}_1, t_1; \mathbf{X}_{0_1}, t_0) = P(\mathbf{X}_2, t_2 | \mathbf{X}_1, t_1; \mathbf{X}_{0_2}, t_0)$$

with $\mathbf{e}_1 = \mathbf{e}_2 = \mathbf{e}$ and $\sigma_1^2 = \sigma_2^2 = \sigma^2$.

Then, (2.15), (2.16), (2.18) and (2.19) are simplified as

$$\mathbf{E}_v = \mathbf{E}_r = \mathbf{e} \quad (2.22)$$

$$\begin{aligned} \Omega_r^2 &= \frac{\Psi_1^3 + 3\Psi_1 \cdot \Psi_2^2 + 3\Psi_1^2 \cdot \Psi_2 + \Psi_2^3}{\Psi^3} \cdot \sigma^2 \\ &= \sigma^2 \end{aligned} \quad (2.23)$$

and

$$\Omega_v^2 = \frac{\Psi_1^2 \cdot \sigma^2 + 2\Psi_1 \cdot \Psi_2 \cdot \sigma_{1,2} + \Psi_2^2 \cdot \sigma^2}{\Psi^2} \leq \sigma^2 \quad (2.24)$$

2.3. The effect of molecular mixing

In the above analysis, the mean \mathbf{E} and variance Ω^2 can be, respectively, interpreted as the center of gravity and the expansion with respect to the center of gravity of the re-diffusion cloud in a single time-step. Then, (2.20) and (2.21) suggest that molecular mixing may generally reduce the expansion of the re-diffusion cloud in a single time-step from the value it would have if molecular mixing was not incorporated into the description. This reduction, however, may not influence the center of gravity of the re-diffusion cloud. In other words, the expansion of the re-diffusion cloud in a single time-step would generally be exaggerated by the classical fluid particle treatment due to exclusion of molecular mixing. This analysis may confirm the notion that, as a controlling agent of the mixing mechanism, molecular mixing is important in every time-step of turbulent diffusion.

From (2.23) and (2.24), we may infer the following: In a laminar flow or a weakly turbulent flow with very low turbulence intensity, the constituent portions of any fluid element at any time should be relatively well correlated, i.e. $\sigma_{1,2} \rightarrow \sigma^2 \rightarrow 0$. Then, the variances of both redistributions $P_r(\mathbf{X}_2, t_2 | \mathbf{X}_1, t_1)$ and $P_v(\mathbf{X}_2, t_2 | \mathbf{X}_1, t_1)$ tend to vanish. This means negligible reduction of the expansion of the re-diffusion cloud in a single time-step by molecular mixing, or negligible exaggeration of the expansion of the re-diffusion cloud in a single time-step by the classical fluid particle treatment. In a flow with high turbulence intensity, however,

the constituent portions of any fluid element at any time may become less correlated, i.e. $\sigma_{1,2}$ decreases when σ^2 increases. Then, the redistribution $P_v(\mathbf{X}_2, t_2 | \mathbf{X}_1, t_1)$ becomes more narrowly distributed, with smaller variance, than the redistribution $P_r(\mathbf{X}_2, t_2 | \mathbf{X}_1, t_1)$. This implies a larger reduction of the expansion of the re-diffusion cloud in a single time-step by molecular mixing, or a more pronounced exaggeration of the expansion of the re-diffusion cloud in a single time-step by the classical fluid particle treatment.

According to (1.1)–(1.6) and (1.7)–(1.12), the above analysis should be applicable in any further time-step development, so that the effect of molecular mixing in reducing the expansion of any intermediate re-diffusion cloud should be continuously renewed. This effect is then accumulated with increasing time so as to change the evolution of the overall diffusion cloud and, simultaneously, the evolution of the mean concentration field. Given a sufficient length of time of accumulation, this change should in principle become experimentally observable.

Previously, scalar concentration fluctuations have been examined by studies which implicitly or explicitly incorporate molecular mixing with (Sawford & Hunt 1986; Stapountzis et al. 1986) or without (Durbin 1980) consideration of the molecular collision-transport (i.e. the molecular momentum and scalar collision transports ν and κ). Their results showed that the decay of scalar concentration fluctuations, in comparison with the fluid particle model (one-particle or "inner limit" two-particle relative dispersion (Durbin 1980)), is mainly caused by molecular mixing, although the molecular collision-transport also have noticeable effects (shown by Sawford & Hunt 1986; Stapountzis et al. 1986). However, these studies were implicitly or explicitly based on the assumption that the influence on the mean concentration field by molecular mixing can be ignored. According to our analysis presented above, this assumption may not be justified. It is usually

supported, in its turn, by a further assumption that the fluid particles move at the local Eulerian fluid velocity (such as Sawford & Hunt 1986, Thomson 1990) This may be inappropriate because, having implicitly incorporated molecular mixing by this second assumption, their fluid elements (moving at the local Eulerian fluid velocity) can only be regarded as virtual fluid parcels (Part 2) In our previous study (Part 1), it has been shown that under the random fluid particle treatment, the assumption of the statistical equivalence between the Lagrangian variables of a single fluid particle and the Eulerian variables at one space-time point is not generally satisfied.

3. Experimental test

3.1 Design

In this section, the results of the above analysis about the effect of molecular mixing are tested in passive scalar turbulent diffusion experiments In order to simulate the situations used in the analysis, and to assure sufficient physical overlap of plumes, the experiments are arranged in two sub-designs, explained in Figure 1..

In the first sub-design, three single instantaneous point sources of a passive scalar are separately released at positions S1, S2 and S3, and their individual diffusion puffs are separately measured at sensor positions In the second sub-design, the instantaneous point source of the passive scalar at S1 is released first. When its center of puff reaches S2, the instantaneous point source at S2 is released. When the center of the joint puff from S1 and S2 reaches S3, the instantaneous point source at S3 is released, Then, the joint diffusion puff from S1, S2 and S3 is observed at sensor positions. The time delays for release of puffs in the second sub-design are estimated from mean flow velocity and source spacings.

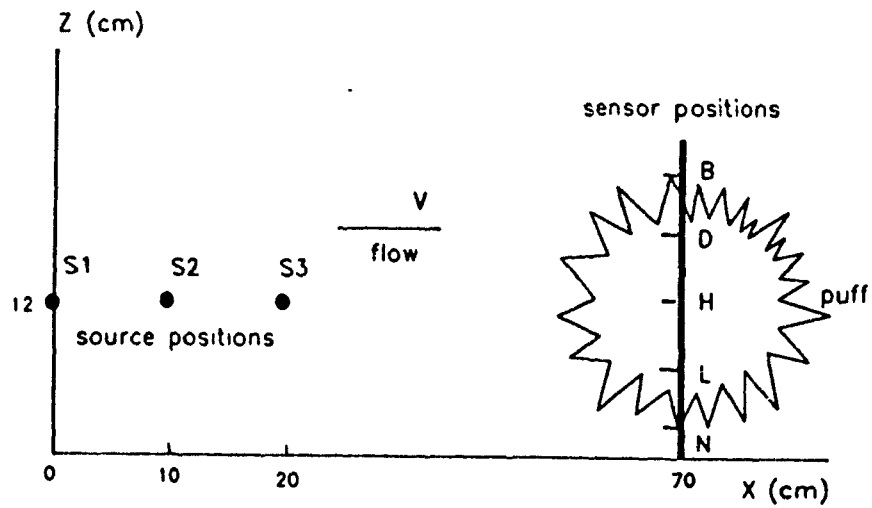


Figure 1. Design of experiments.

The result from the second sub-design would naturally involve molecular mixing between the overlapping puffs developed from S1, S2 and S3, which is the major concern of the virtual fluid parcel treatment. Therefore, the overall diffusion cloud from this sub-design would in principle be expected to be simulated by the virtual fluid parcel description. Under the random fluid particle treatment, however, the overall diffusion is calculated as the statistical superimposition of the contributions from the separate puffs developed from the individual point sources S1, S2 and S3. In the case of passive scalar diffusion, this superimposition is reduced to an independent summation of the separate diffusion puffs from the three point sources, as measured in the first sub-design (Part 1)

3.2. Setup

The experiments were carried out in a closed-circuit water tunnel generally used for electrochemical simulations of heat or mass transfer (e.g. Schuepp 1989). Flow straighteners and 1.2×1.2 mm square-mesh screen precede a working section 110 cm long (x), 28 cm wide (y) and 28 cm high (z), as shown in Figure 2

The source material was a dilute NaOH solution, with concentration equal to 1% of saturation (0.01g/ml, NaOH /H₂O), injected at the source positions by syringes, as approximate instantaneous point sources with constant volumes of about 0.5 cm³. The ions of the source material acted as tracers to be detected by the measurement sensors. Because buoyancy and gravitational settling of the source solution were negligibly small, the source material could be considered to be passive.

The measurement sensors were manufactured by open ends of Cu-K thermocouple wires (1.2 mm diameter), used as electrodes connected to a simple 5V DC loaded circuit. Since the voltage drop between the two electrodes depends

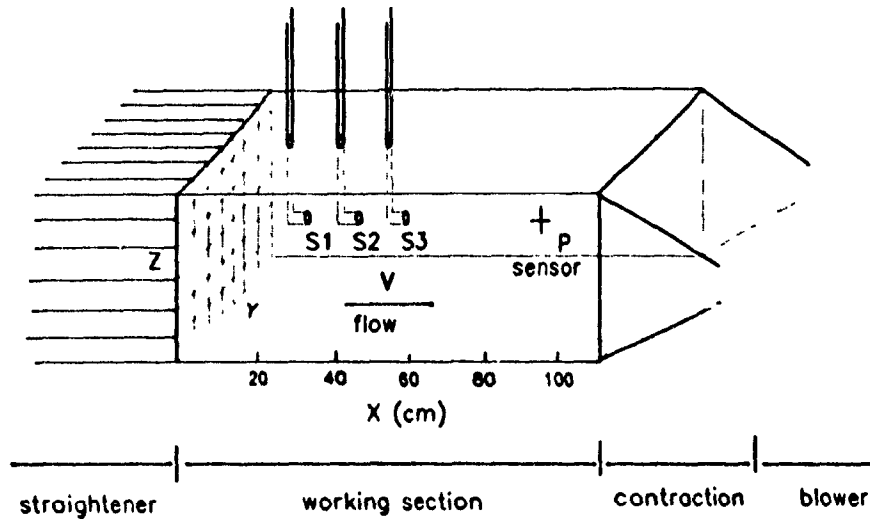


Figure 2. Schematic diagram of the experimental arrangement.

on the ion concentration around the sensor, changes of concentrations are measured as voltage changes. The measurement sensors were calibrated in standard solutions.

Water flow in the central streamline of the working section of the water tunnel was set at a stationary mean velocity of $15 \text{ cm}\cdot\text{s}^{-1}$, with a moderate turbulence intensity (a ratio of mean velocity to the root-mean-squared velocity fluctuations) around 0.1. To avoid boundary effects, the sources were introduced into the working section at points S1, S2 and S3 with 10 cm spacing along the central streamline, through fine tubes penetrating the ceiling of the tunnel. The measurement sensor array was located at P, 50 cm downstream from source S3, where a sufficient length of time of accumulation of molecular mixing effect in the diffusion puff evolution could be expected.

The measurement sensor array is shown in Figure 3. Principal sensors, represented by letters B ... N, were fixed with spacing of 4 cm, and supplementary sensors, represented by $A_1 \dots A_{12}$, were movable. The puffs of NaOH released from the three point sources were expected to hit the center of the array.

Measurements were recorded by CR7X datalogger (Campbell Scientific Inc. model 700) at a frequency of 11 Hz, continuously for 10 s. This sampling interval was sufficient to cover the passage of the diffusion puffs in each experimental run. The recorded signals were transferred to a IBM PC disk storage for analysis. Experiments in both sub-designs were repeated 10 times.

3.3. Results

Figure 4 shows the integrated two-dimensional representations of the observed diffusion puff distributions across the yz plane for the two sub-designs. They were constructed from integrations of the time series of sensor measurement output, covering the full passage of the puffs. Results are shown in flat contour and solid

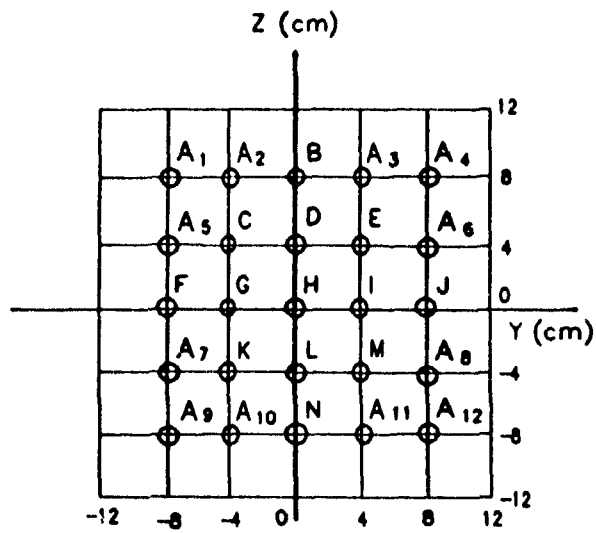
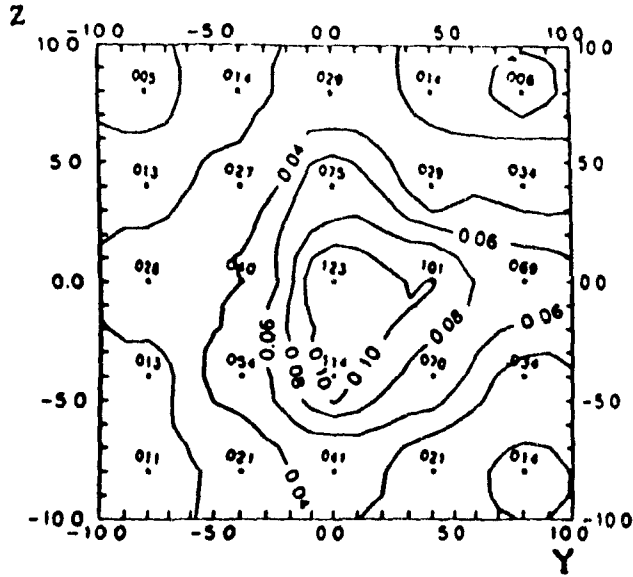
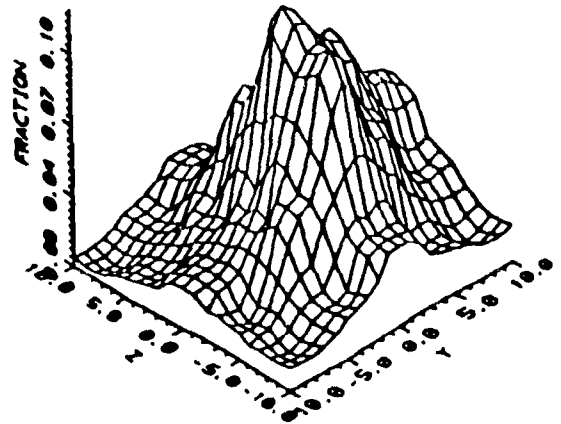


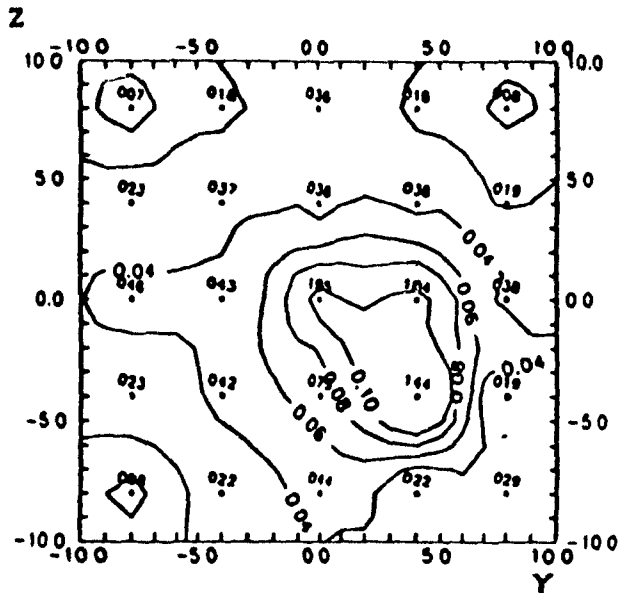
Figure 3. The arrangement of principal measurement sensors B to N and supplementary measurement sensors A₁ to A₁₂.



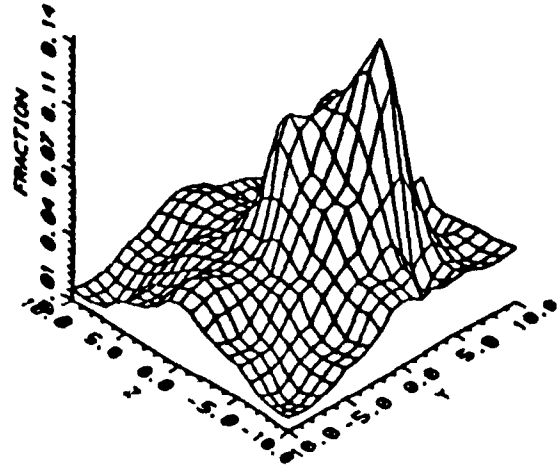
(a1)



(b1)



(a2)



(b2)

Figure 4. The integrated two-dimensional contour (a) and surface (b) plots of the natural joint diffusion distribution P_n of the joint puff measured in the second sub-design (a1 and b1), and the diffusion distribution P_r calculated in principle of the statistical superimposition of the separate puffs individually measured in the first sub-design (a2 and b2), averaged from 10 repetitions. * gives data position.

surface graphs.

Due to imprecise release timing in the second sub-design, the centers of the puffs from the three point sources may not overlap perfectly. The resulting error may, to some degree, enlarge the variance of the natural joint puff distribution in the second sub-design. This would reduce the difference in variances between the natural joint puff distribution in the second sub-design and the one processed in the statistical superimposition of the results from the first sub-design. Moreover, there may exist an internal "contamination" in the first sub-design due to already-existing molecular mixing in the individual puffs from the individual point sources. This "contamination" would also, to some degree, reduce the difference in variances between the natural joint puff distribution in the second sub-design and the one processed in the statistical superimposition of the results from the first sub-design. Quantitative estimation of these errors is, unfortunately, not possible in our experiments. Without these errors, however, the difference in variances between the two treatments should be more observable.

Nevertheless, a non-negligible difference in variances between the two treatments in our experiments is still observed, so that our experimental confirmation of such difference is, at least, qualitatively meaningful.

In our experiments, the means $E_{y'n}$ and $E_{z'n}$ and the variances $\Omega_{y'n}^2$ and $\Omega_{z'n}^2$ of the natural joint puff distribution from the second sub-design (the subscript n denotes the natural joint distribution), and the means $E_{y'r}$ and $E_{z'r}$ and the variances $\Omega_{y'r}^2$ and $\Omega_{z'r}^2$ of the diffusion distribution processed in the statistical superimposition of the results from the first sub-design, are observed as

$$\begin{aligned} E_{y'n} &= 0.82 \text{ cm} & E_{z'n} &= -0.81 \text{ cm} \\ E_{y'r} &= 0.70 \text{ cm} & E_{z'r} &= -0.90 \text{ cm} \end{aligned}$$

and

$$\Omega_{y'n}^2 = 18.13 \text{ cm}^2 \quad \Omega_{z'n}^2 = 17.33 \text{ cm}^2$$

$$\Omega_{y'r}^2 = 21.36 \text{ cm}^2 \quad \Omega_{z'r}^2 = 20.93 \text{ cm}^2$$

where the hypotheses $E_{y'n} = E_{y'r}$, $E_{z'n} = E_{z'r}$, $\Omega_{y'n}^2 < \Omega_{y'r}^2$ and $\Omega_{z'n}^2 < \Omega_{z'r}^2$ are accepted, respectively, with confidence levels 95%, 95%, 65% and 65% in U-tests (Gaussian) and F-tests.

These experimental results qualitatively confirm the analysis in the preceding section. They lend support to the notion that molecular mixing in the natural joint diffusion tends to reduce the diffusion distribution variance, in agreement with the prediction by the virtual fluid parcel treatment. It indicates that the diffusion processed in statistical superimposition under the classical random fluid particle treatment exaggerates the natural joint diffusion by overestimating the diffusion distribution variance, in the same way as it exaggerates the diffusion distribution described by the virtual fluid parcel treatment. It would then appear to confirm the inference stated in the Introduction

4. Conclusion

This study suggests that molecular mixing in turbulent diffusion persistently and cumulatively influences the evolution of the diffusion cloud, and thus influences the evolution of the mean concentration field, by reducing the diffusion distribution variance. This suggestion is presented through a comparison of the classical random fluid particle treatment with the new virtual fluid parcel treatment of the BMDFE, in application to the description of the diffusion cloud evolution on the level of single time-step diffusion redistribution.

According to this suggestion, the description under the random fluid particle

treatment would generally exaggerate the diffusion distribution variance due to exclusion of molecular mixing. This is supported by experiments of passive scalar diffusion in water flow with moderate turbulence intensity. It would then appear to confirm that the virtual fluid parcel treatment, with incorporation of molecular mixing, is more realistic in its description of turbulent diffusion than the classical random fluid particle treatment.

REFERENCES

- Chatwin, P.C. & Sullivan, P.J. 1979 The relative diffusion of a cloud of passive contaminant in incompressible turbulent flow. *J. Fluid Mech.* **91**, 337-355.
- Derman, C., Gleser, L. & Olkin, I. 1973 *A Guide to Probability Theory and Application*. Holt, Rinehart and Winston, Inc., New York.
- Durbin, P.A. 1980 A stochastic model of two-particle dispersion and concentration fluctuations in homogeneous turbulence. *J. Fluid Mech.* **100**, 279-302.
- Kaplan, H. & Dinar, N. 1988 A stochastic model for dispersion and concentration distribution in homogeneous turbulence. *J. Fluid Mech.* **190**, 121-140.
- Monin, A.S. & Yaglom, A.M. 1971 *Statistical Fluid Mechanics: Mechanics of Turbulence*, vol. I. MIT Press, Cambridge, Mass.
- Saffman, P.G. 1960 On the effect of the molecular diffusivity in turbulent diffusion. *J. Fluid Mech.* **8**, 273-283.
- Sawford, B.L. & Hunt, J.C.R. 1986 Effects of turbulence structure, molecular diffusion and source size on scalar fluctuations in homogeneous turbulence. *J. Fluid Mech.* **165**, 373-400.
- Schuepp, P.H. 1989 Microstructure, density and wetness effects on dry deposition to foliage. *Agric. and Forest Meteor.* **47**, 179-198.
- Stapountzis, H., Sawford, B.L., Hunt, J.C.R. and Britter, R.E. 1986 Structure of the temperature field downwind of a line source in grid turbulence. *J. Fluid Mech.* **165**, 401-424.
- Thomson, D.J. 1990 A stochastic model for the motion of particle pairs in isotropic high-Reynolds-number turbulence and its application to the problem of concentration variance. *J. Fluid Mech.* **210**, 113-153.
- Part 1 (attached Y. Guo, 1991): The role of molecular mixing in the description of turbulent diffusion in fluid continuum. Part 1. The limitation of the fluid particle treatment.
- Part 2 (attached Y. Guo, 1991): The role of molecular mixing in the description of turbulent diffusion in fluid continuum. Part 2. The virtual fluid parcel treatment.

Part 4. A Preliminary Simulation of Scalar Turbulent Diffusion under the Virtual Fluid Parcel Treatment

Abstract

A preliminary simplified numerical modeling of scalar turbulent diffusion, based on the virtual fluid parcel treatment of the BMDFE (Basic Macroscopically Describable Fluid Element), is presented. It uses direct experimental observation to estimate the fractional redistribution density of the scalar, to bypass technical difficulties in solving the disintegration equation.

This simplified scheme approximates the fractional redistribution of the scalar by the fractional redistribution of fluid volume, calculated from the probability density distribution of the local real-time Eulerian velocity. It also assumes that sub-grid scale motion, ignored by the discrete Eulerian velocity measurements, is recovered by linear and/or proportional interpolation. Comparison of numerical model predictions against experimental simulation of ammonia diffusion in wind tunnel models shows encouraging general agreement, particularly in the case of low turbulence intensity.

1. Introduction

An exploratory virtual fluid parcel treatment has been proposed in our previous study (Part 2), which conceptually incorporates molecular mixing by permitting disintegration of individual BMDFEs (Basic Macroscopically Describable Fluid Element) in turbulent fluids. This treatment is expected to improve the classical random fluid particle treatment in the description of turbulent diffusion, by introducing a feedback mechanism through physically coupled disintegrations and integrations of the BMDFEs (Part 2, Part 3) It describes turbulent diffusion, in successive time steps, through cascaded integration of the fractional contributions from continuously disintegrating virtual fluid parcels in the flow. For scalar diffusion in an incompressible fluid, this description is given by the following recurring joint equations (Part 2):

$$\begin{aligned} & \frac{\partial}{\partial s} \bar{\Psi}(\mathbf{Y}, t_i + s; \mathbf{X}, t_i) + (\bar{\mathbf{V}}(\mathbf{Y}, t_i + s; \mathbf{X}, t_i) \cdot \nabla_{\mathbf{y}}) \cdot \bar{\Psi}(\mathbf{Y}, t_i + s; \mathbf{X}, t_i) \\ & = \kappa \cdot \nabla_{\mathbf{y}}^2 \cdot \bar{\Psi}(\mathbf{Y}, t_i + s; \mathbf{X}, t_i) - \overline{(\mathbf{V}'(\mathbf{Y}, t_i + s; \mathbf{X}, t_i) \cdot \nabla_{\mathbf{y}}) \cdot \Psi'(\mathbf{Y}, t_i + s; \mathbf{X}, t_i)} \\ & + (\Psi(\mathbf{X}, t_i) + \mathbf{E}(\mathbf{X}, t_i) \cdot \Delta t) \cdot \delta(\mathbf{Y} - \mathbf{X}) \cdot \delta(s) \\ & \quad (0 \leq s \leq \Delta t) \end{aligned} \quad (1.1)$$

$$F_C(\mathbf{Y}, t_{i+1} | \mathbf{X}, t_i) = \frac{\bar{\Psi}(\mathbf{Y}, t_{i+1}; \mathbf{X}, t_i)}{\Psi(\mathbf{X}, t_i) + \mathbf{E}(\mathbf{X}, t_i) \cdot \Delta t} \quad (1.2)$$

$$\Psi(\mathbf{Y}, t_{i+1}) = \int (\Psi(\mathbf{X}, t_i) + \mathbf{E}(\mathbf{X}, t_i) \cdot \Delta t) \cdot F_C(\mathbf{Y}, t_{i+1} | \mathbf{X}, t_i) \cdot d\mathbf{X} \quad (1.3)$$

$$t_{i+1} = t_i + \Delta t, \quad i = 0, 1, 2, \dots$$

Terms in these equations are defined as follows: $\bar{\mathbf{V}}(\mathbf{Y}, t_i + s; \mathbf{X}, t_i)$ and $\bar{\Psi}(\mathbf{Y}, t_i + s; \mathbf{X}, t_i)$

are the approximate fractional contributions to the velocity and volumetric concentration of scalar of the virtual fluid parcel at $(\mathbf{Y}, t_i + s)$ from the unit volume virtual fluid parcel at (\mathbf{X}, t_i) , respectively. $\mathbf{V}'(\mathbf{Y}, t_i + s; \mathbf{X}, t_i)$ and $\Psi'(\mathbf{Y}, t_i + s; \mathbf{X}, t_i)$ are the deviations from $\bar{\mathbf{V}}$ and $\bar{\Psi}$, respectively. $F_C(\mathbf{Y}, t_{i+1} | \mathbf{X}, t_i)$ is the fractional redistribution density coefficient for scalar disintegrated from the virtual fluid parcel at (\mathbf{X}, t_i) and then mixed into the unit volume virtual fluid parcel at (\mathbf{Y}, t_{i+1}) . $E(\mathbf{X}, t_i)$ is the (Eulerian) external volumetric source strength of scalar at (\mathbf{X}, t_i) . $\Psi(\mathbf{X}, t_i)$ and $\Psi(\mathbf{Y}, t_{i+1})$ are the (Eulerian) volumetric concentrations of scalar at (\mathbf{X}, t_i) and (\mathbf{Y}, t_{i+1}) respectively. Δt is the time interval comparable to the minimum period of the significant fluctuation of the scalar volumetric concentration $\Psi(\mathbf{X}, t_i)$. κ is the molecular collision-transport coefficient for scalar. $\nabla_{\mathbf{Y}}$ and $\nabla_{\mathbf{Y}}^2$ are del operator and the Laplace operator with respect to \mathbf{Y} , respectively, and δ is the Dirac delta function.

In practice, however, the solution of (1.1) may involve technical difficulties in the nonlinearity of the equation and in the parameterization of the flow character with macroscopic inhomogeneity of both flow scale and turbulence intensity (e.g. Thomson 1984; van Dop, Nieuwstadt & Hunt 1985; Sawford 1986; Pope 1987; Jones & Musong 1988; Luhar & Britter 1989). Up to now, successful solutions to these difficulties have not generally been available.

This preliminary test of the virtual fluid parcel treatment is based on a simplified numerical modeling, where measurements are used to bypass some of the difficulties in solving (1.1). In particular, the fractional redistribution density $F_C(\mathbf{Y}, t_{i+1} | \mathbf{X}, t_i)$, will be directly estimated from observations of the velocity field. Such simplified numerical modeling should be feasible, in principle, because the information required is obtainable through Eulerian measurements, although approximations may have to be used for reasons of practical convenience.

The simplified numerical modeling is applied to the diffusion of ammonia (NH_3) from a continuous point source in two wind tunnel models, representing open-surface and plant canopy, respectively. A corresponding type of numerical simulation under the classical random fluid particle treatment cannot be executed because of our current inability to obtain direct and reliable Lagrangian measurements. Therefore, the predictions of this study cannot be compared against those of the classical random fluid particle approach. Instead, this study is limited to the first practical application of the virtual fluid parcel treatment to a situation where the numerical predictions can be tested against experimental observations.

2. Alternative approximate disintegration

Generally, $F_C(\mathbf{Y}, t_{i+1} | \mathbf{X}, t_i)$ must be linked to the fractional redistribution density of the virtual fluid parcel volume. As a very rough approximation, we may use the latter to estimate $F_C(\mathbf{Y}, t_{i+1} | \mathbf{X}, t_i)$ for reasons of practical convenience, under the implied assumptions that the scalar is completely mixed in every virtual fluid parcel at any time, and that the redistribution of the scalar perfectly follows the redistribution of fluid volume. Given that the virtual fluid parcel is defined in such a way that it always moves at the local Eulerian fluid velocity (Part 2), the displacements $\mathbf{Y} - \mathbf{X}$ of the disintegrated fragments of fluid volume from the virtual fluid parcel at (\mathbf{X}, t_i) can be approximated, under assumption of ergodicity, by the measurements of the local real-time Eulerian velocity $\mathbf{V}(\mathbf{X}, t_i)$ during the small time interval Δt . We then have

$$\mathbf{Y} - \mathbf{X} = \mathbf{V}(\mathbf{X}, t_i) \cdot \Delta t \quad (2.1)$$

and $F_C(\mathbf{Y}, t_{i+1} | \mathbf{X}, t_i)$ can be estimated as

$$\begin{aligned}
 F_C(\mathbf{Y}, t_{i+1} | \mathbf{X}, t_i) &= P_{\mathbf{V}}(\mathbf{V} | \mathbf{X}, t_i) \cdot \frac{1}{\Delta t^3} \\
 &= P_{\mathbf{V}}\left(\frac{\mathbf{Y} - \mathbf{X}}{\Delta t} | \mathbf{X}, t_i\right) \cdot \frac{1}{\Delta t^3}
 \end{aligned}
 \tag{2.2}$$

Here $P_{\mathbf{V}}(\mathbf{V} | \mathbf{X}, t_i)$ is the probability density distribution of the local real-time Eulerian velocity measurements at space-time point (\mathbf{X}, t_i) . If the frequency-response of the measurement sensor is sufficiently high, $P_{\mathbf{V}}(\mathbf{V} | \mathbf{X}, t_i)$ can be statistically determined from a large number of observations.

It should be emphasized here, that the classical random fluid particle treatment does not provide theoretical access to the above approximation. It has been shown in our previous study (Part 1), that under the random fluid particle treatment the assumption of the statistical equivalence between the Lagrangian variables of a fluid particle and the Eulerian variables at one space-time point is not generally satisfied due to the multi-to-one Lagrangian-Eulerian transformations.

Multiplying both sides of (2.2) by $d\mathbf{Y}$, we have

$$F_C(\mathbf{Y}, t_{i+1} | \mathbf{X}, t_i) \cdot d\mathbf{Y} = P_{\mathbf{V}}\left(\frac{\mathbf{Y} - \mathbf{X}}{\Delta t} | \mathbf{X}, t_i\right) \cdot d\mathbf{V}
 \tag{2.3}$$

This means that the volume redistribution $F_C(\mathbf{Y}, t_{i+1} | \mathbf{X}, t_i) \cdot d\mathbf{Y}$ is equivalent to the velocity distribution $P_{\mathbf{V}}(\mathbf{V} | \mathbf{X}, t_i) \cdot d\mathbf{V}$ under the following scale transform

$$\Delta t = \frac{dx}{du} = \frac{dy}{dv} = \frac{dz}{dw}
 \tag{2.4}$$

where the time step Δt could be interpreted as the time grid size, expressed as a function of the space grid size (dx , dy and dz) and the velocity grid size (du , dv

and dw).

With the above approximation, the joint equations (1.1)–(1.3) are simplified as

$$F_C(\mathbf{Y}, t_{i+1} | \mathbf{X}, t_i) = P_{\mathbf{V}}\left(\frac{\mathbf{Y} - \mathbf{X}}{t_{i+1} - t_i} | \mathbf{X}, t_i\right) \cdot \frac{1}{(t_{i+1} - t_i)^3} \quad (2.5)$$

$$\Psi(\mathbf{Y}, t_{i+1}) = \int (\Psi(\mathbf{X}, t_i) + \mathbf{E}(\mathbf{X}, t_i) \cdot \Delta t) \cdot F_C(\mathbf{Y}, t_{i+1} | \mathbf{X}, t_i) \cdot d\mathbf{X} \quad (2.6)$$

$$t_{i+1} = t_i + \Delta t, \quad i = 0, 1, 2, \dots$$

Their numerical solutions require information about the probability density distribution $P_{\mathbf{V}}(\mathbf{V} | \mathbf{X}, t_i)$ of the local real-time Eulerian velocity, the external source strength $\mathbf{E}(\mathbf{X}, t_i)$ of the scalar, the initial volumetric concentration distribution $\Psi(\mathbf{X}_0, t_0)$ and appropriate boundary conditions.

3. Experimental details

3.1. Laboratory set-up

An open-top and open-ended laboratory wind tunnel was constructed, with 3:1 volume contraction over a 50 cm section of flow straighteners, and $1.2 \times 1.2 \text{ mm}^2$ square-mesh grid screen upstream of a working section 240 cm long (x), 43.2 cm wide (y) and 32 cm high (z), as shown in Figure 1a.

Two types of physical models were used: open-surface (empty tunnel) and artificial plant canopy, respectively. The open-surface consists of a wooden board commensurate with the size of the wind tunnel floor. The artificial canopy is

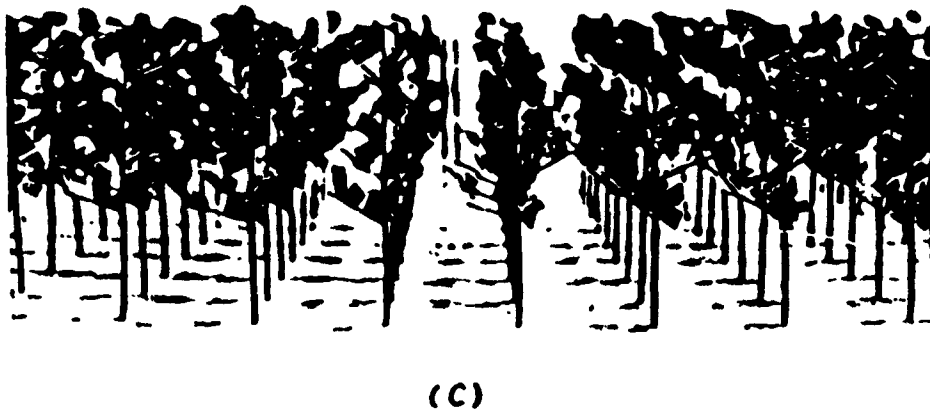
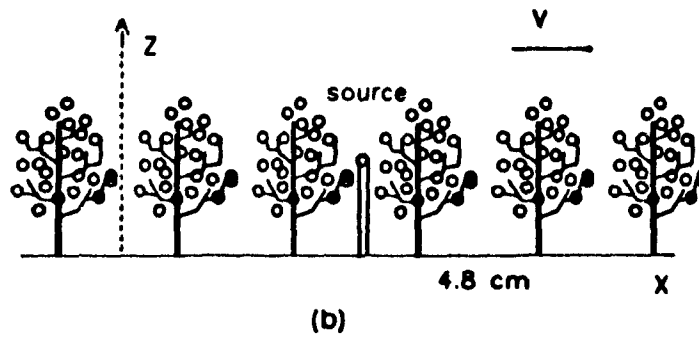
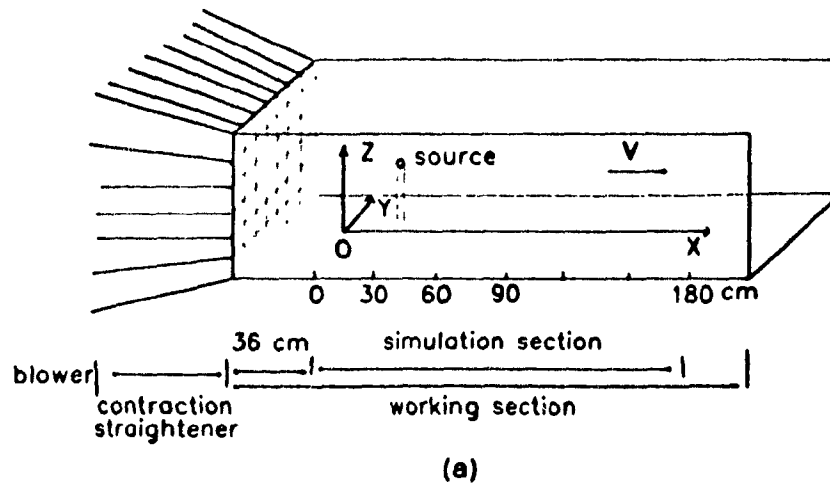


Figure 1. Schematic diagram of wind tunnel (a), artificial plant canopy diagram (b) and photograph (c).

composed of an array of small artificial trees installed in a regular square cell pattern of 4.8 cm spacing (Figures 1b,c), over a length (x) of 182.4 cm and width (y) equal to that of the wind tunnel. Trunk, branches and leaves of artificial trees are made of 2 mm diameter wire, 0.5 mm diameter wire and $6 \times 12 \text{ mm}^2$ rigid paper strips, respectively. Each tree is 11 cm tall, with 5 cm trunk and $2.4 \times 2.4 \times 6 \text{ cm}^3$ crown.

To avoid leading and tailing edge effects, the area used for simulations (simulation section) starts at 36 cm into the working section, and ends at 160.8 cm and 218.4 cm, respectively, for canopy and open-surface models. Coordinate origins are defined by the start of the simulation section ($x = 0$), the central streamline ($y = 0$) and the surface ($z = 0$).

An external continuous point source was introduced in both models, located at position $x = 4.8 \text{ cm}$, $y = 0.0 \text{ cm}$, $z = 9.6 \text{ cm}$, along the central streamline for open-surface, and at the center of the central cell pattern for the canopy model (Figure 1b). The source location splits the simulation section into two symmetrical parts about the central xz plane ($y = 0$). Source material is a 98% ammonia (NH_3) solution, introduced by a small glass tube with 38.5 mm^2 opening on the top.

To assure a relatively steady plume development, winds in both models were set stationary with free-stream velocity $U_\infty = 210 \text{ cm}\cdot\text{s}^{-1}$. Simulations started at initial time t_0 when the simulation sections were clean of external source material, i.e. $\Psi(x_0, t_0) = 0$. Since the simulations were not aimed at any specific application, no special boundary treatment was imposed. Boundary conditions on both sides and at the bottom of the models were assumed to be elastic reflections, and the thermal stratification measured to be neutral.

The results of the experimental simulations were directly measured as NH_3 concentration distributions of the steady plumes, at measurement positions shown

in Figure 2. Since the plumes are symmetrical about the central xz plane ($y = 0$), only one side ($y \geq 0$) of the plumes was measured. Measurement positions were arranged in six profiles, three on the xz plane at $y = 0$, three on the xz plane at $y = 9.6$ cm, with five sensors per profile. Sensors were located at centers of cell patterns in the canopy model.

3.2. Measurements

The NH_3 concentration Ψ in the experimental simulations was measured through an air sampling system, consisting of sampling tubes, plastic tubing and vacuum pumps. The sampling tubes were silica gel absorbent tubes, 7 cm long, 4 mm inner diameter and 6 mm outer diameter (Supelco Chromatography Supplies, ORBO-52, 1987), functioning like NH_3 filters. During sampling, they were mounted at the measurement positions (Figure 2), pointing open-ended into the prevailing wind, with the downwind opening connected through 4 mm diameter plastic tubings to two vacuum pumps. Airflow in the sampling tubes was controlled and adjusted to approximate local flow speed. For calculation of concentration, air flow F ($\text{L} \cdot \text{min}^{-1}$) for each sampling tube was measured by flow meter (Union Carbide Corp., Model 201-4334).

After simultaneous sampling of the steady plumes for one minute, sampling tubes were disconnected and sealed at both ends. The silica gel absorbent in each sampling tube was washed into 10 mL of water, in which the NH_3 concentration Ψ_S ($\text{mol} \cdot \text{L}^{-1}$) was measured by pH meter (Fisher Accumet, Model 610) with Ammonia Electrode (ORION 951000, 1978). Due to the wide range of NH_3 concentrations, two calibrated ammonia electrodes were used. One is filled with normal ammonium chloride solution (ORION 951006), covering the Ψ_S range from 10^{-2} to 10^{-7} $\text{mol} \cdot \text{L}^{-1}$, the other diluted half-normal ammonium chloride solution, covering the

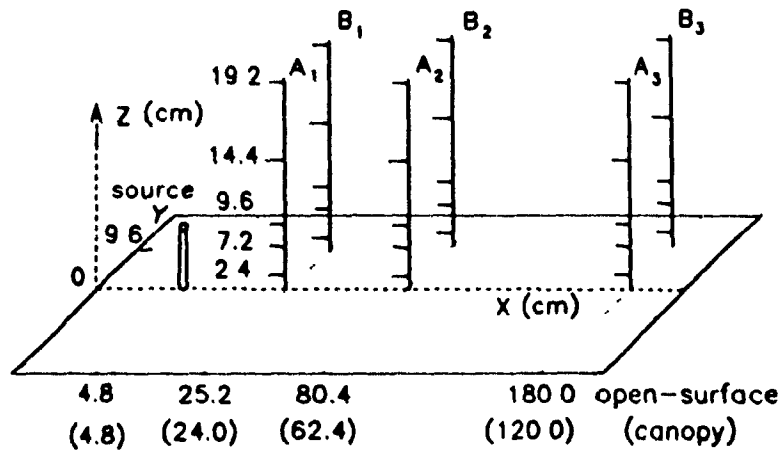


Figure 2. The arrangements of concentration measurement positions: A₁, A₂, A₃, B₁, B₂ and B₃ are measurement profiles, each with five sensors at levels of 2.4, 7.2, 9.6, 14.4 and 19.2 cm respectively. Sensors are located at centers of cell patterns in the canopy model.

Ψ_s range from 10^{-7} to 10^{-12} mol·L⁻¹. The final mean NH₃ concentration Ψ in the steady plumes is calculated as

$$\Psi = \frac{0.1703 \cdot \Psi_s}{F} \quad (\text{mg} \cdot \text{cm}^{-3})$$

The strength E of the continuous point source of NH₃ was determined from the evaporation rate of NH₃, which is the product of the specific weight of NH₃ solution and the volumetric evaporation rate. The specific weight was measured as 714.9 mg·ml⁻¹ and the volumetric evaporation rate read from the scales of the glass tube of the source solution. Because airflow conditions in both models were stationary, E was found to be very steady over the time intervals concerned, at 0.0834 mg·s⁻¹·cm⁻³ and 0.0477 mg·s⁻¹·cm⁻³ for the open-surface and canopy models, respectively.

The three components (u , v , w) of the Eulerian wind velocity were measured by three mutually perpendicular hot-film sensors, as shown in Figure 3a, and the directions in v and w determined by another two pairs of mutually perpendicular hot-film sensors, as shown in Figures 3b and 3c. Hot-film sensors were 2 mm long, 0.025 mm in diameter, with 20 KHz frequency response (Thermo-Systems Inc., Model 1210-20).

The hot-film sensor output from constant-temperature anemometers (Thermo-Systems Inc., Model 1050) with 2KHz low-pass filters and linearizers, was digitized by a data acquisition and control system interfaced with IBM PC (Tecmar Incorporated, 5712 module, 1984) and sampled at 1000 Hz continuously for 10 seconds at each measurement position. The sampled signals were converted into time series, which were used to calculate the probability density distributions

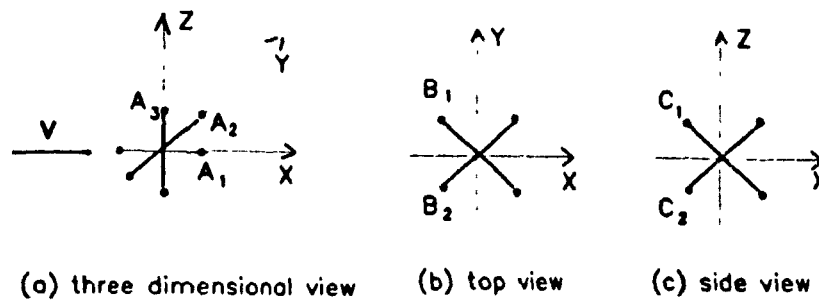


Figure 3. The design of hot-film sensors for the measurement of the value of the three components of the Eulerian wind velocity (a), the direction of v (b) and the direction of w (c). A_1 , A_2 , A_3 , B_1 , B_2 , C_1 and C_2 are sensors.

$P_V(\mathbf{v}|\mathbf{x},t_i)$ of the Eulerian wind velocity.

Some measured aerodynamic features are summarized in Figure 4. In the open-surface model, the flow is shown to be weakly turbulent with relatively big mean velocity and relatively small turbulence intensity. In the canopy model, however, the mean velocity is reduced by the canopy crown and consequently transformed into higher turbulence intensity. The along-wind and cross-wind variations of mean velocity and turbulence intensity in both models are shown to be small except near the boundaries. This is contrasted by the dramatic vertical variations. In the open-surface model, the mean velocity logarithmically increases from the surface to a height of 15 cm then decreases to the top (Figure 4 a3), while the turbulence intensity profile shows a pronounced dip between 3 and 15cm (Figure 4 b3). The relative reduction in mean wind and increase in turbulence intensity, in the canopy model, are shown in Figures 4 a3 and 4 b3, respectively.

Similar phenomena are reflected in the spectra of Figure 5. In the open-surface model, the down-transport of energy is normally cascaded from the height of 15cm to the surface. In the canopy model, however, this down-transport of energy is resisted by the canopy crown and, consequently, large eddies are broken into small eddies by canopy elements with their dominant scales (near the peaks of the spectra) shifted to smaller values (higher frequencies).

4. Numerical details

4.1. Interpolations

In order to run the numerical simulations based on (2.5) and (2.6), the input information of external source strength and Eulerian velocity, synchronized with the plume development, must be provided. In principle, detailed real-time observations of the Eulerian velocity are required at all spatial positions in the

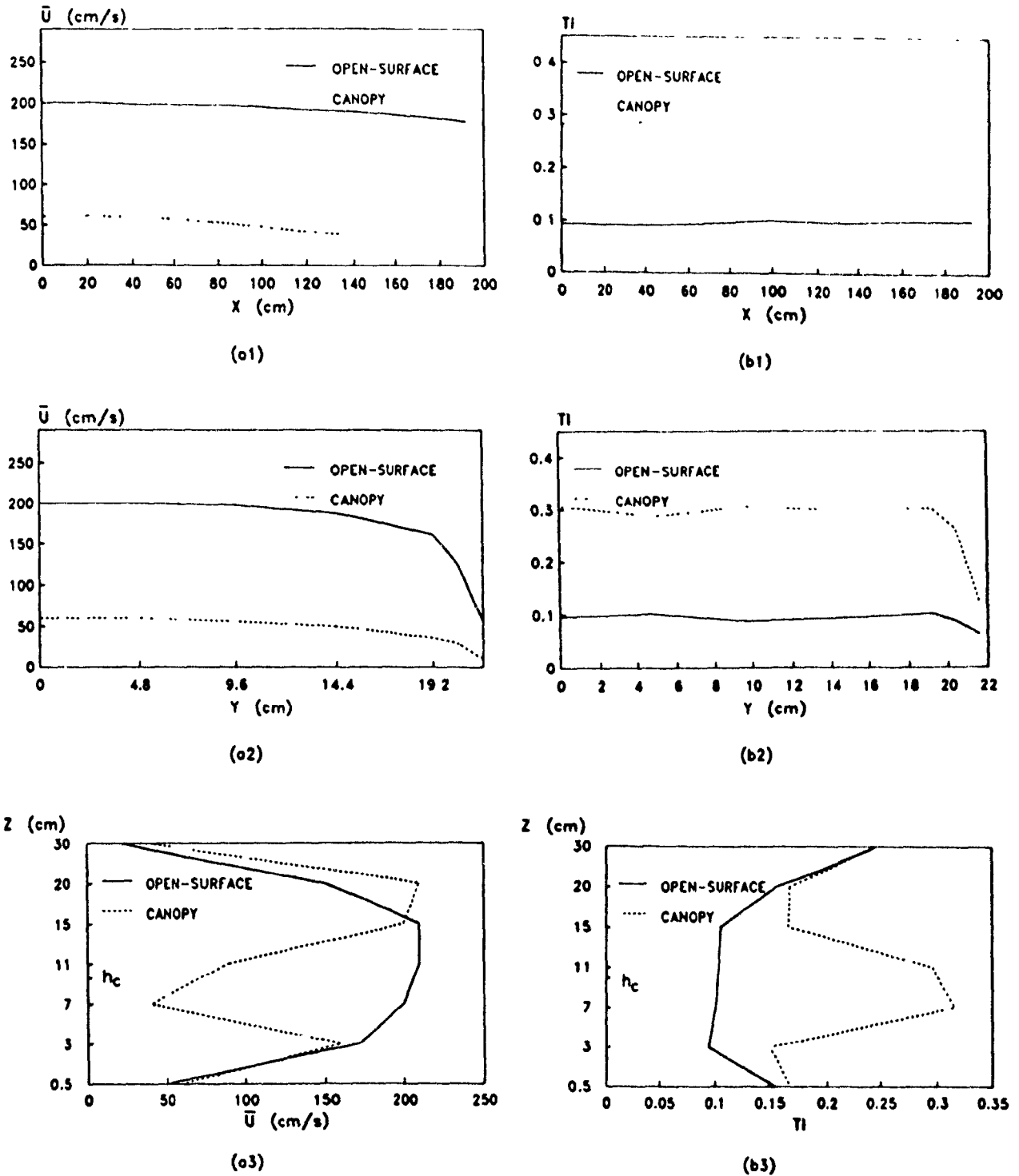


Figure 4. The profiles of mean velocities \bar{U} and turbulence intensities TI at source height in along-wind direction (a1, b1), cross-wind direction (a2, b2) and vertical direction (a3, b3), in the middle of the simulation sections. Measurements are taken at centers of cell patterns in the canopy model.

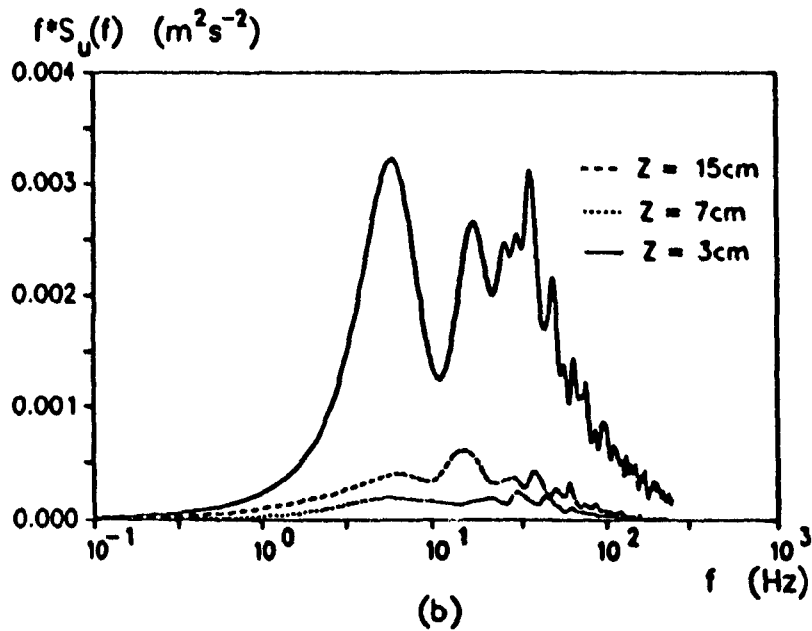
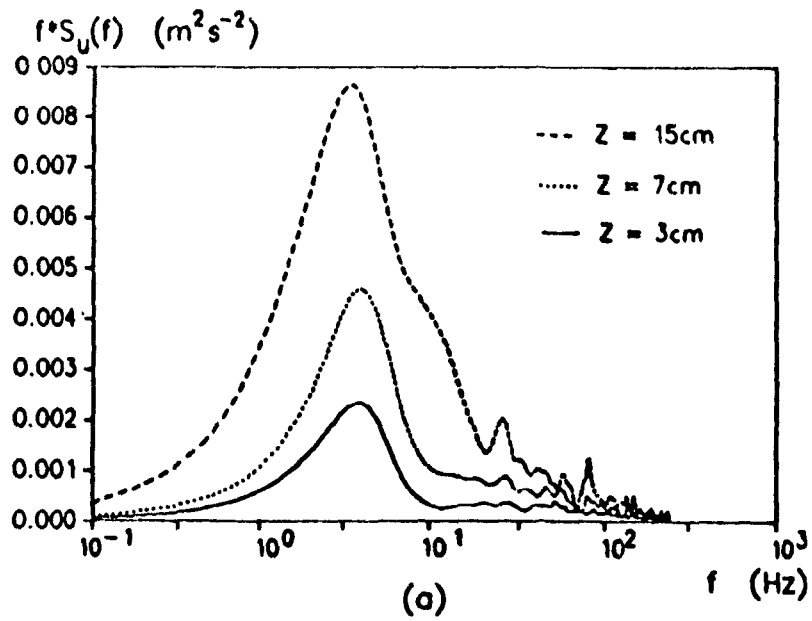


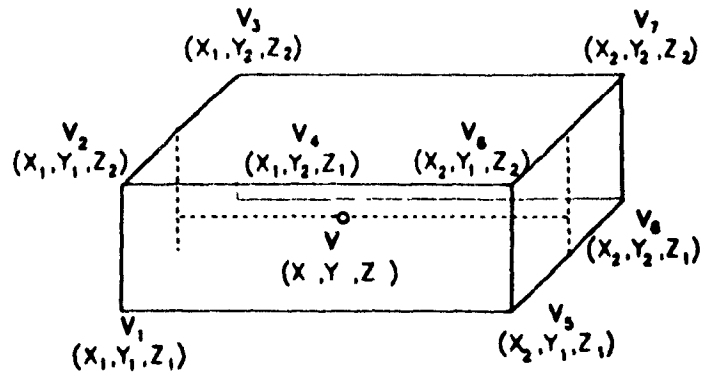
Figure 5. Spectra for u measured at $x = 90\text{cm}$, $y = 0\text{cm}$ in open-surface model (a) and at $x = 62.4\text{ cm}$, $y = 0\text{ cm}$ in canopy model (b).

simulation section, with infinitely fine grids. In practice, however, measurements are restricted to a limited number of positions with relatively large discrete spacing, and interpolations between these measurement positions are used.

Based on the preliminary observations of spatial variation in the wind field (Figure 4), the simulation section was divided into linear rectangular sub-sections bounded by $y = 0, 9.6, 19.2, 21.6$ cm, $z = 0, 2.4, 7.2, 12.0, 14.4, 16.8, 19.2, 33.6$ cm and $x = 0, 91.2, 182.4$ cm for the open-surface model, or $x = 0, 62.4, 124.8$ cm for the canopy model. In each of the sub-sections, the Eulerian velocity V at any position (x,y,z) was linearly interpolated from the measurements at all corners of the sub-section (measurements V_1 to V_8), as illustrated in Figure 6a

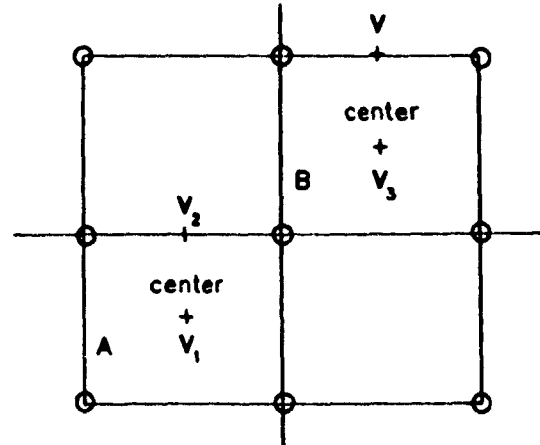
In the canopy model, the above linear interpolation was only applicable to the center of each cell pattern formed by four surrounding trees. For any other position within each cell pattern, a further proportional interpolation was used under the assumption of similarity between cell patterns. As symbolized in Figure 6b, a central cell pattern A was chosen as being representative, in which the Eulerian velocities at various positions V_2 , inside the cell pattern and along the cell pattern periphery, were measured in addition to the central velocity V_1 . Any other cell pattern B in the simulation section was assumed to be dynamically similar to A, and the Eulerian velocity V at any position in cell B was proportionally interpolated on the basis of V_3 (itself linearly interpolated as described above).

By not providing information about sub-grid scale motion, the Eulerian velocity measurements at discrete spatial positions may not adequately reflect the natural spatial coherence of flow structures. The proposed interpolations (both linear and proportional) from isolated point measurements can only approximate such structures in a statistical sense; it cannot reproduce a dynamic picture of such structures. The potential error introduced by this procedure will be discussed later.



$$\begin{aligned}
 v = & \frac{1}{(x_2-x_1)(y_2-y_1)(z_2-z_1)} (v_1(x_2-x)(y_2-y)(z_2-z) \\
 & + v_2(x_2-x)(y_2-y)(z-z_1) + v_3(x_2-x)(y-y_1)(z-z_1) \\
 & + v_4(x_2-x)(y-y_1)(z_2-z) + v_5(x-x_1)(y_2-y)(z_2-z) \\
 & + v_6(x-x_1)(y_2-y)(z-z_1) + v_7(x-x_1)(y-y_1)(z-z_1) \\
 & + v_8(x-x_1)(y-y_1)(z_2-z))
 \end{aligned}$$

(a)



$$v = v_3 \frac{v_2}{v_1}$$

(b)

Figure 6. Linear (a) and proportional (b) interpolation procedures: V is the interpolated value, V₁, V₂, V₃, V₄, V₅, V₆, V₇ and V₈ are measured values. Circles represent trees.

1054

4.2. Gridding

The simulation sections were numerically divided into space grids. To minimize computational errors within the limitations imposed by available computing facilities, the division of the space grids was subject to the conditions that the space grid size dx , dy and dz be smaller than the dominant eddy scales reflected in the spectrum measurement. For optimum comparison of numerical and experimental simulation, the Eulerian velocity measurement positions described in Section 4.1. should also be located at centers of the space grids. According to these conditions, the space grid size in both open-surface and canopy models was chosen to be $dx = dy = dz = 1.2$ cm. The loss of information from eddies below this cut-off scale (at frequencies around 170 Hz) would be expected to be small (Figure 5).

With the above space grid size, the simulation sections were divided into three-dimensional $152 \times 36 \times 28$ space grids in the open-surface model and $104 \times 36 \times 28$ space grids in the canopy model, respectively, starting at the coordinate origins. The source was then located at space grid point ($x = 4$, $y = 0$, $z = 8$). in both open-surface and canopy models.

In order to calculate the probability density distribution $P_{\mathbf{v}}(\mathbf{v} | \mathbf{x}, t_1)$, the measured or interpolated time series of the Eulerian velocity at each space grid point were divided into three-dimensional $7 \times 7 \times 7$ velocity grids, with grid size $du = dv = dw = 26 \text{ cm} \cdot \text{s}^{-1}$, covering fluctuations from -90 to $90 \text{ cm} \cdot \text{s}^{-1}$. The time step Δt was then determined as $\Delta t = \frac{1.2}{26} = 0.046154 \text{ s}$ according to (2.4).

The numerical simulations were carried out until steady plumes were developed. Since the plumes were expected to be symmetrical about the central xz plane ($y = 0$), only halves of plumes ($y \geq 0$) were actually simulated. Calculations were coded by FORTRAN 77 and performed in the mainframe computer systems

MVS and MUSICA (McGill University, Computing Center). Each simulation required about 15 hr CPU time. For later reference, the main parameters are listed in Table 1.

5. Results

5.1. Comparison of numerical simulations with experimental observations

The concentration profiles of the steady numerical plumes are compared with observed concentration profiles of the steady experimental plumes in Figures 7 and 8, at the measurement positions indicated in Figure 2.

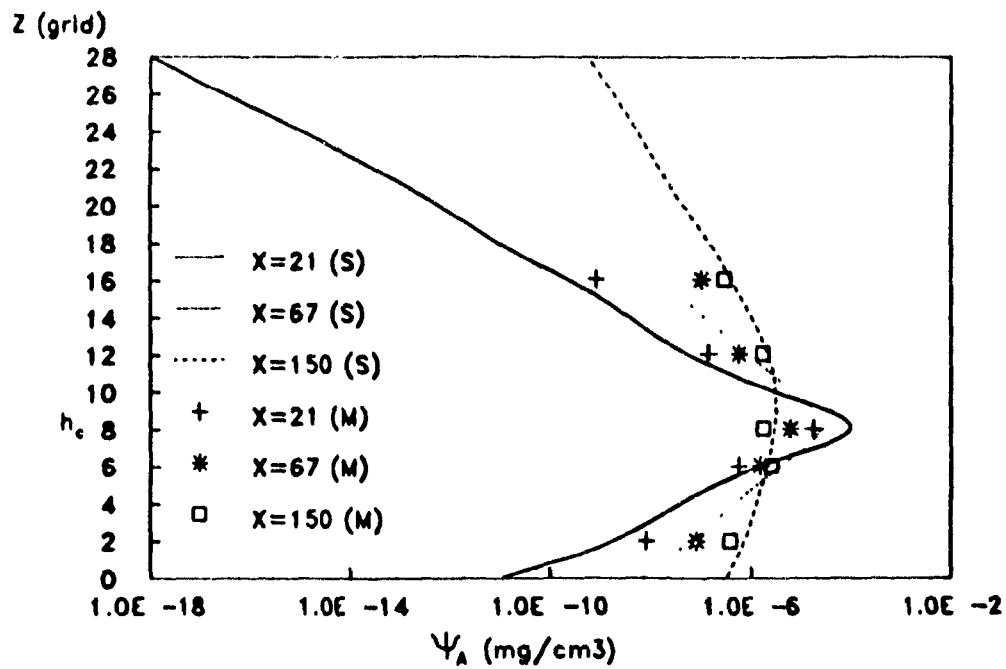
Considering that the sampling tubes of the experimental measurements occupy non-negligible space in the fluid, a proper spatial averaging has been imposed on the numerical profiles, without significant changes from original results.

In the open-surface model, numerical predictions show good agreement with experimental observations (Figure 7), except for a tendency towards overestimation close to the source ($z = 8$) and underestimation at some distance from it. These minor discrepancies might be attributed to the wake structure introduced by the glass tube that contains the source solution (Figure 1), which might contaminate the fluid flow. This would retard NH_3 diffusion in a way not reflected and recovered by the discrete Eulerian velocity measurements and the linear interpolation approximation used in the numerical simulation (Figure 6a). The influence of this wake flow would be expected to decrease with increasing distance from the source. This appears to be confirmed by the close agreement between numerical predictions and experimental observations at $x = 150$.

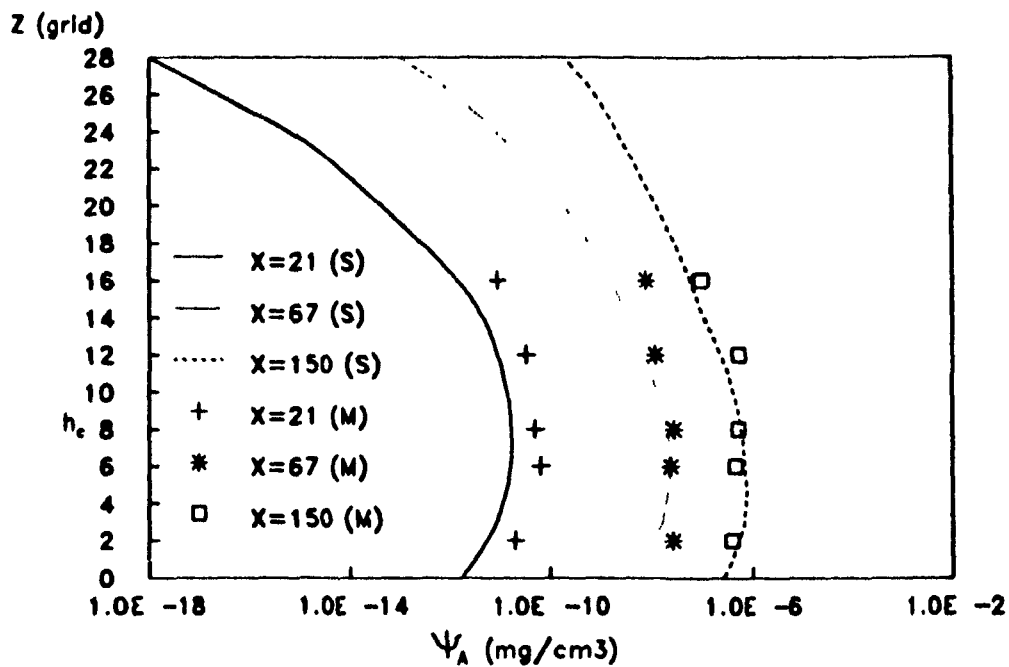
In the canopy model, the numerical predictions also show general agreement with the experimental observations (Figure 8), at least in the central xz plane. However, the agreement is not as good as in the open-surface model. In particular,

Table 1. List of simulation parameters.

Parameters:	Open Surface:	Canopy:
Canopy height (h_c) cm	n. a.	11
Canopy cell shape	n. a.	square
Canopy cell spacing cm	n. a.	4.8
Velocity grids ($U \times V \times W$)	$7 \times 7 \times 7$	$7 \times 7 \times 7$
Velocity grid size (du) cm s^{-1}	26	26
Space grids ($X \times Y \times Z$)	$152 \times 36 \times 28$	$104 \times 36 \times 28$
Space grid size (dx) cm	1.2	1.2
Time step (Δt) s	0.046154	0.046154
Initial concentration (Ψ_A) mg cm^{-3}	0.0	0.0
Source material	98% NH_3	98% NH_3
Source location (X, Y, Z) grid	(4,0,8)	(4,0,8)
Source strength (E_A) $\text{mg s}^{-1} \text{cm}^{-3}$	0.0834	0.0477
Boundary condition	reflection	reflection
Free-stream velocity (U_w) cm s^{-1}	210	210
Mean velocity at h_c cm s^{-1}	200	60
Turbulence intensity at h_c	0.102	0.306
Simulation duration s	10.0	16.0



(a)



(b)

Figure 7. NH_3 concentration profiles of the steady numerical plume (S) and steady experimental plume (M) from continuous point source in the open-surface model at three downwind distances (x) from the source, on each of two xz planes at $y = 0$ (a) and $y = 8$ (b).

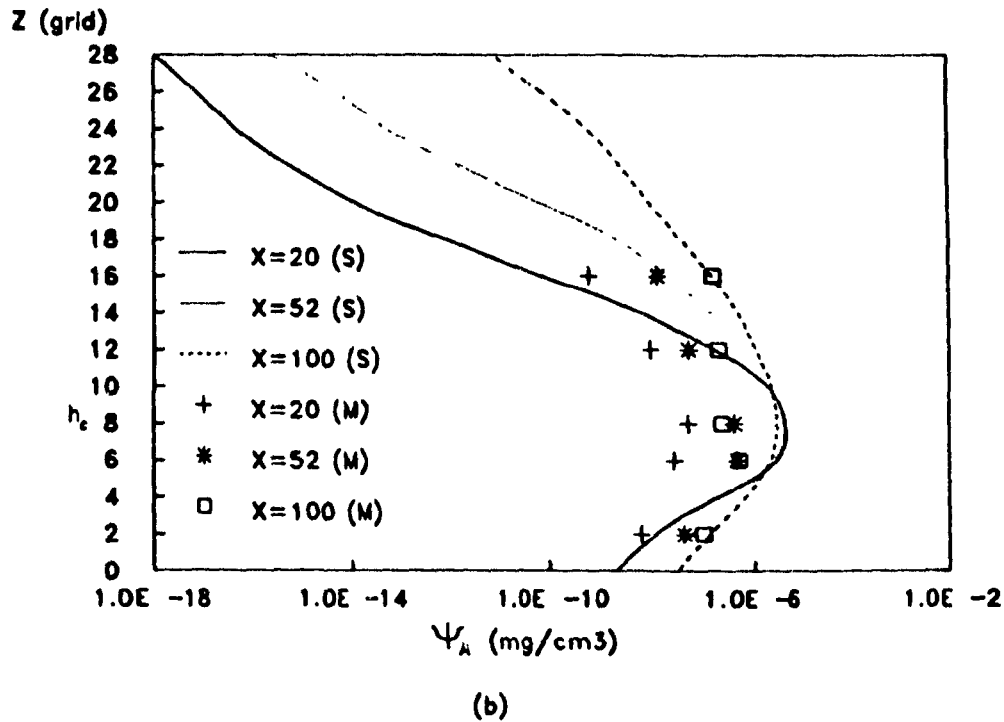
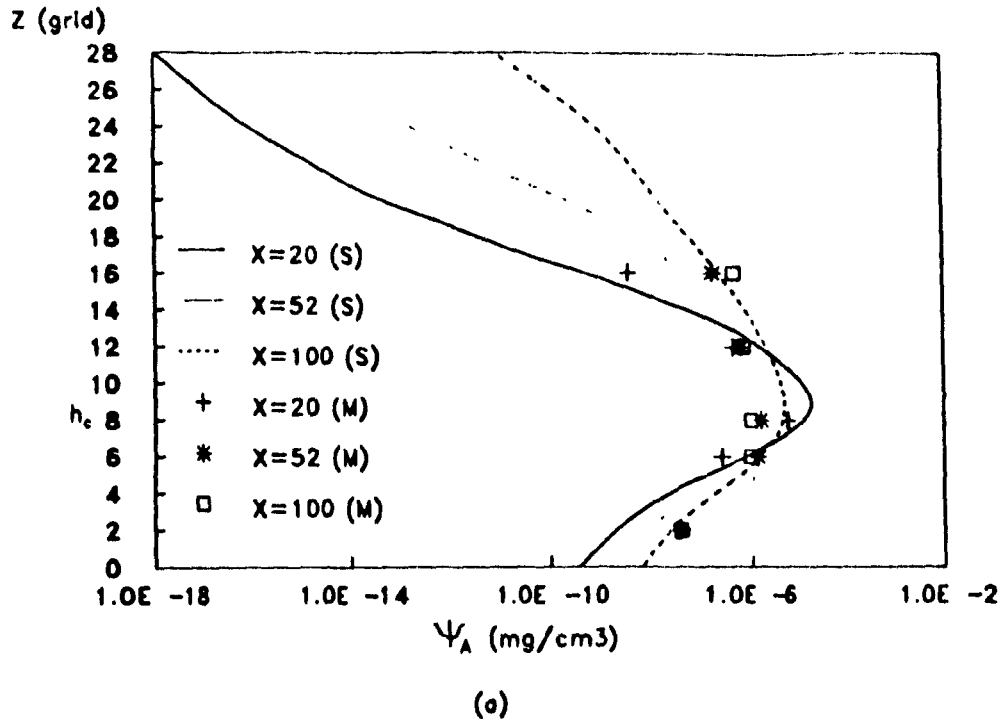


Figure 8. NH_3 concentration profiles of the steady numerical plume (S) and steady experimental plume (M) from continuous point source in the canopy model at three down-wind distances (x) from the source, on each of two xz planes at $y = 0$ (a) and $y = 8$ (b).

the numerical overestimations are more pronounced around the canopy crown, both above and within, where strong turbulence intensity has been measured (Figure 4b). These overestimations do not seem to diminish with increasing distance, as observed in the open-surface model. On the contrary, they tend to grow and spread with plume development. The strong turbulence intensity structure in the canopy crown may be the main cause for persistent overestimation. It is almost certainly too complex in detail to be reflected and recovered by the discrete Eulerian velocity measurements and the interpolation approximations used in the numerical simulations (Figure 6).

In general, it might be concluded, in both open-surface and canopy models, that the numerical simulations deviate from experimental observations primarily in areas of high concentration, like the centroid of the plume, and/or in areas of complex flow with strong turbulence intensity, like the wake structure behind the source tube and within the canopy.

5.2. Development of the numerical plumes

For interest only, the development with time of the numerical plumes in both open-surface and canopy models are presented here. Since continuous time in the numerical simulations was separated into a discrete time series, with the time step $\Delta t = t_{i+1} - t_i$, the sources were perceived as periodic trains of NH_3 puffs whose further development was simulated. This can be seen in the cutaway views of the central xz plane ($y = 0$) in the open-surface model (Figure 9a), where the train of puffs persists over some distance in the field of weak turbulence intensity. In the canopy model, the individual puffs are not distinguishable since the strong turbulence intensity generated by the canopy destroys the consistency of the flow (Figure 9b). Due to the resistance of the canopy crown, the plume is distorted into

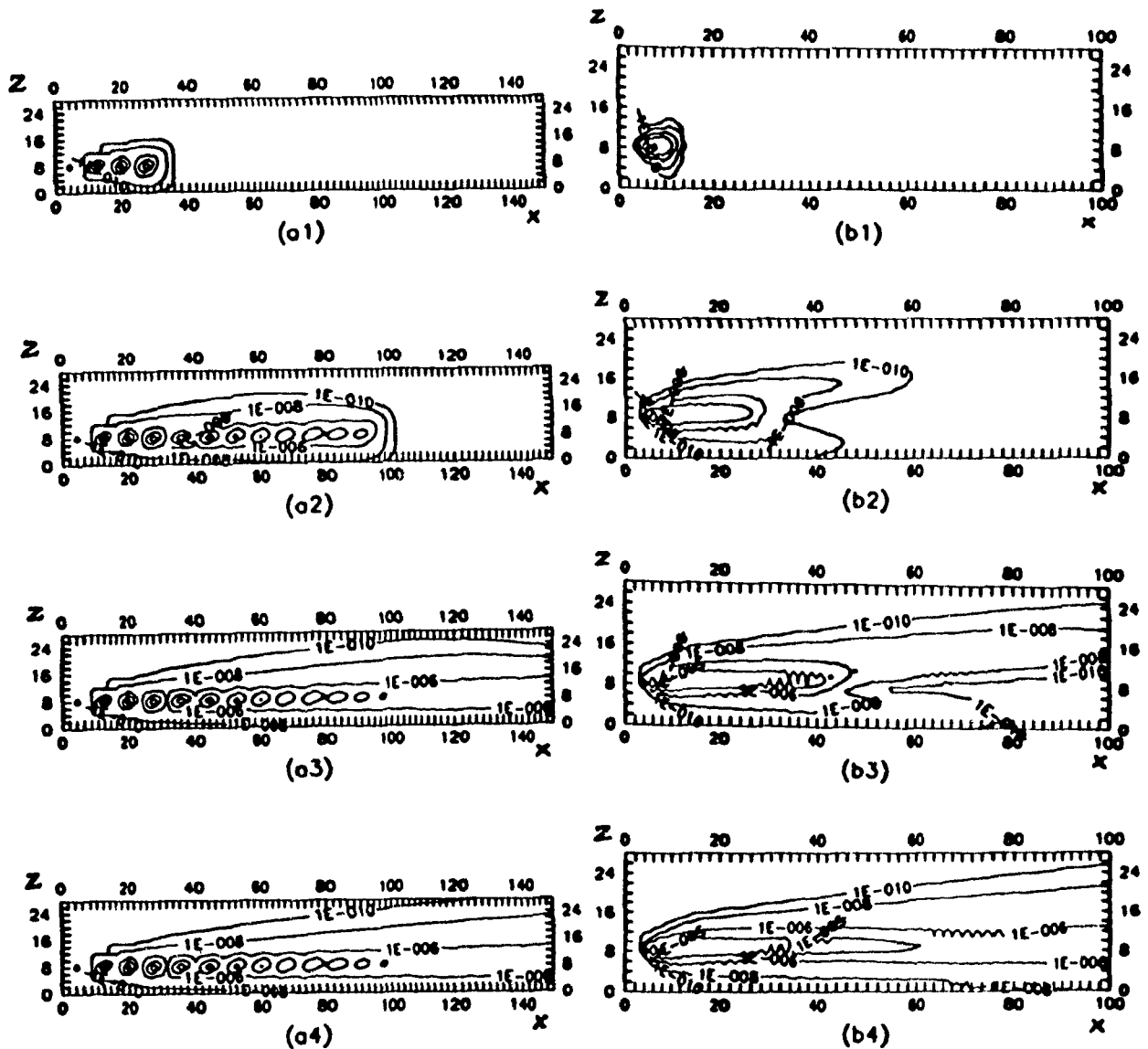


Figure 9. The developments of NH_3 concentration contours on the central xz plane ($y = 0$) of the numerical plumes from continuous point sources in the open-surface model (a) and the canopy model (b) at simulation times 0.1s (a1, b1), 0.5s (a2, b2), 2.0s (a3, b3), 10.0s (a4) and 16.0s (b4).

two fronts, spreading above the canopy and into the trunks space, respectively. Similar developments of the numerical plumes are shown in the cutaway views of the horizontal xy plane at source height ($z = 8$) in Figure 10, which again shows a clearly defined plume in the open-surface model. In the canopy model, however, the shape of the plume is blurred by rapid lateral spread of source material.

Figures 9 and 10 also illustrate that the numerical plume in the open-surface model develops at almost twice the speed of the plume in the canopy model, so that the numerical formation of stable plumes takes less time (about 8 seconds) in the former model than in the latter (about 14 seconds). This is in agreement with the observed higher mean velocity and source release rate in the open-surface model, compared to the canopy model.

Differences in fully developed plumes between the two models become evident in the longitudinal cuts along the xz plane at $y = 0, 4, 8$ and 18 in Figure 11. In the open-surface model (Figure 11a), the flow of weak turbulence intensity smoothly spreads source material into a narrow and orderly plume with clear outline and strong cross-wind concentration gradients. In the canopy model (Figure 11b), the high turbulence intensity diffuses the source material into a broad and disorderly plume with vague outline and weak cross-wind concentration gradients.

To illustrate these structures more clearly, the concentration profiles of the steady numerical plumes are presented in Figure 12 at three distances from the source ($x = 21, 67$ and 150 in the open-surface model; $x = 20, 52$ and 100 in the canopy model) on each of the xz planes at $y = 0, 8$ and 18 . These concentration profiles again demonstrate the effective lateral mixing in the canopy model, because concentration profiles do not change much in the cross-wind direction. By contrast, the plume in the open-surface model, with poor lateral mixing, shows rapidly

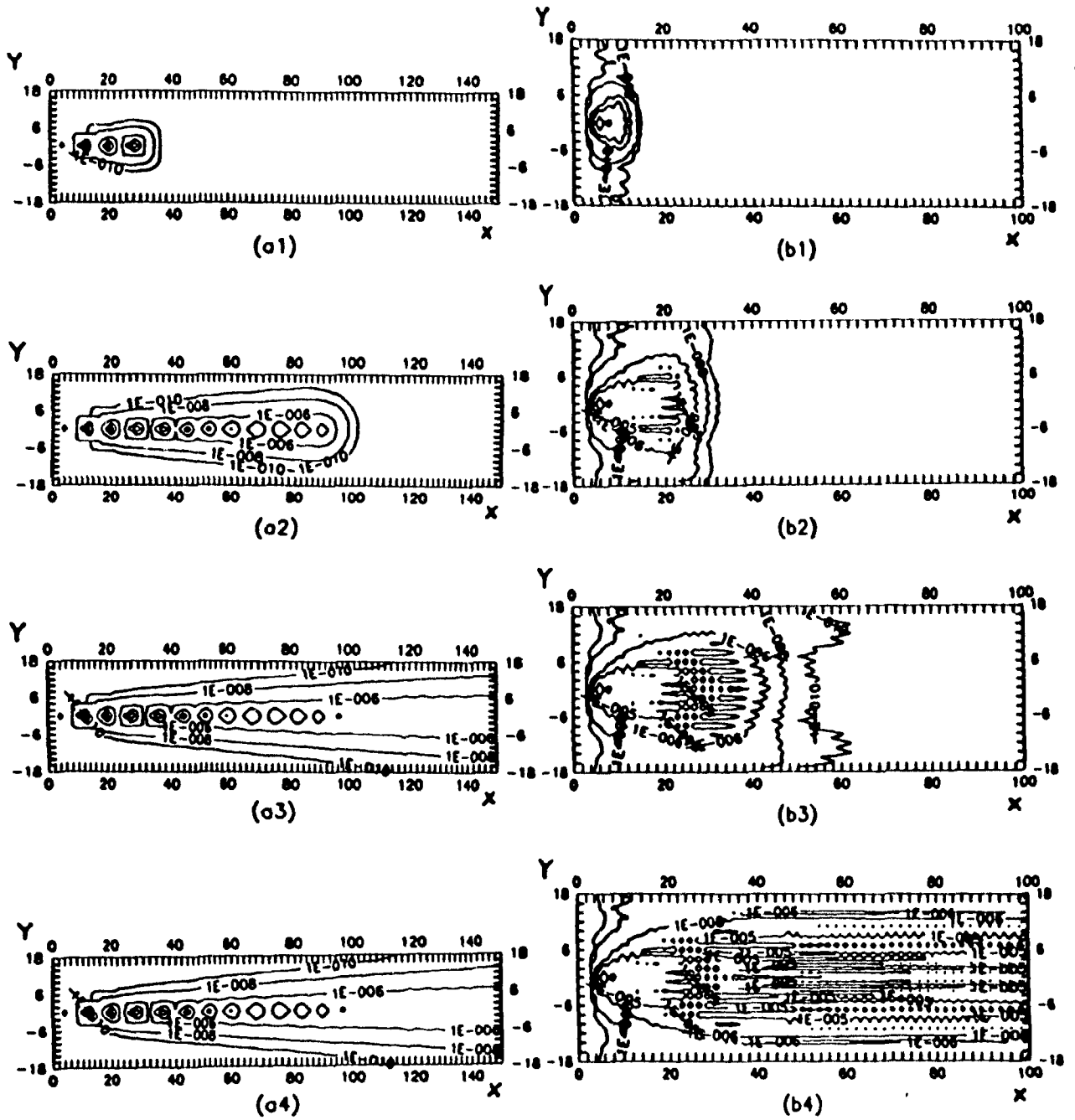


Figure 10. The developments of NH_3 concentration contours on the xy plane ($z = 8$, source height) of the numerical plumes from continuous point sources in the open-surface model (a) and the canopy model (b) at simulation times 0.1s (a1, b1), 0.5s (a2, b2), 2.0s (a3, b3), 10.0s (a4) and 16.0s (b4).

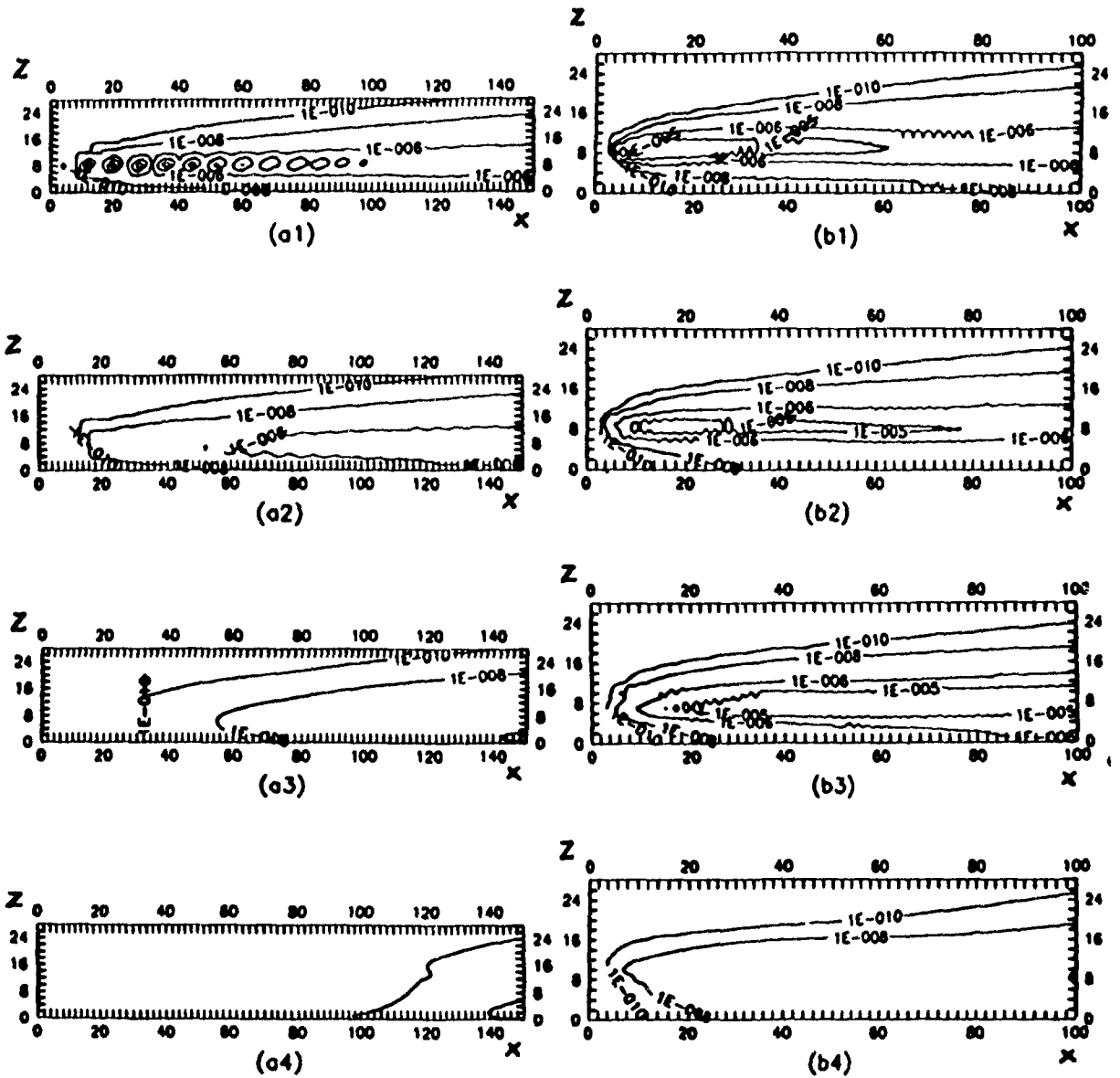
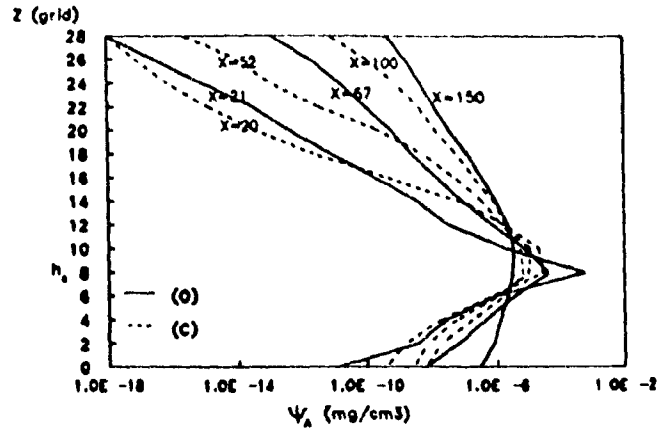
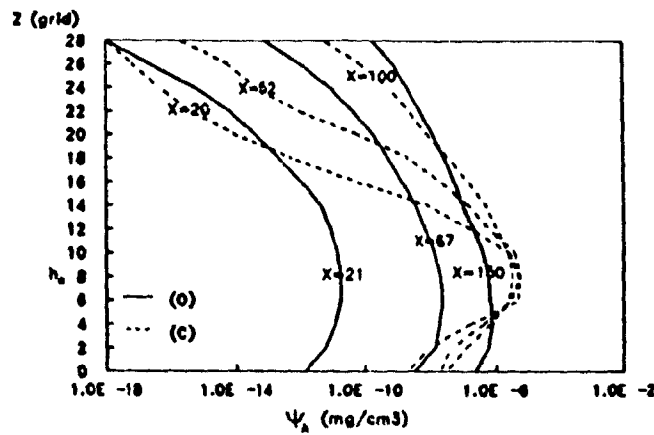


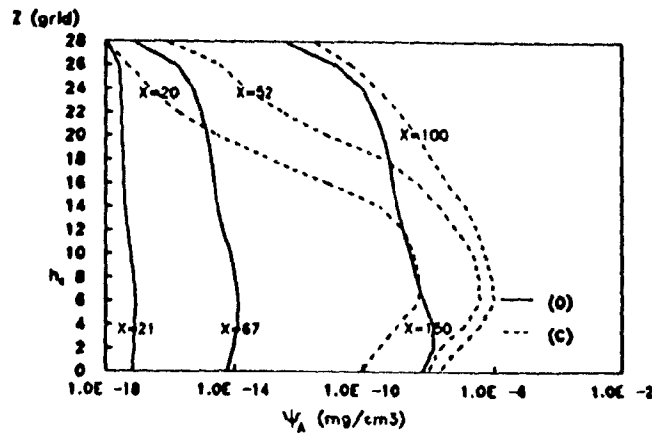
Figure 11. NH_3 concentration contours of the steady numerical plumes from continuous point sources in the open-surface model (a) and the canopy model (b) on different xz planes at $y = 0$ (a1, b1), $y = 4$ (a2, b2), $y = 8$ (a3, b3) and $y = 18$ (a4, b4).



(a1)



(a2)



(a3)

Figure 12. NH_3 concentration profiles of the steady numerical plumes from continuous point sources in the open-surface model (O) and the canopy model (C) at three down-wind distances (x) from the source, on each of three xz planes at $y = 0$ (a1), $y = 8$ (a2) and $y = 18$ (a3).

decreasing concentration profiles in the cross-wind direction. Similar results can be seen from the concentration profiles, presented in Figure 13, at the three cross-wind distances $y = 0, 8$ and 18 , on each of the yz planes at $x = 21, 67$ and 150 in the open-surface model, and at $x = 20, 52$ and 100 in the canopy model. However, sufficiently far downwind from the source, the difference of the steady numerical plumes in cross section between the open-surface model and the canopy model becomes small, because the simulation sections are limited in space and boundary-induced contaminations may be unavoidable.

6. Error analyses

In spite of generally encouraging agreement between numerical simulations and experimental observations in this preliminary application, discrepancies do exist. They could conceivably result from the following errors: (a) loss of tracer concentration unreclaimed by the sampling tubes of the experimental observations in areas of high concentration; (b) idealized boundary condition treatments due to the assumption of elastic reflection; (c) deficiency of flow information due to the discrete Eulerian velocity measurements and inadequate interpolation procedures; (d) loss of eddies smaller than the space grid size of 1.2 cm; (e) perturbations of the Eulerian velocity measurement from directional contaminations of the three velocity components (u, v, w) through the limited accuracy provided by the hot-film measurement array; (f) imprecise estimate of the fractional redistribution density F_C by the approximation (2.2) or (2.5).

Error (a) most likely occurs along the centroid of the experimental plumes. It would flatten the peaks of the observed concentration profiles. In the experimental simulations, however, tracer concentrations are of the same order of magnitude in both models, so that error (a) is expected to be comparable in both, and unlikely

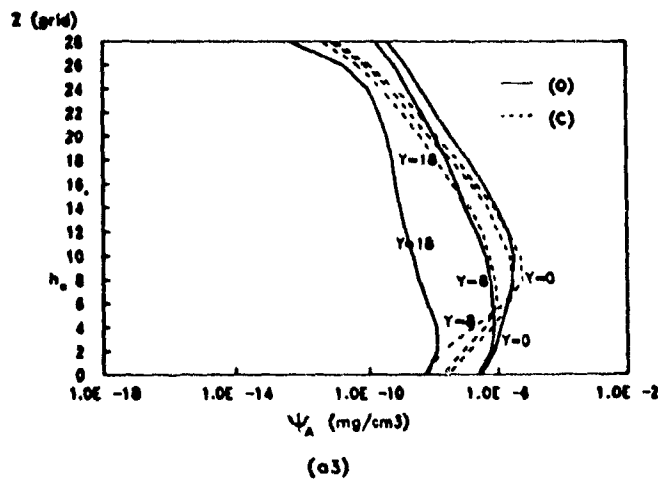
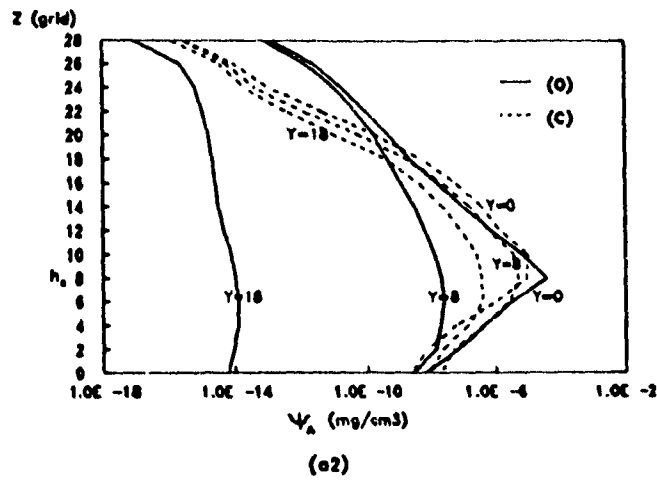
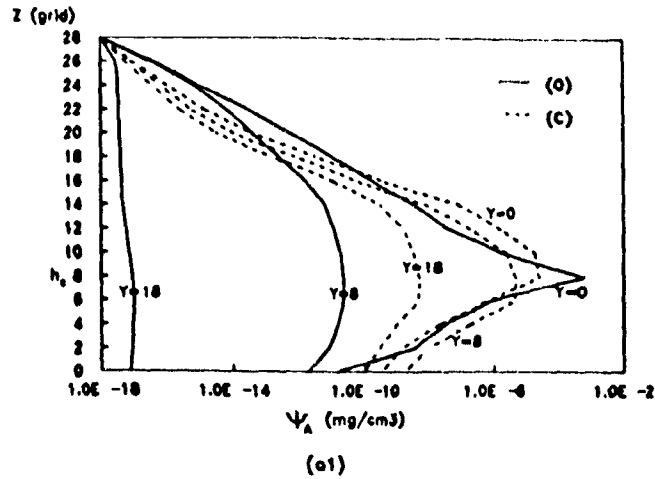


Figure 13. NH_3 concentration profiles of the steady numerical plumes from continuous point sources in the open-surface model (O) and the canopy model (C) at three crosswind distances (y), on each of three yz planes at $x = 21$ (O) or 20 (C) in (a1), $x = 67$ (O) or 52 (C) in (a2) and $x = 150$ (O) or 100 (C) in (a3).

to explain relative differences between their respective degrees of success.

Error (b) may cause the numerical plumes to be contaminated by the boundaries, while errors (c) and (d) may unduly simplify the numerical plumes. The magnitude of error (c), stemming from neglect of sub-grid scale motion, is likely a function of the complexity of the flow structure. It is potentially more worrisome in the case of coherently inhomogeneous and intermittent flow with strong turbulence intensity, so that it might be more pronounced in the canopy model, while errors (b) and (d) may be expected to be comparable in the two models under the same boundary and gridding treatments.

Error (e) may distort the calculated Eulerian velocity probability density distribution $P_{\mathbf{V}}(\mathbf{V} | \mathbf{x}, t_1)$ used by (2.5) in the numerical simulations. However, this error has been reduced to some degree by directional corrections so that, as a first approximation, it could be expected to be comparable in the two models.

Error (f) cannot be directly evaluated, but its existence certainly distorts the true fractional redistribution density F_C , and thus the numerical plumes. It stems from the assumptions that the scalar tracer (NH_3) is completely mixed in every virtual fluid parcel at any time, and that the redistribution of the scalar perfectly follows the redistribution of the fluid volume. In laminar or weakly turbulent flow with small turbulence intensity, these assumptions may be justified. However, in strongly turbulent flow with large turbulence intensity, such as in the canopy model, they may introduce noticeable error since the fluid may become non-uniformly mixed with the scalar. The weakness of the assumption (2.5), that the fractional redistribution density F_C can be deduced from the probability density distribution $P_{\mathbf{V}}$ of the local real-time Eulerian velocity, where the significant influence of the scalar concentration distribution is not incorporated, then becomes apparent.

It may thus be said that the larger discrepancy between the numerical simulations and the experimental observations in the canopy model is expected to be due primarily to errors (c) and (f), with a relative distribution between them that cannot be ascertained within the framework of this preliminary study.

7. Conclusion

As a preliminary trial, this study explores a simplified numerical modeling of turbulent diffusion under the virtual fluid parcel treatment of the BMDFE. It has been based on the approximation of the fractional redistribution of the scalar by the fractional redistribution of fluid volume, calculated from the probability density distribution of the local Eulerian velocity. It is also based on the assumption that the sub-grid scale motion, ignored by the discrete Eulerian velocity measurements, can be recovered by linear and/or proportional interpolations. This simplified numerical modeling has been applied to the simulations of diffusion of ammonia (NH_3) from a continuous point source in open-surface and canopy models in a wind tunnel. The numerical simulations showed general agreement with the experimental observations, with partial discrepancies.

The discrepancies in the canopy model have been shown to be bigger than in the open-surface model, presumably because of the existence of the inhomogeneous and intense turbulence in the canopy flow. In such turbulent flow, the above approximations may produce significant errors, since the mixing of fluid may be too severe for its scalar distribution to be precisely estimated by its volume distribution, and since the structure of the flow may be too complex in detail for its sub-grid scale motion to be accurately represented by simple interpolations.

Overall, the relative success of the simplified numerical modeling encourages tests of the full numerical modeling, based on the joint equations (1.1)–(1.3), for

which proper (closure) parameterization in the disintegration equation (1.1) should be explored.

REFERENCES

- Jones, W.P. & Musong, P. 1988 Closure of the Reynolds stress and scalar flux equations. *Phys. Fluids* **31**, 3589–3604.
- Luhar, A.K. & Britter, R.E. 1989: A random walk model for dispersion in inhomogeneous turbulence in a convective boundary layer. *Atmos. Environ.* **23**, 1911–1924.
- Pope, S.B. 1987 Consistency conditions for random-walk models of turbulent dispersion. *Phys. Fluids* **30**, 2374–2379.
- Sawford, B.L. 1986 Generalized random forcing in random-walk turbulent dispersion models. *Phys. Fluids* **29**, 3582–3585.
- Thomson, D.J. 1984 Random walk modeling of diffusion in inhomogeneous turbulence. *Q. J. R. Met. Soc.* **110**, 1107–1120.
- van Dop, H., Nieuwstadt, F.T.M. & Hunt, J.C.R. 1985 Random walk models for particle displacements in inhomogeneous unsteady turbulent flows. *Phys. Fluids* **28**, 1639–1653.
- Part 1 (attached Y. Guo, 1991): The role of molecular mixing in the description of turbulent diffusion in fluid continuum. Part 1. The limitation of the fluid particle treatment.
- Part 2 (attached Y. Guo, 1991): The role of molecular mixing in the description of turbulent diffusion in fluid continuum. Part 2. The virtual fluid parcel treatment.
- Part 3 (attached Y. Guo, 1991): The role of molecular mixing in the description of turbulent diffusion in fluid continuum. Part 3. Application to the diffusion cloud.

General Summary

This thesis examined the role of molecular mixing in the description of turbulent diffusion in continuum framework at the level of conceptualization (or mathematical treatment) of the BMDFE (Basic Macroscopically Describable Fluid Element). The classical fluid particle treatment of the BMDFE is compared with a new virtual fluid parcel treatment of the BMDFE. Main findings are summarized as follows:

With its postulated constraint that individual BMDFEs maintain their integrities in motion, the classical fluid particle treatment excludes molecular mixing between different BMDFEs. The randomization supplementary treatment does not alleviate this fact because it does not change the nature of the postulated fluid particle moving as an entity. As a result, turbulent diffusion under the random fluid particle treatment can only be described as the random fluid particle dispersions in process of the non-feedback statistical superimposition of the shadow-like ensemble mean contributions from individual fluid particles in the flow. Due to the existence of molecular mixing between the BMDFEs in real turbulent fluids, this description may lead to a potential mathematical-physical inconsistency in the understanding of turbulent diffusion.

By relaxing the above constraint to permit disintegration of individual BMDFEs, a new virtual fluid parcel treatment is proposed to incorporate molecular mixing between different BMDFEs. The main improvement made by the new virtual fluid parcel treatment lies in the introduction of a feedback mechanism in the form of physically coupled disintegration and integration of the BMDFEs. This improvement suggests that molecular mixing is a controlling agent of the mixing mechanism in every time-step of turbulent diffusion, whose significance could be

cumulatively increased.

By applying the above two treatments to the evolution of the diffusion cloud, analysis shows that molecular mixing persistently and cumulatively influences the evolution of the diffusion cloud by reducing the diffusion distribution variance. This indicates that the exclusion of molecular mixing in the classical fluid particle treatment could lead to an exaggeration of the diffusion distribution variance. This analysis is qualitatively supported by scalar diffusion experiments in water flow with moderate turbulence intensity.

As a preliminary trial, a simplified numerical modeling of scalar diffusion based on the virtual fluid parcel treatment is executed in two wind tunnel models. The simplification is made by direct estimation of the fractional redistribution density of scalar from measurements. The numerical predictions show general agreement with the experimental observations.

Suggestions for Future Study

Future study would be primarily pursued in quantitative examination of the effect of molecular mixing on turbulent diffusion. This would involve numerical experiments to compare the virtual fluid parcel treatment and the random fluid particle treatment in the description of the diffusion cloud evolution.

The (closure) parameterization of the macroscopic inhomogeneity in both flow scale and turbulence intensity is the common technical difficulty in solving the diffusion equations under both the virtual fluid parcel and the random fluid particle treatments. In order to minimize the influence of this difficulty, the diffusion in stationary and homogeneous turbulence will be a start of the study. As a working hypothesis, the errors caused by parameterization in the two descriptions are expected to be comparable.

According to Part 3, the reduction of the diffusion distribution variance by molecular mixing (or the exaggeration of the diffusion distribution variance by the random fluid particle treatment due to exclusion of molecular mixing) is expected to become more pronounced when the Reynolds number, the Peclet number, or the turbulence intensity in general, increases. Quantitative confirmation of this analysis should be done by numerical experiments under variation of the Reynolds number, the Peclet number or the turbulence intensity. The results may then be used to evaluate the role of molecular mixing in the transition from laminar flow, through weakly turbulent flow to highly turbulent flows. The numerical experiments can also be easily adjusted to account for the effect of molecular collision-transport if the dependence on the Prandtl or Schmidt number is considered in the diffusion equations.